PORPHYRIN POLYSILOXANES AND THEIR APPLICATIONS

STRATEGIES FOR THE INCORPORATION OF PORPHYRINS IN POLYSILOXANES AND THEIR APPLICATIONS

By CODY B. GALE H.B.Sc

A Thesis Submitted to the School of Graduate Studies in Partial Fulfillment of the Requirements of the Degree of Doctor of Philosophy

McMaster University DOCTOR OF PHILOSOPHY (2021) Hamilton, Ontario

Chemistry

TITLE: Strategies for the Incorporation of Porphyrins in Polysiloxanes and their Applications.

AUTHOR: Cody B. Gale, H.B.Sc (McMaster University)

SUPERVISOR: Professor Michael A. Brook.

NUMBER OF Pages: xx, 171

Lay Abstract

Porphyrins have attracted the attention of scientists for generations who have sought to exploit their unique chemical, physical, optical, and electronic properties. Their unique properties have led to them being utilized in a multitude of applications. Despite the wide array of applications investigated, the utilization of porphyrins in polysiloxane (silicone) chemistry has received comparatively little attention. Polysiloxanes and porphyrins possess potentially mutually beneficial properties that could lead to the development of interesting materials. Unfortunately, their development is not straightforward, as porphyrins and polysiloxanes are not naturally compatible with one another. Therefore, to realize the potential benefit of porphyrin-polysiloxane materials synthetic techniques must be first developed that allow for the reliable incorporation of porphyrins into polysiloxane matrices Two techniques were investigated for the incorporation of porphyrins into polysiloxanes. The Piers-Rubinsztajn reaction and ionic crosslinking. These methods allowed for the development of materials that had interesting applications including dielectric elastomers, reactive oxygen species generating materials and catalytic elastomers.

Abstract

Porphyrins are a class of natural and synthetic aromatic macrocycles that have received extensive investigation because of their unique chemical and optoelectronic properties. They are excellent ligands, photosensitizers and catalysts and serve critical roles in numerous biochemical reactions. Their properties and diverse applications have fascinated chemists from multiple fields, and porphyrins have been investigated in applications such as dye-sensitized solar cells, cancer treatments, and conjugated polymers among others. While porphyrins have made in-roads in multiple fields they have received at best minimal attention in the field of polysiloxane chemistry.

Polysiloxanes are a class of inorganic polymers widely used in industrial applications that possess properties including low glass transition temperatures, high thermal and oxidative stabilities, high optical transparency, and low refractive indices that are largely unmatched by organic polymers. These properties, if properly utilized, could compliment those possessed by porphyrins and lead to the development of new applications in the fields of porphyrin and polysiloxane chemistry. Unfortunately, porphyrins and polysiloxanes are not readily compatible with one another and synthetic techniques must be developed to allow for the reliable incorporation of porphyrins into polysiloxane matrices.

The objectives of this thesis are to develop strategies that allow for the ready incorporation of porphyrins into polysiloxane materials to improve existing and develop new applications for porphyrin-polysiloxane materials. These investigations led to the development of two techniques for the incorporation of porphyrins into polysiloxanes, the

Piers-Rubinsztajn reaction, and ionic crosslinking. Several siloxane and polysiloxane porphyrins were prepared utilizing the Piers-Rubinsztajn reaction. These porphyrins were easily incorporated into silicone elastomers that could be utilized as dielectric, or reactive oxygen species-generating elastomers. Alternatively, ionic crosslinks could be utilized to incorporate the natural porphyrin hemin into silicone elastomers. Elastomers manufactured via this method retained the catalytic capabilities of hemin, opening the door to a new class of synthetic peroxidases. Regardless of the method of application controlling the natural tendency of porphyrins to aggregate was essential to achieving the desired properties.

Acknowledgments

First and foremost, I want to thank my Ph.D. supervisor, Dr. Michael A. Brook, for allowing me to work in his lab during my undergraduate thesis and for allowing me to stay for a Ph.D. Mike's enthusiasm for chemistry and constant encouragement to pursue my research interests have allowed me to develop from an undergraduate student continually questioning why he chose to go into chemistry at all into a trained chemist who enjoys the challenge and only occasionally questions why he went into chemistry, usually only after multiple failed experiments! I greatly appreciate all the advice and opportunities that Mike has provided me over the past four years, and I will miss hearing him say, "We should totally do that."

I would also like to thank Dr. Anne Ladegaard Skov for allowing me to work in her lab at the Danish Technical University (DTU) for four months and for providing by far one of the best personal and professional experiences of my degree. I appreciate all the help provided by all the Danish Polymer Centre members during my stay there. Special thank you to Dr. Liyun Yu for her training and useful discussions on dielectric elastomers, and Dr. Piotr Mazurek and Dr. Elisa Ogliani for their help and friendship during my stay.

Thank you to Dr. Goward and Dr. Blossom Yan for lending your expertise in EPR, which was instrumental in completing my research project. A special thank you to Blossom for her positivity and encouragement during the six-month period where nothing was working. I would also like to thank my committee members, Dr. McNulty and Dr. Pelton, for their helpful suggestions and discussions throughout my degree. To my fellow Brook Lab members, both past and present, thank you for all your help and friendship over the

past four years. It has been a pleasure to work with a fantastic group of people who made coming into the lab every day an enjoyable experience even when things were not working as expected. I could not have gotten through these past four years without you all. A special thank you to Dr. Daniel Chen for providing valuable insight during my projects and keeping the lab running smoothly.

Finally, I would like to thank my family and friends for their constant support in the past four years. To my parents, we often joked that you knew nothing about what I did, but you were always ready to listen and help me through moments where I wanted to give up. Thank you for encouraging me to see this to the end. Without all of you, this would not have been possible. Thank you.

Declaration of Academic Achievement

I hereby certify that the work described within this thesis is the original work of the author under the supervision of Dr. Michael A. Brook.

Published Manuscripts:

1. C. B. Gale, Z. Blossom. Yan, M. Fefer, G. R. Goward, and M. A. Brook, *Macromolecules.* In press.
2. C. B. Gale, M.A. Brook, and A. Ladegaard Skov, *RSC Adv.,* 2020, **10,** 18477-18486.[1]
3. C. B. Gale and M. A. Brook, *Green Chem.*, 2018, **20**, 3717–3721.[1]
4. C. B. Gale, B. Chin, C. Tambe, D. Graiver and M. A. Brook, *ACS Sustain. Chem. Eng.*, 2019, **7**, 1347–1352.

Manuscripts in Preparation:

1. C. B. Gale, and M. A. Brook, Hemin-doped, Ionically Crosslinked Silicone Elastomers with Peroxidase-like Reactivity.
   (to be submitted by May 2021)

Author Contributions

Chapter 2: The author was responsible for all experimental work.

Chapter 3: Z. Blossom Yan and the author contributed equally to the EPR experiments.

The synthesis and preparation of the materials was conducted by the author

Chapter 4: The author was responsible for all experimental work.

[1] Publications 3 and 4 were completed during the first year and a half of my Ph.D. and are focused on projects unrelated to the goals of my thesis and therefore were not included.

Table of Contents

Table of Figures

Table of Tables

List of Abbreviations and Symbols

AMS-152	Aminopropylmethylsiloxane (4-5%)-dimethylsiloxane copolymer
AMS-233	Aminoethylaminopropylmethylsiloxane (2-4%)-dimethylsiloxane copolymer
BCF	Tris(pentaflurophenyl)borane
Bis-H	Bis(trimethylsiloxy)methylsilane
BODIPY	4-4-difluoro-4-bora-3a,4a-diaza-s-indacene
CDC	Centers for Disease Control and Prevention
CPO	Copper phthalocyanine oligomers
d	Thickness
DAI	Device acquired infection
DCM	Dichloromethane
DE	Dielectric elastomers
DMS-H31	Hydride-terminated polydimethylsiloxane, 28 000 g mol^{-1}
DMS-HV15	α-Monovinyl-ω-monohydride-terminated polydimethylsiloxane
DMS-V22	Vinyl-terminated polydimethylsiloxane, 9400 g mol^{-1}

DMSO	Dimethylsulfoxide
DPBF	1,3-Diphenylisobenzofuran
E_b	Dielectric breakdown strength
ε_o	Permittivity in a vacuum
ε_r	Relative permittivity
EPR	Electron paramagnetic resonance spectroscopy
ESI-MS	Electrospray ionization mass spectroscopy
FOM	Figure of merit
G’	Storage modulus
G’’	Loss modulus
HMBC	Heteronuclear multiple bond correlation
HMS-301	Trimethylsiloxy-terminated dimethylsiloxane-hydromethyl-siloxane copolymer (25-35% hydromethylsiloxane)
HSQC	Heteronuclear single quantum coherence
IPA	Isopropanol
M_n	Number average molecular weight
NMR	Nuclear magnetic resonance spectroscopy
$^1O_2$	Singlet oxygen
4-oxo-TEMP	2,2,6,6-Tetramethyl-4-piperidone
4-oxo-TEMPO	4-Oxo-2,2,6,6-tetramethyl-1-pirperidinyl
PR	Piers-Rubinsztajn
PDMS	Polydimethylsiloxane

PMMA	Poly(methyl methacrylate)
PS	Photosensitizer
ROS	Reactive oxygen species
SOSG	Singlet oxygen sensor green
SWNT	Single-walled carbon nanotubes
tanδ	Dielectric loss or loss tangent
TEOS	Tetraethyl orthosilicate
TFA	Trifluoracetic acid
T_g	Glass transition temperature
TMB	3',3',5',5'-Tetramethylbenzidine
TPMP	5,10,15,20-(Tetra-3-methoxyphenyl)porphyrin
UV	Ultraviolet
V	Voltage
Y	Young's modulus
Zn-TPMP	Zinc 5,10,15,20-(Tetra-3-methoxyphenyl)porphyrin

Chapter 1 Introduction

1.1 Porphyrins

Porphyrins are a unique class of aromatic macrocyclic chromophores, comprised of four pyrrole rings connected by methene bridges.[1] While they can exist in their free base form, porphyrins are prolific ligands and commonly bind various metals (Figure 1.1).[2] The delocalized aromatic network gives rise to their unique optoelectronic properties, including intense optical absorbances and luminescence and high intersystem crossing efficiencies.

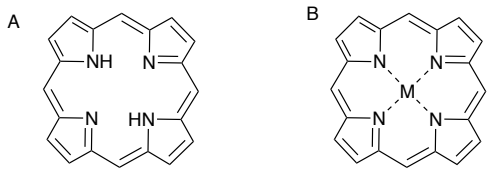

Figure 1.1: A) General structure of a free base porphyrin. B) General structure of a metallated porphyrin.

1.1.1 Aromaticity of porphyrins

Porphyrins contain an extensively delocalized network of 22π electrons; this conjugated network is responsible for many of the unique optoelectronic and physiochemical properties observed in porphyrins. Aromaticity in organic chemistry is traditionally described by Hückel's 4n+2 rule and porphyrins abide by this rule.[3,4] However, it was determined by Franz Sondheimer and Emanuel Vogel that the aromatic character of porphyrins is better explained using an 18π conjugation pathway based on [18]annulene (Figure 1.).[5,6] NMR, X-ray crystallography, heat of formation experiments,

and porphyrins' reactivity all indicate they are aromatic molecules and support the theoretical predictions based on Hückels rule.[7]

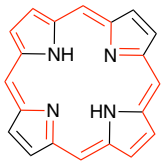

Figure 1.2: Illustration of the 18 π conjugation pathway in red used to explain aromaticity in porphyrins.

While some have disputed the [18]annulene model and proposed alternative models for porphyrin aromaticity, the 18π conjugation pathway remains the standard for describing porphyrin aromaticity.[8]

1.1.2 Optoelectronic Properties of Porphyrins

Porphyrins are excellent chromophores and absorb light in two distinct regions of the UV-visible spectrum. These regions are associated with π to π* electronic transitions and consist of an intense absorption band at 395-425 nm referred to as the B or Soret band after its discoverer, and two to four weaker bands between 480-700 nm referred to as the Q bands.[1,7] Significant information about porphyrins can be obtained by analyzing the UV-visible spectra, including whether it is a free base or metallated porphyrin,[1,7] and its substitution pattern.[9]

Exposure of the porphyrin to light results in its excitation to a singlet excited state (S_x). From this excited state, numerous pathways exist for the relaxation of the porphyrin back to the ground state S_0. Regardless of the pathway, the porphyrin first converts back to the lowest excited state, S_1. From S_1, the porphyrin can undergo radiationless decay via internal conversion to S_0, emit radiation in the form of fluorescence, which in porphyrins

can be observed from 630-700nm, or alternatively undergo intersystem crossing to the triplet state, T_1.[10,11] The latter gives rise to perhaps one of the most interesting properties of porphyrins, their ability to act as photosensitizers (PS).[12,13]

A porphyrin in the T_1 state can produce reactive oxygen species (ROS) by two methods. In a type 1 pathway, the triplet state PS transfers an electron to oxygen or a biological substrate to produce superoxide or hydroxyl radicals. In a type 2 pathway, the triplet state PS transfers energy to O_2 to produce the excited singlet oxygen $^1O_2$ (Figure 1.3).[14]

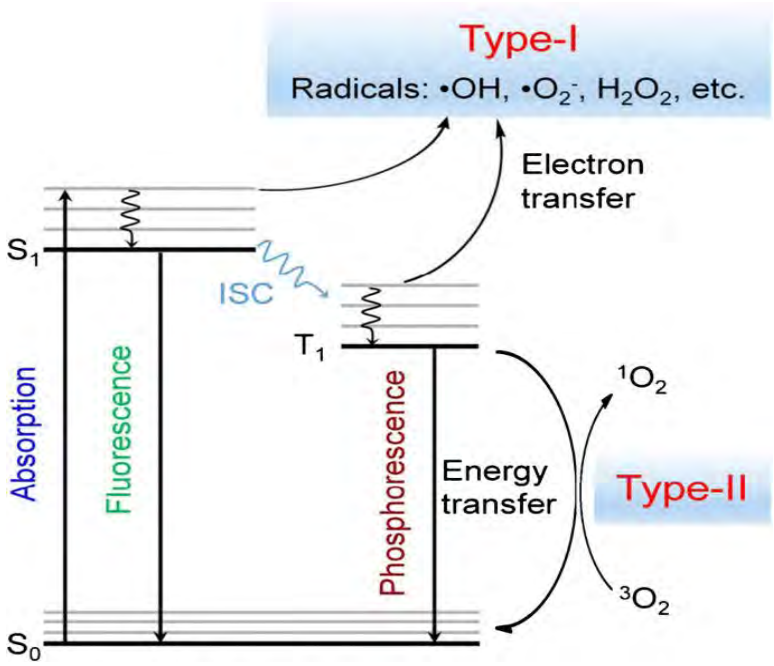

Figure 1.3: Jablonski diagram illustrating the general photosensitization process for the production of ROS. Reproduced with permission.[15] Copyright SpringerNature 2019.

In reality, these reactions are occurring simultaneously, and the predominant route is determined by a number of factors, including oxygen concentration, environment and type of photosensitizer used.[16] ROS are incredibly reactive, and the photosensitized

production of reactive oxygen species has been used extensively in photodynamic therapy as a treatment for cancer and as an antimicrobial.[17]

1.1.3 Porphyrins as Ligands

The binding of metals by porphyrins is entropically favourable and is referred to as the macrocycle effect, and porphyrins will even distort from planarity to maximize metal-binding interactions.[1,18–20] Variation of the chelated metal and periphery modification remains a principal method to control the optoelectronic and chemical properties of porphyrins. The metal centre can be used to modulate intersystem crossing efficiencies, fluorescence lifetimes and catalytic properties of porphyrins.[21–23] This has led to extensive investigations into metalloporphyrins and their properties, including those found in nature.

1.1.4 Natural Porphyrins

Porphyrins can be divided into two general categories: natural and synthetic. Porphyrins such as those in the chlorophyll, bacteriochlorophyll and heme families are widely found in nature and are essential to everyday life, leading to them being referred to as the pigments of life (Figure 1.4).[24]

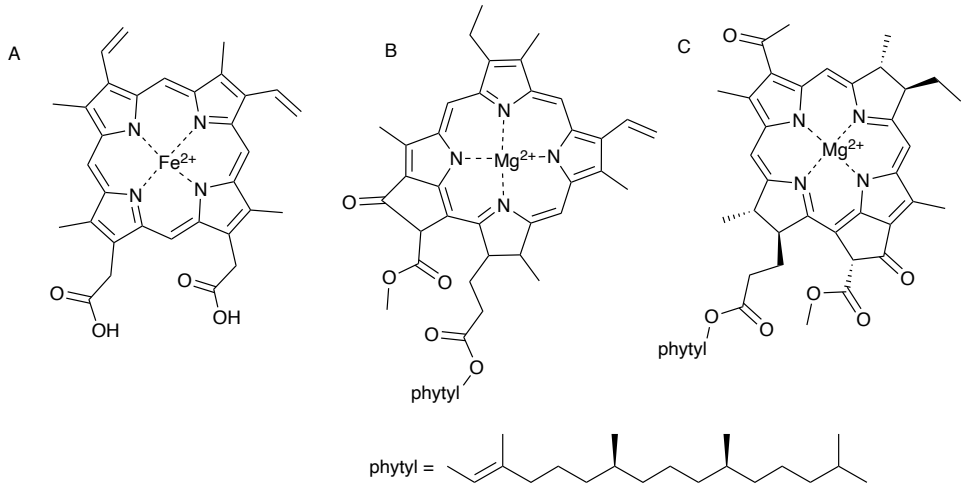

Figure 1.4: Selected structures of A) Heme a. B) Chlorophyll a. C) Bacteriochlorophyll a.

Chlorophylls and bacteriochlorophylls are photosynthetic pigments containing magnesium that act as electron transport agents in photosynthesis. Hemes are iron porphyrins found in various hemoproteins, such as hemoglobin and myoglobin, and participate in oxygen transport in the body.[25] Hemes are also key components of peroxidases, dismutases, and catalases that act as the first line of defence against ROS.[26,27]

The synthesis of naturally occurring porphyrins occurs via complex biosynthetic pathways involving multiple enzymes and cofactors. The porphyrins chlorophyll and heme can be easily isolated, albeit in very low yields, from spinach and blood, respectively.[28–30] Alternatively, these porphyrins can be produced synthetically. In 1930, Hans Fischer won the Nobel Prize for his work on the artificial synthesis of hemin,[31] while Robert Woodward received the Nobel Prize in part for his total synthesis of chlorophyll in 1965.[32] Woodward's synthesis consists of 49 steps and is still considered one of the greatest achievements in organic synthesis.[33] These initial accomplishments have led to multiple investigations into the synthesis of biologically relevant porphyrins, and numerous synthetic procedures have

been developed towards this goal. Even in light of the amazing accomplishments in organic synthesis, porphyrins, with a few exceptions, remain very challenging targets.

1.1.5 Synthesis of 5,10,15,20-tetraarylporphyrins

Tetraarylporphyrins are a class of synthetic porphyrins first reported by William Rothemund, who synthesized tetraphenylporphyrin by heating pyrrole, benzaldehyde and pyridine in a sealed tube.[34,35] The syntheses of these compounds are relatively simple in comparison to their naturally occurring cousins, e.g., chlorophyll.

More efficient strategies for 5,10,15,20-tetraarylporphyrins have since been employed by many famous chemists. Famous porphyrin chemists, Alan Alder and Frederick Longo showed that tetraarylporphyrins are accessible by refluxing pyrrole and benzaldehyde in propionic acid at atmospheric pressure.[36–38] The harsh conditions of this reaction are disadvantageous in that they preclude the use of aldehydes that contain sensitive functional groups and, furthermore, the process suffers from a challenging purification.[39,40] Later, Lindsey showed that symmetrical 5,10,15,20-tetra-arylporphyrins are readily accessible through a one-pot two-step synthesis.[39] In this route, commonly referred to as the Lindsey synthesis, pyrrole and benzaldehyde are mixed in an organic solvent with a Lewis or Brønsted acid catalyst and react via condensation of the pyrrole and aldehyde to produce a porphyrinogen. Following ring formation, either DDQ or *p*-chloroanil is added to irreversibly oxidize the porphyrinogen to the corresponding porphyrin (Figure 1.5).[39]

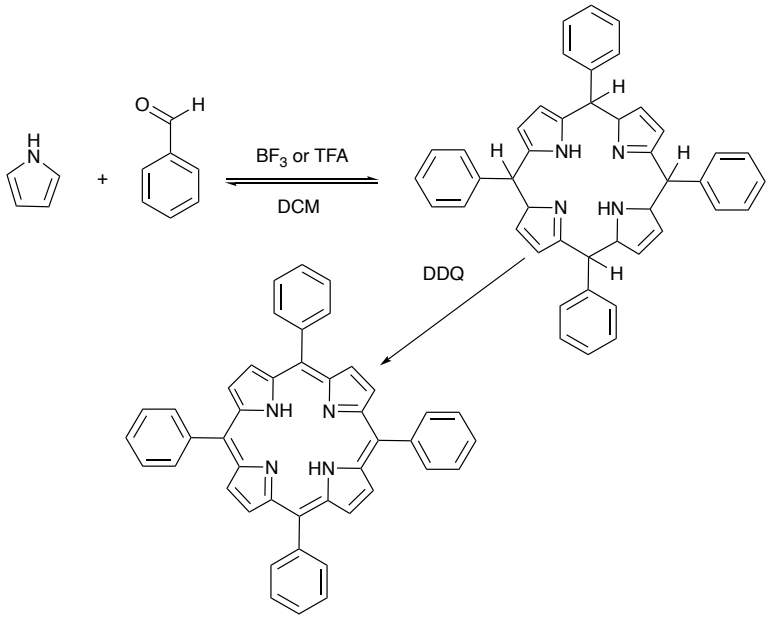

Figure 1.5: Lindsey synthesis of tetraphenylporphyrin.

This reaction is incredibly versatile and tolerant to numerous substituted benzaldehydes, and over 30 substituted porphyrins were made by Lindsey. Theoretically, the number of different porphyrins available through this route is limited only by the number of benzaldehyde derivatives available and their tolerance to the reaction conditions. However, the final yield of the reaction is highly dependent on the aldehyde, acid catalyst, water scavenger, and oxidant and, to achieve the maximum yield for a specific porphyrin, all these parameters must be optimized.[39]

The periphery of the porphyrin can be further modified by utilizing benzaldehyde derivatives that contain reactive or synthetically useful functional groups. This approach has dramatically expanded the library of 5,10,15,20-tetraarylporphyrins reported in the literature; a comprehensive review of the strategies available for porphyrin modification is available.[41] Despite some initial skepticism by the porphyrin community,

tetraarylporphyrins have proven to be valuable materials in multiple fields because of their synthetic accessibility and versatility for various applications.[42]

1.2 Applications of Porphyrins

The development of more accessible porphyrins has contributed to a dramatic expansion in their use, and they are now being investigated in a variety of applications. Among the most investigated applications are photodynamic therapy,[43] catalysts,[44] dye-sensitized solar cells,[45,46] metal and covalent organic frameworks.[47] These applications rely on the unique photochemical and physiochemical properties of porphyrins noted above. Despite the current interdisciplinary nature of porphyrin research, there has been little investigation into porphyrins and their application in polysiloxane chemistry.

1.3 Polysiloxanes

Polysiloxanes, commonly referred to as silicones, are an inorganic class of polymers composed of repeating R_2SiO units. First reported by Frederick S. Kipping in the 1900s, he considered silicones to be of little practical relevance and deserving only of academic investigation.[48,49] However, individual pioneering work by James Franklin Hyde, Richard Mueller and Eugene Rochow enabled mass production of silicone precursors (chloromethylsilanes) by the Mueller-Rochow Process (the Direct Process) that brought silicone polymers into the industrial realm.[50–52] In 2013, the silicone industry was an $11 billion industry, and ~2.12 million tonnes of silicones are produced each year.[53,54] Now widely available and mass-produced, silicones have attracted attention from academic and industrial communities looking to utilize their unique properties.

1.3.1 Synthesis of Polydimethylsiloxanes

The industrial-scale synthesis of PDMS relies on the precursor dichlorodimethylsilane produced using the Direct Process. In this process, elemental silicon is heated to ~ 350°C with chloromethane and a copper catalyst to produce dichlorodimethylsilane.[55,56] In the presence of water, dichlorodimethylsilane hydrolyzes to produce silanols that condense, producing linear and cyclic oligomers. These cyclic oligomers are utilized in a base or acid-catalyzed ring-opening condensation polymerization to produce longer chain polydimethylsiloxanes; the addition of trimethylsilyl chloride caps the polymer (Figure 1.6). [57]

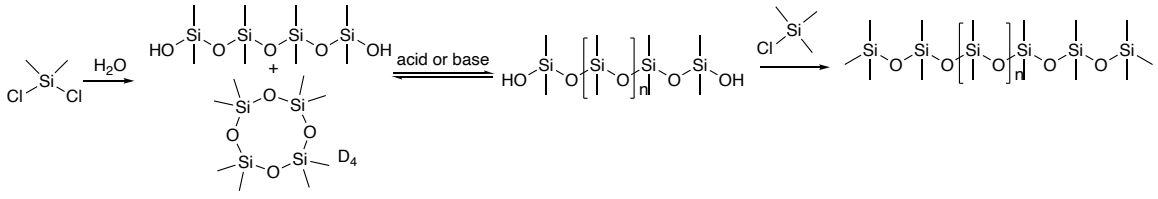

Figure 1.6: Synthesis of polydimethylsiloxane from dichlorodimethylsilane.

1.3.2 Properties of Polysiloxanes and their Benefits to Porphyrin Chemistry

Silicones possess properties unmatched by their organic counterparts, including low glass transition temperatures (T_g), high thermal and oxidative stabilities. The polymers are highly gas-permeable, hydrophobic, and optically transparent.[57] These properties are directly related to the properties of the polymer backbone, including the Si-O bond strength, the Si-O-Si bond angle, low resistance to torsional stress, and the nature of the alkyl groups bound to silicon, usually but not always methyl. The low T_g, hydrophobicity and gas permeability of silicones stem from the large 145° Si-O-Si bond angle; the large bond angle

makes the siloxane chain flexible, while the low torsional force constant makes segmental motion easy. This is manifested in the physical properties of the polymers leading to low T_gs, ranging from -127 °C to -70 °C, depending on the alkyl/aryl groups bound to silicon.[58] The ability of silicone chains to rapidly reorient creates free volume internally, which results in high gas permeability, and water-repellent interfaces at which hydrophobic organic groups are presented.[3957,59] To an extent, these properties can be modified by changing the sidechain groups on the backbone. Adding bulky substituents capable of reducing the segmental motion, such as phenyl groups, can lead to minor increases in the T_g and reductions in the gas permeability.[59]

The thermal and oxidative stability of silicones is primarily a result of the Si-O bond strength.[60,61] The Si-O bond has a bond energy of 452 kJ mol^{-1}; comparatively, the C-C bond strength is ~347 kJ mol^{-1}. This makes direct thermal cleavage of the Si-O unlikely even at exceptionally high temperatures and provides silicones with high thermal stability.[61] In fact, the thermal degradation of silicones does not normally occur via direct cleavage of the Si-O bond. Instead, between 753-900 K, thermal degradation occurs via an intramolecular cyclic four-centred transition state that facilitates siloxane bond rearrangement/metathesis and produces cyclic monomers (Figure 1.7A).[61–63] The formation of the transition state is possible because of the segmental motion of the chain.[60,61] Higher temperatures > 900 K result in degradation via a radical-mediated mechanism (Figure 1.7B).[64]

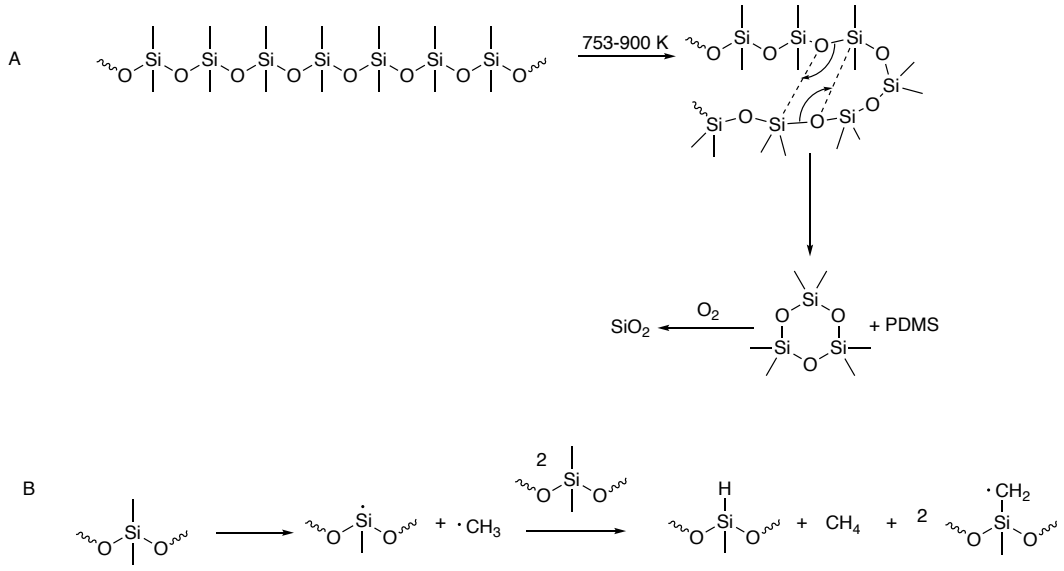

Figure 1.7: A) Degradation by cyclic formation. B) Proposed radical mechanism for polysiloxane degradation.

Similar to hydrophobicity, T_g and gas permeability, modification of the alkyl/aryl groups on silicon can reduce thermal stability by creating alternative pathways for thermal degradation. This allows the properties of the silicone to be tailored to the intended application.[61]

Polysiloxanes normally possess no chromophores and exhibit excellent optical transparency because of their high transmittance of visible and UV light; provided they are homogenous and contain no structural defects, they do not scatter light.[65] This makes them well suited for application in conjunction with porphyrin chemistry, as the silicone polymers would be unlikely to interfere with the optoelectronic properties of porphyrins. Porphyrins very easily self-associate/aggregate, which is detrimental to the optical properties noted above. It is proposed, due to their low T_g, that the modification of porphyrins with polysiloxanes or even simple siloxanes could improve solubility in non-

polar solvents including silicones and reduce aggregation.[66] The high oxidative and thermal stability of silicones would be a benefit in porphyrin facilitated ROS-producing materials, as they could be utilized without fear of degrading the polymer matrix. Furthermore, their high gas permeability would be beneficial in these applications, as they would allow for high concentrations of dissolved oxygen and, theoretically, more ROS production. Conversely, the optoelectronic properties of porphyrins such as the electric susceptibility could be utilized in applications where polysiloxanes are considered ideal materials such as dielectric elastomers.[67]

1.3.3 Porphyrin-Polysiloxane Materials

Despite their potential, polysiloxanes have barely been used in the field of porphyrin materials chemistry. In the research that has been reported, porphyrins are physically doped into polysiloxane elastomers using a swell-encapsulation technique. In use in oxygen sensors and reactive oxygen species-generating antimicrobial coatings, the silicone is simply utilized as a carrier of the porphyrin. While there are numerous examples of polysiloxanes being used in these applications, they often suffer from difficulties in introducing the porphyrin into the silicone, and aggregation of the porphyrins in the silicone.

Porphyrin-containing disiloxanes have been reported but failed to exhibit any of the beneficial properties associated with silicones and, therefore, little interest;[68,69] presumably, these small molecules cannot really behave as do real polymers. Unfortunately, the modification of porphyrins with polysiloxanes is more challenging, and very few strategies for their synthesis have been described. Previously, 5-(4-hydroxyphenyl)-10,15,20-

triphenylporphyrin was modified with polysiloxanes. In this case, the porphyrin served as a nucleophile reacting with the chlorobenzyl groups on the polysiloxane to create the modified porphyrin. Using this methodology, only ~8% of the chlorobenzyl groups present on the polymer reacted to form the new porphyrin derivative.[66]

Ji et al. utilized a more precise synthesis and modified 5,10,15,20-tetrakis(4-carboxyphenyl)porphyrin with mono(hydroxyalkyl) PDMS using *N,N′*-diisopropylcarbodiimide as a coupling agent to produce a class of porphyrin polysiloxane surfactants. These materials were isolated as oils and proved to be excellent surfactants for the dispersion of single-walled carbon nanotubes (SWNTs) in petroleum ether. The porphyrin-polysiloxane surfactants were also naturally compatible with silicone elastomer formulations and were able to be dispersed into elastomers with SWNT to create composite materials.[70] This work highlights the potential for polysiloxane-modified porphyrins in materials science and serves as an excellent example of the benefits of modifying porphyrins with polysiloxanes.

1.3.4 Current Limitations and Potential of Porphyrin-Polysiloxane Hybrid Materials

Current porphyrin-polysiloxane materials suffer from one significant shortcoming; the limited techniques available for the synthesis of porphyrin-polysiloxanes. This has prevented the in-depth investigation of hybrid materials and limited the number of potential applications for these materials. However, the work by Ji et al. suggests that there exists a potentially complementary relationship between the optoelectronic properties of porphyrins and the physicochemical properties of polysiloxanes, their adaption of a liquid form following modification while retaining some porphyrin properties. Therefore, to fully

realize this potentially mutualistic relationship, additional synthetic strategies that allow for their incorporation into polysiloxanes while leaving the optoelectronic properties of porphyrins untouched need to be developed. This will allow for additional applications to become apparent, as well as further the understanding of the potential properties and benefits that can be imparted to porphyrins upon their modification with polysiloxanes.

1.4 Incorporating Aromatic Groups into Polysiloxanes

1.4.1 The Piers-Rubinsztajn Reaction

Porphyrins represent a challenging class of aromatic molecules to incorporate into polysiloxanes; the two materials are not naturally compatible with one another. Reliable and reproducible incorporation will be dependent on the functionalization of the porphyrin with siloxanes or polysiloxanes such that they will dissolve in silicones without the assistance of solvents. One potential strategy for the incorporation of porphyrins is the Piers-Rubinsztajn (PR) reaction.[71]

The PR reaction was first described by Warren Piers as something to worry about, and recognized by Slawomir Rubinsztajn as a new route to siloxane bonds. It utilizes the strong Lewis acid tris(pentaflurophenyl)borane $B(C_6F_5)_3$ to catalyze the formation of a new silicon-oxygen bond and an alkane byproduct from the reaction of a hydrosilane and alkoxysilane (Figure 1.8A).[72–77] It was later realized that the alkoxysilane could be substituted for other oxygen nucleophiles such as silanols, aryl ethers and phenols (Figure 1.8B).[74] The mechanism of the reaction is generally agreed to proceed as follows: the hydrosilane first coordinates to $B(C_6F_5)_3$; followed by nucleophilic attack of the silicon

atom by the oxygen nucleophile; and, the borohydride complex then cleaves the carbon-oxygen bond to form the new silicon-oxygen bond with a simple alkane as a byproduct.[78,79]

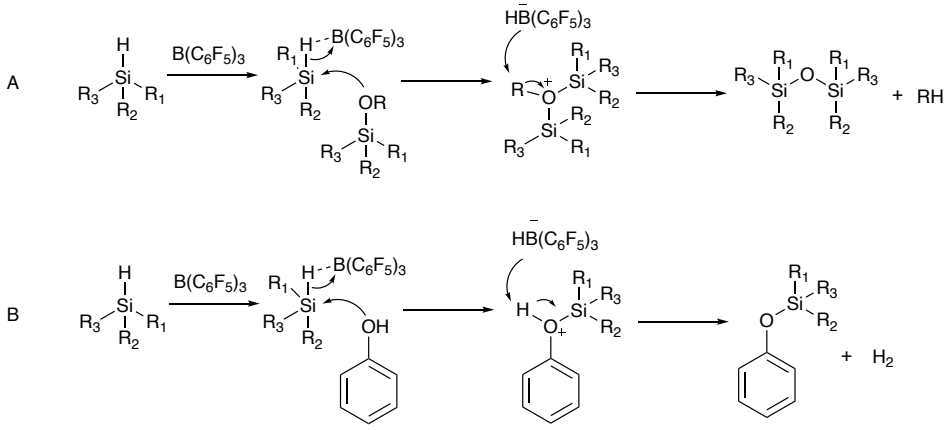

Figure 1.8: A) Mechanism of the PR reaction of an alkoxysilane with a hydrosilane. B) Mechanism of the PR reaction of a hydrosilane with phenol.

1.4.2 Introduction of Multifunctional and Complex Aromatic Groups via the Piers-Rubinsztajn Reaction

Initially, the PR reaction was used by silicone chemists to create precise silicone structures, including dendrimers, foams and polymers from alkoxysilanes and hydrosilanes, and this still remains an active area of research.[80] However, the realization that the alkoxysilane could be replaced by aryl ethers and phenols created a new strategy for the incorporation of aromatic groups that has since been widely utilized and could, with the correct porphyrin, be utilized to create a new family of porphyrin-polysiloxane materials.

The PR reaction provides silicone chemists with a significant and previously unachievable degree of control over the aromatic content in polysiloxanes. Rubinsztajn and Cella were the first to use the reaction for aromatic groups and created linear polysiloxane polymers containing bisphenol and silphenylene units.[74] Bender and coworkers utilized the PR reaction to synthesize phenoxylated polysiloxanes by reacting the phenols 3-

pentadecylphenol, 4-*tert*-octylphenol, and phenol with polydimethylsiloxane-co-methylhydrosiloxane and were able to control the functional group density of the material, illustrating the potential of the PR reaction to synthesize precise silicone polymers.[81] Later, Schneider et al. utilized the PR reaction to synthesize $C_x(AB)_yC_x$ triblock silicone copolymers from *p*-dimethoxybenzene and hydride terminated PDMS, reliably producing copolymers with precise control of the aromatic group placement and molecular weight.[82] Using a similar approach, they were able to synthesize phenyl silicones via the PR reaction and crosslink them with trimethoxybenzene to produce foams and elastomers with tunable properties.[83]

1.4.3 Incorporation of Structurally Complex Aromatic Molecules via the Piers-Rubinsztajn Reaction

The aromatic groups susceptible to modification by the PR reaction are not limited to the simple phenols and aryl ethers. More complex aromatic systems, including naturally occurring aromatic groups and aromatic groups that have unique and useful physiochemical properties, have been successfully incorporated using the PR reaction.

There are numerous naturally occurring aromatic molecules that possess the necessary functional groups to partake in the PR reaction. The first example of utilizing the PR reaction to incorporate a natural molecule was done by the Brook group, who utilized the PR reaction to incorporate lignin, a complex naturally occurring aromatic polymer containing an abundance of phenols and aryl ethers.[84,85] Surprisingly, despite the complex and random structure of lignin, significant control over the material properties could be achieved, and the final materials contained high quantities of lignin.[85,86] Unexpectedly, and despite the high quantities of organic matter contained, the materials had high flame

resistance. This highlighted the potential of the PR reaction to incorporate complex aromatic molecules into silicone materials and the potential beneficial properties that could result.[87,88]

In an extension of this work, Laengert et al. were able to selectively react the phenol group present on the natural compound eugenol while leaving both the vinyl and aryl ether group untouched.[89] Subsequent hydrosilylation, or a second PR reaction could then be used to target the vinyl or aryl ether group, respectively. Depending on the order of the reactions, silicone elastomers or foams could be made to give precise networks with tunable properties.[89] In a similar example, eugenol was functionalized with benzocyclobutene via the PR reaction to create silicone polymers that could be crosslinked thermally.[90]

Normally, triarylamines are relatively insoluble and difficult-to-process materials. Pioneering work by the Bender and Brook groups showed that triarylamines, a class of *p*-type semiconducting materials useful in organic electronic devices, could be easily modified with small siloxane units using the PR reaction to create room-temperature liquid triarylamines that retained their semiconducting capabilities.[91,92] Alternatively, the same reaction could be used to install triarylamines pendent on the backbone of polysiloxanes or, depending on the number of reactive functional groups on the triarylamine, crosslinked into elastomers.[93–95] The tolerance of the PR reaction towards triarylamines has been extensively investigated, and even complex triarylamines can be easily incorporated into polysiloxanes.[96] The ability of the PR reaction to modify and impart polysiloxane properties to triarylamines without impeding their semiconductor capabilities suggests that the PR reaction could be a viable method for accomplishing the same goal with porphyrins.

1.5 Alternate Strategies for Incorporating Aromatic Groups

The utility of the Piers-Rubinsztajn reaction is limited by the substrate requirements, the catalyst functional group tolerance, and the selectivity of the reaction.[97] The PR reaction is only applicable for aromatic groups that contain phenols or aryl ethers. However the PR reaction is not selective for phenols or aryl ethers; other functional groups including carbonyls,[73] alcohols,[98] ethers,[98] epoxides,[97] thiols, [97] and amides [99,100] will competitively react, limiting the number of substrates that can be utilized with the PR reaction. Furthermore, the presence of Lewis bases such as alkylamines are known to irreversibly deactivate the catalyst or dramatically retard the rate of reaction.[97,100] Thus, the reactivity profile of many functional groups to PR conditions limits the number of porphyrins capable of being modified via the PR reactions. For example, natural porphyrins such as heme and chlorophyll both contain carbonyls that would prevent their modification using the PR reaction.

Fortunately, alternatives do exist for incorporating aromatic groups into polysiloxanes. These include but are not limited to azide-alkyne [101,102] and thiol-ene click reactions, [103] ester or amide formation[104] and dynamic imine formation.[105] These provide potential alternative approaches for functionalization and subsequent incorporation of porphyrins into polysiloxanes. They have been successfully used to incorporate a wide variety of aromatic groups into polysiloxane polymers and elastomers.[106] However, like the PR reaction, each reaction requires the aromatic group to have a suitable synthetic handle or, in some cases, must be modified to contain a suitable handle.

The presence of carboxylic acids on natural porphyrins such as heme (Figure 1.1) opens the door to an intriguing method for their incorporation into polysiloxanes; ionic crosslinking. Polysiloxanes containing ionic crosslinks formed via the reaction of aminosilicones and carboxylic acids have been previously reported but have yet to be applied to aromatic groups.[107–111] This method would eliminate the need for extensive functional group modification potentially providing the simplest route for porphyrin incorporation.

1.6 Thesis Objectives

The use of porphyrins in polysiloxane polymers and materials represents an untapped area of research worthy of investigation. Currently, the literature on porphyrin-silicones is limited, and there is little understanding of the potential benefits that could be achieved from creating polysiloxane porphyrin hybrid materials that benefit from the interesting properties of each constituent. This thesis aims to address some the current limitations in this field and is composed of two principal research themes; developing strategies for the reliable incorporation of porphyrins into silicone materials, and examining potential applications of porphyrin-polysiloxane materials.

The incorporation of porphyrins into polysiloxanes will be examined utilizing two strategies. First, modification of 5,10,15,20-(tetra-3-methoxyphenyl)porphyrin, a porphyrin perfectly suitable for modification via the Piers-Rubinsztajn reaction, will allow the creation of derivatives that can be physically or covalently incorporated into polysiloxanes. Second, ionic crosslinking with aminosilicones will be used to bind hemin. Three potential applications for porphyrin-silicone materials have been identified that make

use of their unique properties: dielectric elastomers; antimicrobial coatings; and, catalytic membranes.

1.7 References

1 L. R. Milgrom and U. L. D. of C. L. R. Milgrom, *The Colours of Life: An Introduction to the Chemistry of Porphyrins and Related Compounds*, Oxford University Press, 1997.

2 M. Kielmann and M. O. Senge, *Angew. Chem. Int. Ed.*, 2019, **58**, 418–441.

3 F. A. Carey and R. J. Sundberg, in *Advanced Organic Chemistry: Part A: Structure and Mechanisms*, eds. F. A. Carey and R. J. Sundberg, Springer US, Boston, MA, 1990, pp. 499–538.

4 A. D. Zdetsis, *J. Phys. Chem. C*, 2018, **122**, 17526–17536.

5 Franz. Sondheimer, Reuven. Wolovsky and Yaacov. Amiel, *J. Am. Chem. Soc.*, 1962, **84**, 274–284.

6 E. Vogel, *Pure Appl. Chem.*, 1993, **65**, 143–152.

7 *Porphyrins and metalloporphyrins :a new edition based on the original volume by J.E. Falk /*, Amsterdam , 1975.

8 T. D. Lash, *J. Porphyr. Phthalocyanines*, 2011, **15**, 1093–1115.

9 M. Gouterman, *J. Chem. Phys.*, 1959, **30**, 1139–1161.

10 M. Imran, M. Ramzan, A. K. Qureshi, M. A. Khan and M. Tariq, *Biosensors*, 2018, **8**, 95.

11 D. C. Harris, *Exploring Chemical Analysis*, W. H. Freeman, 2008.

12 L. G. Arnaut, in *Advances in Inorganic Chemistry*, eds. R. van Eldik and G. Stochel, Academic Press, 2011, vol. 63, pp. 187–233.

13 R. Bonnett and M. Berenbaum, in *Ciba Foundation Symposium 146 - Photosensitizing Compounds: Their Chemistry, Biology and Clinical Use*, John Wiley & Sons, Ltd, pp. 40–59.

14 M. S. Baptista, J. Cadet, P. D. Mascio, A. A. Ghogare, A. Greer, M. R. Hamblin, C. Lorente, S. C. Nunez, M. S. Ribeiro, A. H. Thomas, M. Vignoni and T. M. Yoshimura, *Photochem. Photobiol.*, 2017, **93**, 912–919.

15 Y. Wang, Z. Dong, H. Hu, Q. Yang, X. Hou and P. Wu, *Anal. Bioanal. Chem.*, 2019, **411**, 4415–4423.

16 L. Huang, Y. Xuan, Y. Koide, T. Zhiyentayev, M. Tanaka and M. R. Hamblin, *Lasers Surg. Med.*, 2012, **44**, 490–499.

17 P. R. Ogilby, *Chem. Soc. Rev.*, 2010, **39**, 3181–3209.

18 J. A. Shelnutt, X.-Z. Song, J.-G. Ma, S.-L. Jia, W. Jentzen, C. J. Medforth and C. J. Medforth, *Chem. Soc. Rev.*, 1998, **27**, 31–42.

19 H. Ryeng and A. Ghosh, *J. Am. Chem. Soc.*, 2002, **124**, 8099–8103.

20 M. Weller, T. Overton, J. Rourke and F. Armstrong, *Inorganic Chemistry*, OUP Oxford, 2014.

21 M.-H. Ha-Thi, N. Shafizadeh, L. Poisson and B. Soep, *J. Phys. Chem. A*, 2013, **117**, 8111–8118.

22 B. C. D. Simone, G. Mazzone, N. Russo, E. Sicilia and M. Toscano, *Molecules*, 2017, **22**, 1093.

23 M. Pineiro, A. L. Carvalho, M. M. Pereira, A. M. d'A. R. Gonsalves, L. G. Arnaut and S. J. Formosinho, *Chem. – Eur. J.*, 1998, **4**, 2299–2307.

24 A. R. Battersby, *Nat. Prod. Rep.*, 2000, **17**, 507–526.

25 M. A. Sowole, S. Vuong and L. Konermann, *Anal. Chem.*, 2015, **87**, 9538–9545.

26 X. Huang and J. T. Groves, *Chem. Rev.*, 2018, **118**, 2491–2553.

27 T. L. Poulos, *Chem. Rev.*, 2014, **114**, 3919–3962.

28 J. A. Ciaccio and K. Hassan, *J. Chem. Educ.*, 2020, **97**, 2362–2365.

29 H. T. Quach, R. L. Steeper and G. W. Griffin, *J. Chem. Educ.*, 2004, **81**, 385-387.

30 S. F. Russo and R. B. Sorstokke, *J. Chem. Educ.*, 1973, **50**, 347-350.

31 Hans Fischer, in *Nobel Lecture*, 1930.

32 R. B. Woodward, W. A. Ayer, J. M. Beaton, F. Bickelhaupt, R. Bonnett, P. Buchschacher, G. L. Closs, H. Dutler, J. Hannah, F. P. Hauck, S. Itô, A. Langemann, E. Le Goff, W. Leimgruber, W. Lwowski, J. Sauer, Z. Valenta and H. Volz, *J. Am. Chem. Soc.*, 1960, **82**, 3800–3802.

33 Y. Liu, S. Zhang and J. S. Lindsey, *Nat. Prod. Rep.*, 2018, **35**, 879–901.

34 P. Rothemund, *J. Am. Chem. Soc.*, 1935, **57**, 2010–2011.

35 P. Rothemund, *J. Am. Chem. Soc.*, 1936, **58**, 625–627.

36 A. D. Adler, F. R. Longo, J. D. Finarelli, J. Goldmacher, J. Assour and L. Korsakoff, *J. Org. Chem.*, 1967, **32**, 476–476.

37 A. D. Adler, L. Sklar, F. R. Longo, J. D. Finarelli and M. G. Finarelli, *J. Heterocycl. Chem.*, 1968, **5**, 669–678.

38 A. D. Adler, F. R. Longo and William. Shergalis, *J. Am. Chem. Soc.*, 1964, **86**, 3145–3149.

39 J. S. Lindsey, I. C. Schreiman, H. C. Hsu, P. C. Kearney and A. M. Marguerettaz, *J. Org. Chem.*, 1987, **52**, 827–836.

40 J. S. Lindsey, in *Metalloporphyrins Catalyzed Oxidations*, eds. F. Montanari and L. Casella, Springer Netherlands, Dordrecht, 1994, pp. 49–86.

41 S. Hiroto, Y. Miyake and H. Shinokubo, *Chem. Rev.*, 2017, **117**, 2910–3043.

42 K. M. Smith, *New J. Chem.*, 2016, **40**, 5644–5649.

43 Y. Lin, T. Zhou, R. Bai and Y. Xie, *J. Enzyme Inhib. Med. Chem.*, 2020, **35**, 1080–1099.

44 J. C. Barona-Castaño, C. C. Carmona-Vargas, T. J. Brocksom and K. T. De Oliveira, *Molecules*, 2016, **21**, 310.

45 M. Urbani, M. Grätzel, M. K. Nazeeruddin and T. Torres, *Chem. Rev.*, 2014, **114**, 12330–12396.

46 Ö. Birel, S. Nadeem and H. Duman, *J. Fluoresc.*, 2017, **27**, 1075–1085.

47 X. Zhang, M. C. Wasson, M. Shayan, E. K. Berdichevsky, J. Ricardo-Noordberg, Z. Singh, E. K. Papazyan, A. J. Castro, P. Marino, Z. Ajoyan, Z. Chen, T. Islamoglu, A. J. Howarth, Y. Liu, M. B. Majewski, M. J. Katz, J. E. Mondloch and O. K. Farha, *Coord. Chem. Rev.*, 2021, **429**, 213615.

48 N. R. Thomas, *Silicon*, 2010, **2**, 187–193.

49 F. S. Kipping and L. L. Lloyd, *J. Chem. Soc. Trans.*, 1901, **79**, 449–459.

50 J. F. Hyde and R. C. DeLong, *J. Am. Chem. Soc.*, 1941, **63**, 1194–1196.

51 D. Seyferth, *Organometallics*, 2001, **20**, 4978–4992.

52 E. G. Rochow, *J. Am. Chem. Soc.*, 1945, **67**, 963–965.

53 Global Silicones Council, 2016.

54 L. Xu, S. Xu, Q. Zhang, Q. Xu, S. Zhang and Y. Cai, *Environ. Sci. Technol.*, 2018, **52**, 9835–9844.

55 Y. Zhang, J. Li, H. Liu, Y. Ji, Z. Zhong and F. Su, *ChemCatChem*, 2019, **11**, 2757–2779.

56 W. Kalchauer and B. Pachaly, in *Handbook of Heterogeneous Catalysis*, American Cancer Society, 2008, pp. 2635–2647.

57 M. A. Brook, *Silicon in Organic, Organometallic, and Polymer Chemistry*, Wiley, 1999, pp.256-308.

58 P. R. Dvornic, in *Silicon-Containing Polymers: The Science and Technology of Their Synthesis and Applications*, eds. R. G. Jones, W. Ando and J. Chojnowski, Springer Netherlands, Dordrecht, 2000, pp. 185–212.

59 C.-L. Lee, H. L. Chapman, M. E. Cifuentes, K. M. Lee, L. D. Merrill, K. L. Ulman and K. Venkataraman, *J. Membr. Sci.*, 1988, **38**, 55–70.

60 E. Ogliani, L. Yu, P. Mazurek and A. L. Skov, *Polym. Degrad. Stab.*, 2018, **157**, 175–180.

61 S. Hamdani, C. Longuet, D. Perrin, J.-M. Lopez-cuesta and F. Ganachaud, *Polym. Degrad. Stab.*, 2009, **94**, 465–495.

62 K. Chenoweth, S. Cheung, A. C. T. van Duin, W. A. Goddard and E. M. Kober, *J. Am. Chem. Soc.*, 2005, **127**, 7192–7202.

63 T. H. Thomas and T. C. Kendrick, *J. Polym. Sci. Part -2 Polym. Phys.*, 1969, **7**, 537–549.

64 G. Camino, S. M. Lomakin and M. Lageard, *Polymer*, 2002, **43**, 2011–2015.

65 K. Su, J. Jon V. DeGroot, A. W. Norris and P. Y. Lo, in *ICO20: Materials and Nanostructures*, International Society for Optics and Photonics, 2006, vol. 6029, p. 60291C.

66 E. Tarabukina, E. Fagadar-Cosma, C. Enache, N. Zakharova and M. Birdeanu, *J. Macromol. Sci. Part B*, 2013, **52**, 1092–1106.

67 F. B. Madsen, A. E. Daugaard, S. Hvilsted and A. L. Skov, *Macromol. Rapid Commun.*, 2016, **37**, 378–413.

68 J. Almeida, M. E. Fortună, L. Pricop, A. Lobiuc, A. Leite, A. M. N. Silva, R. P. Monteiro, M. Rangel, V. Harabagiu and A. M. G. Silva, *J. Porphyr. Phthalocyanines*, 2019, **23**, 1001–1012.

69 X.-H. Dai, W.-H. Yang, W.-L. Yan, J.-M. Hu, Y.-R. Dai, J.-M. Pan and Y.-S. Yan, *Colloids Surf. Physicochem. Eng. Asp.*, 2017, **520**, 222–230.

70 Y. Ji, Y. Y. Huang, A. R. Tajbakhsh and E. M. Terentjev, *Langmuir*, 2009, **25**, 12325–12331.

71 M. A. Brook, J. B. Grande and F. Ganachaud, in *Silicon Polymers*, ed. A. M. Muzafarov, Springer, Berlin, Heidelberg, 2011, pp. 161–183.

72 J. M. Blackwell, E. R. Sonmor, T. Scoccitti and W. E. Piers, *Org. Lett.*, 2000, **2**, 3921–3923.

73 D. J. Parks and W. E. Piers, *J. Am. Chem. Soc.*, 1996, **118**, 9440–9441.

74 J. Cella and S. Rubinsztajn, *Macromolecules*, 2008, **41**, 6965–6971.

75 J. Chojnowski, S. Rubinsztajn, W. Fortuniak and J. Kurjata, *J. Inorg. Organomet. Polym. Mater.*, 2007, **17**, 173–187.

76 J. Chojnowski, W. Fortuniak, J. Kurjata, S. Rubinsztajn and J. A. Cella, *Macromolecules*, 2006, **39**, 3802–3807.

77 J. Chojnowski, S. Rubinsztajn, W. Fortuniak and J. Kurjata, *Macromolecules*, 2008, **41**, 7352–7358.

78 J. Chojnowski, S. Rubinsztajn, J. A. Cella, W. Fortuniak, M. Cypryk, J. Kurjata and K. Kaźmierski, *Organometallics*, 2005, **24**, 6077–6084.

79 W. E. Piers, A. J. V. Marwitz and L. G. Mercier, *Inorg. Chem.*, 2011, **50**, 12252–12262.

80 M. A. Brook, *Chem. – Eur. J.*, 2018, **24**, 8458–8469.

81 A. M. Szawiola, N. de M. Souza, B. H. Lessard and T. P. Bender, *Polym. Int.*, 2017, **66**, 1324–1328.

82 A. F. Schneider, E. K. Lu, G. Lu and M. A. Brook, *J. Polym. Sci.*, 2020, **58**, 3095–3106.

83 A. F. Schneider and M. A. Brook, *Chem. – Eur. J.*, 2019, **25**, 15367–15374.

84 E. Adler, *Wood Sci. Technol.*, 1977, **11**, 169–218.

85 J. Zhang, Y. Chen, P. Sewell and M. A. Brook, *Green Chem.*, 2015, **17**, 1811–1819.

86 J. Zhang, Y. Chen and M. A. Brook, *ACS Sustain. Chem. Eng.*, 2014, **2**, 1983–1991.

87 J. Zhang, E. Fleury and M. A. Brook, *Green Chem.*, 2015, **17**, 4647–4656.

88 J. Zhang, E. Fleury, Y. Chen and M. A. Brook, *RSC Adv.*, 2015, **5**, 103907–103914.

89 S. E. Laengert, A. F. Schneider, E. Lovinger, Y. Chen and M. A. Brook, *Chem. – Asian J.*, 2017, **12**, 1208–1212.

90 X. Chen, L. Fang, X. Chen, J. Zhou, J. Wang, J. Sun and Q. Fang, *ACS Sustain. Chem. Eng.*, 2018, **6**, 13518–13523.

91 B. A. Kamino, J. B. Grande, M. A. Brook and T. P. Bender, *Org. Lett.*, 2011, **13**, 154–157.

92 B. A. Kamino, T. P. Bender and R. A. Klenkler, *J. Phys. Chem. Lett.*, 2012, **3**, 1002–1006.

93 M. J. Gretton, B. A. Kamino, M. A. Brook and T. P. Bender, *Macromolecules*, 2012, **45**, 723–728.

94 M. J. Gretton, B. A. Kamino and T. P. Bender, *Macromol. Symp.*, 2013, **324**, 82–94.

95 B. A. Kamino, A. M. Szawiola, T. Plint and T. P. Bender, *Can. J. Chem.*, 2019, 97, 378–386.

96 B. A. Kamino, B. Mills, C. Reali, M. J. Gretton, M. A. Brook and T. P. Bender, *J. Org. Chem.*, 2012, **77**, 1663–1674.

97 J. B. Grande, D. B. Thompson, F. Gonzaga and M. A. Brook, *Chem. Commun.*, 2010, **46**, 4988–4990.

98 V. Gevorgyan, M. Rubin, S. Benson, J.-X. Liu and Y. Yamamoto, *J. Org. Chem.*, 2000, **65**, 6179–6186.

99 R. C. Chadwick, V. Kardelis, P. Lim and A. Adronov, *J. Org. Chem.*, 2014, **79**, 7728–7733.

100 E. Blondiaux and T. Cantat, *Chem. Commun.*, 2014, **50**, 9349–9352.

101 A. S. Fawcett and M. A. Brook, *Macromolecules*, 2014, **47**, 1656–1663.

102 F. B. Madsen, I. Dimitrov, A. E. Daugaard, S. Hvilsted and A. L. Skov, *Polym. Chem.*, 2013, **4**, 1700–1707.

103 H. Yang, M.-X. Liu, Y.-W. Yao, P.-Y. Tao, B.-P. Lin, P. Keller, X.-Q. Zhang, Y. Sun and L.-X. Guo, *Macromolecules*, 2013, **46**, 3406–3416.

104 Z. M. Hudson, D. J. Lunn, M. A. Winnik and I. Manners, *Nat. Commun.*, 2014, **5**, 3372.

105 R. Bui and M. A. Brook, *Polymer*, 2019, **160**, 282–290.

106 Z. Ren and S. Yan, *Prog. Mater. Sci.*, 2016, **83**, 383–416.

107 S. Zheng, Y. Chen and M. A. Brook, *Polym. Chem.*, 2020, **11**, 7382–7392.

108 J. Shi, N. Zhao, D. Yan, J. Song, W. Fu and Z. Li, *J. Mater. Chem. A*, 2020, **8**, 5943–5951.

109 H. Lu and S. Feng, *J. Polym. Sci. Part Polym. Chem.*, 2017, **55**, 903–911.

110 F. B. Madsen, L. Yu and A. L. Skov, *ACS Macro Lett.*, 2016, **5**, 1196–1200.

111 A. Genest, D. Portinha, E. Pouget, K. Lamnawar, F. Ganachaud and E. Fleury, *Macromol. Rapid Commun.*, 2021, **42**, 2000372.

Chapter 2 Compatibilization of Porphyrins for use as High Permittivity Fillers in Low Voltage Actuating Silicone Dielectric Elastomers

2.1 Abstract

Polysiloxanes represent, because of their unusual properties, a material with great potential for use in dielectric elastomers (DEs), a promising class of electroactive polymers. Currently, their application as actuators is limited by the need for high driving voltages, because of the low relative permittivity possessed by polysiloxanes (~2-3). Reducing these voltages can be achieved to some degree by using high permittivity additives to improve the permittivity of the polysiloxane. However, modifying such additives so that they are compatible with, and can be dispersed within, polysiloxane elastomers remains challenging. For reliable actuation, full miscibility is key. In this work the porphyrin 5,10,15,20-(tetra-3-methoxyphenyl)porphyrin (TPMP) was investigated as a high permittivity additive. Its behaviour was compared to the analogue that was derivatized with bis(trimethylsiloxy)methylsilane groups using the Piers-Rubinsztajn reaction to improve compatibility with silicone formulations. The derivatized porphyrin was dispersed in elastomers and their dielectric and mechanical properties were evaluated. It was discovered that only low levels of incorporation (1-10%) of the siliconized TPMP – much lower than the parent TPMP – were needed to elicit improvements in the permittivity and electromechanical actuation of the elastomers; actuation strains of up to 43% could be achieved using this method.

2.2 Introduction

Dielectric elastomers (DEs), commonly referred to as "artificial muscles", are a class of electroactive polymers receiving considerable attention for their potential applications in soft robotics and clean energy applications.[1,2] They consist of two components; a thin incompressible elastomer, and two compliant electrodes that are assembled such that the elastomer is sandwiched between the compliant electrodes that are connected to an external voltage source.[3] When a voltage is applied, charge builds up on the electrodes exerting a pressure on the elastomer. The actuation of the elastomer is spontaneous, as it serves to reduce the charge density present on the electrodes while simultaneously bringing the oppositely charged electrodes into proximity to one another.[4]

Three parameters govern the electromechanical response or strain exhibited by DEs; the relative permittivity (ε_r) or susceptibility of elastomer to polarization; Young's modulus (Y); and dielectric breakdown strength (E_b), which is the maximum voltage that can be applied to the elastomer before it short circuits. The actuation can be described by equation 1,

$$s = \frac{\varepsilon_o \varepsilon_r}{Y}\left(\frac{V}{d}\right)^2 \quad (1)$$

and the ideal elastomer is one that exhibits a high relative permittivity and dielectric breakdown strength while simultaneously having a low Young's modulus.[1,5] Given the potential of DEs as artificial muscles, there has been widespread investigation into materials that possess optimal properties.

While a variety of elastomeric materials have been investigated, polysiloxanes have come to be considered the premier material for dielectric applications due to their excellent

mechanical and physicochemical properties. Specifically, polysiloxanes show minimal aging effects, reproducible actuation for millions of cycles, high thermal stability and lower viscous losses than their competitors.[1] Unfortunately, polysiloxanes suffer from one critical flaw; low relative dielectric permittivities (~2-3), which results in the need for higher driving voltages to achieve actuation strains comparable to other materials such as VHB from 3M. As a consequence, there is significant interest in developing strategies to increase the permittivity of polysiloxanes.[1,4,6]

Of the multiple strategies investigated to improve the permittivity of polysiloxanes, including conductive fillers, and the grafting of permanent dipoles, the most prevalent strategy involves the doping of elastomers with high permittivity inorganic additives. This strategy has received attention due to its simplicity; control over the permittivity can be realized simply by adding dopants into commercially available silicone elastomer formulations.[7,8] Additives such as TiO_2,[9–11] ZnO,[12] and $BaTiO_3$[13,14] have all been tested as high permittivity fillers. In each case, these fillers have resulted in improved permittivities the magnitude of which depends on the loading of the additive. The increase in the dielectric permittivity of the elastomers was usually maximum of the order of 2. Unfortunately, this strategy is not without its challenges. Achieving reproducible dispersions and minimizing particle aggregation is difficult, and aggregates significantly and negatively impact the final dielectric properties of the composite.[15] In addition, inorganic additives act as fillers that increase the Y of the materials, ultimately resulting in materials with poorer actuation performance since the Young's modulus was usually increased by more than a factor of 2.[16]

Electro-stabilization by means of inorganic fillers, such as ZnO and $BaTiO_3$, has also been explored [17,18] but again the favourable dielectric properties achieved are outweighed by the increased Young's modulus.[12,19]

While inorganic fillers such as those discussed above have been widely investigated, organic fillers have received considerably less attention. The investigation into organic fillers has largely been limited to conjugated polymers with limited miscibility with silicone, such as polyaniline, and poly(hexylthiophene), which all serve to increase the dielectric performance but only to a limited extent: increasing the concentration of the dopant within the elastomer is challenging due to the immiscibility of the two components.[20,21] Phase separation leads to unfavourable properties due to the resulting inhomogeneous electrical fields. An excellent example of the use of a high-permittivity organic filler in DE applications was conducted by Zhang et al. Using copper-phthalocyanine oligomers (CPO), they were able to increase the permittivity of silicone elastomers to ~11 at a loading of 40%, which represents a 250% increase in the permittivity.[22,23] Macrocycles such as phthalocyanines have a tendency to form aggregates, particularly in silicones due to their low solubility.[24,25] Zhang et al. observed aggregation of the CPO in their elastomers, which contributed to a significant lowering of the dielectric breakdown strength.[22,23]

Despite the promise shown by these organic fillers there has been little additional investigation into the use of these or other high permittivity fillers aromatic macrocycles, such as porphyrins (a closely related class of molecules to phthalocyanines) for silicone

elastomers. We reasoned that the benefits of this class of molecules could be better realized if the materials were more soluble in silicones.

It has been shown that highly insoluble triarylamines could be rendered soluble in silicones by grafting small silicone units onto the aromatic ring. The Piers-Rubinsztajn (PR) reaction was used to convert arylmethoxy into arylsiloxy groups, analogous to the reaction shown in B, after which they became soluble in a variety of non-polar solvents.[26–28] We hypothesized that the same reaction could be used with an appropriate porphyrin and silane to create liquid porphyrins that, due to their silicone functionality, would similarly show improved dispersion in silicone elastomers. In this work, 5,10,15,20-(tetra-3-methoxyphenyl)porphyrin (TPMP) was derivatized with bis(trimethylsiloxy)methylsilane and the resulting silicone-modified porphyrin was incorporated into silicone elastomer formulations at various loadings. The physical and dielectric properties of the elastomers were evaluated and compared to elastomers containing unmodified TPMP. A comparison with unmodified silicone elastomers was also performed.

2.3 Experimental

2.3.1 Materials

5,10,15,20-(Tetra-3-methoxyphenyl)porphyrin (TPMP) was purchased from Porphychem, France. Zinc acetate dihydrate, tris(triphenylphosphine) rhodium (I) chloride (Wilkinson's Catalyst), neutral alumina Brockmann I activity, dichloromethane, methanol, n-pentane and deuterated chloroform were purchased from Sigma-Aldrich. Wilkinson's catalyst was dissolved in toluene to provide a stock solution of 7.6 mg mL^{-1} (76 mg in 10 mL).

Bis(trimethylsiloxy)methylsilane, trimethylsiloxy-terminated dimethylsiloxane-hydromethyl-siloxane copolymer (25-35% hydromethylsiloxane, HMS-301, M_w= 1900-2000 g/mol, 25- 35 cSt), and vinyl-terminated polydimethylsiloxane (DMS-V22, M_w= 9400 g/mol, 200 cSt) were purchased from Gelest. Elastosil RT 625 Parts A and B were purchased from Wacker Chemie. Tris(pentaflurophenyl)borane ($B(C_6F_5)_3$, BCF) was purchased from TCI chemicals and dissolved in dichloromethane to provide a stock solution of 10 mg $mL^{-1.}$ Karstedt's catalyst, platinum divinyl-tetramethyl disiloxane complex, was purchased from ABCR chemicals. All chemicals were used as received without further purification. Carbon Grease (Nyogel 756G, Lot# MY121102) was purchased from Nye Lubricants Inc. The Dual Asymmetric Centrifuge (DAC) Model DAC 150.1 FV7-K and FlackTek cups were purchased from FlackTek Incorporated.

2.3.2 NMR Analysis

^{1}H, ^{13}C NMR and ^{29}Si NMR spectra were performed on a Bruker Avance 600 MHz NMR. $CDCl_3$ was used as the solvent in each case.

2.3.3 Infrared Spectroscopy

Fourier Transform Infrared Spectroscopy was performed using a Nicolet Is50 Ft-IR instrument.

2.3.4 Electrospray Ionization Mass Spectrometry

Electrospray ionization mass spectrometry (ESI-MS) was performed using an Agilent 6340 Ion Trap mass spectrometer. Sample concentrations were ~50-100 μM.

2.3.5 Dielectric Spectroscopy

Dielectric Spectroscopy was performed using a Novocontrol Alpha-A High Performance Frequency Analyzer (Novo-control Technologies GmbH & Co. KG, Germany). Measurements were taken in the frequency range of 10^{-1} to 10^{-6} Hz at 25 °C. Samples were sandwiched between two gold-coated electrode plates prior to measurement. The electrode geometry was 20 mm.

2.3.6 Dielectric Breakdown

Electrical breakdown strength was measured using an in-house-built device based on international standards (IEC 60243-1 (1998) and IEC 60243-2 (2001). Samples were prepared with a thickness of 100 μm. The film was placed between two spherical electrodes (diameter of 20 mm). The electrical breakdown measurement was taken at the point of contact with a stepwise. increasing voltage applied (50 – 100 V per step) at a rate of 0.5 -1 steps per s. The electrical breakdown measurement was repeated 12 times for each sample, and the average of these values was then stated as the electrical breakdown strength.

2.3.7 Young's Modulus

Young's moduli were measured using an Instron 3345 instrument. Samples were prepared as thin films of ~200μm and were stretched at a rate of 500 mm/min. The Young's moduli were calculated by taking the tangent of the stress-strain curve at 10% strain. Each sample was subject to three trials.

2.3.8 Synthesis of Zinc 5,10,15,20-(Tetra-3-methoxyphenyl)porphyrin (Zn-TPMP)

TPMP (5.00 g, 6.80 mmol) was added to a 2 L round-bottomed flask and dissolved in 1 L of a DCM:methanol mixture (1:1). Zinc acetate dihydrate (2.98 g ,14.0 mmol) was added, and the reaction mixture was stirred vigorously for 5 h. The solvent was removed *in vacuo* to yield a purple solid that was suspended in methanol and collected via vacuum filtration. The product was rinsed with water (3x100 mL) to remove excess zinc acetate and dried overnight to yield a purple solid (5.15 g, 6.45 mmol, 95%). ^{1}H NMR (600 MHz, $CDCl_3$) δ 8.99 (s, 8H), 7.83-7.77 (m), 7.63 (t, *J*=7.9 Hz, 4H), 7.31 (dd, *J*=8.6, 2.5 Hz, 4H), 3.95 (s, 12H). ^{13}C NMR (151 MHz, $CDCl_3$) δ 157.77, 150.13, 144.11, 132.00, 127.60, 127.31, 120.87, 120.34, 113.44, 55.48. MS-ESI: calc. for $C_{48}H_{36}N_4O_4Zn$, 796.2028; found, 796.2026.

2.3.9 Synthesis of Zn-TPMP-Bis-H

Zn-TPMP (5.00 g, 6.26 mmol) and bis(trimethylsiloxy)methylsilane (11.1 g, 50.1 mmol, 14.0 mL) were added to a 1 L round-bottomed flask and dissolved in 250 mL of DCM. Tris(pentaflurophenyl)borane solution (14.0 mL, 255 mg, 0.498 mmol, 1 mol%) was added. The reaction was monitored via thin-layer chromatography using a 1:1 *n*-pentane:DCM mixture, the reaction was judged complete when all the Zn-TPMP was consumed (~3 h). The solvent was removed *in vacuo* and the product was purified using column chromatography on Brockman Neutral Alumina Activity I with 1:1 pentane:DCM to yield a purple liquid (9.27g, 5.71 mmol, 91.2%). ^{1}H NMR (600 MHz, $CDCl_3$) δ 9.16 (s, 8H), 8.09 – 7.89 (m, 8H), 7.84 – 7.67 (m, 4H), 7.57-7.42 (m, 4H), 0.46 (s, 12H), 0.25 (q, *J*=1.3 Hz, 72H). ^{13}C NMR (151 MHz, $CDCl_3$) δ 152.54, 150.18, 144.21, 132.03, 128.50, 127.26,

126.52, 120.76, 119.12, 1.74, -3.02. ^{29}Si NMR (119 MHz, $CDCl_3$) δ 9.82, -60.09. Calc. for $C_{72}H_{108}N_4O_{12}Si_{12}Zn$ 1623.4528; found 1623.4533.

2.3.10 Preparation of Stock Hydrosilylation Pre-elastomer (without platinum catalyst)

HMS-301 (3.13 g, 1.56 mmol, 12.8 mmol Si-H) and DMS-V22 (60.0 g, 6.38 mmol, 12.8 mmol vinyl) were added to a 60 mL FlackTek cup (Si-H: vinyl=1:1) and mixed at 3500 rpm for five minutes to ensure a homogenous mixture. Silicone pre-elastomers were subject to high vacuum treatment after mixing, but prior to cure to reduce bubble formation in the elastomers.

2.3.11 Preparation of Porphyrin Elastomers-Physical Dispersion of Zn-TPMP and Zn-TPMP-Bis-H in Stock Pre-elastomer

Stock pre-elastomer and Zn-TPMP or Zn-TPMP-Bis-H were added to a 25 mL FlackTek cup and mixed at 3500 rpm for 2 min in the DAC to disperse the respective porphyrin additives (Table 2.1). Karstedt's catalyst (0.5 μL, 6 ppm) was added and then mixed at 1500 rpm for 30 s. The mixture was poured into 1 mm square molds and cured at 80^{o}C for 5 h, providing an elastomer ~ 1 mm thick to measure dielectric properties.

2.3.12 Preparation of Porphyrin Elastomers-Physical Dispersion of Zn-TPMP-Bis-H in Elastosil 625

Zn-TPMP-Bis-H and Elastosil 625 Parts A and B were added to a 25 mL FlackTek cup and mixed at 3500 rpm for 2 min (Table 2.2). Additional Karstedt's catalyst (0.5 μL, 6 ppm) or Wilkinson's catalyst (1.2 μL, 6 ppm) was added to each elastomer to ensure consistency, and the formulation was mixed for an additional 1 min at 2500 rpm. The final crosslinked films were prepared in three thicknesses: 1 mm to measure LVE and dielectric properties, 100 μm to measure dielectric breakdown strength, and 200 μm to measure Young's modulus. Each sample was cured at 80 °C for 5 h.

Table 2.1: Required masses for porphyrin elastomers using HMS-301+DMS-V22 mixture.

Weight Percent Porphyrin (%)	Mass Zn-TPMP or Zn-TPMP-Bis-H (g)	Mass Silicone Mixture (g)*	Total Mass (g)
0	0	1.500	1.50
0.5	0.00750	1.493	1.50
1	0.0150	1.485	1.50
2	0.0300	1.470	1.50
4	0.0600	1.440	1.50
6	0.0900	1.410	1.50
8	0.120	1.380	1.50
10	0.150	1.350	1.50

Table 2.2:Required masses for the synthesis of porphyrin elastomers using Elastosil 626.

Weight Percent Porphyrin (%)	Total Mass (g)	Mass Zn-TPMP-Bis-H (g)	Mass Silicone (g)	Mass RT 625 Part A (g)	Mass RT 625 Part B (g)
0	1.500	0	1.500	1.350	0.150
2	1.500	0.0300	1.470	1.323	0.147
6	1.500	0.0900	1.410	1.269	0.141
10	1.500	0.150	1.350	1.215	0.135

2.3.13 Actuation Tests

Elastomers containing 0, 2 6 and 10% Zn-TPMP-Bis-H were made using the procedure described above and cast as 50 μm films. The films were stretched over a rigid ring mold (inner diameter = 5 cm, outer diameter = 7 cm) such that a 10% pre-strain was applied. A 25 mm diameter circular carbon grease electrode was applied to each side and connected to a Stanford Research Systems Model PS37 high voltage source. An initial voltage of 100 V was applied, and the voltage was gradually increased in 50 V increments until dielectric breakdown was observed. The change in diameter of the electrode was measured by analyzing the videos with the software tracker and this data was used to calculate the % area strain.

2.4 Results and Discussion

2.4.1 Synthesis of Zn-TPMP and Zn-TPMP-Bis-H

The addition of zinc to the parent TPMP porphyrin to give Zn-TPMP (Figure 2.1A) was readily achieved at room temperature in high yields (95%); metalation of the porphyrin was confirmed after 5 h by monitoring the 1H-NMR spectrum for the absence of a peak at -2 ppm in the 1H-NMR, corresponding to N-H protons of the pyrrole units.[29] The final

product required minimal purification; rinsing the product with water provided a product of sufficient purity for synthesis of Zn-TPMP-Bis-H

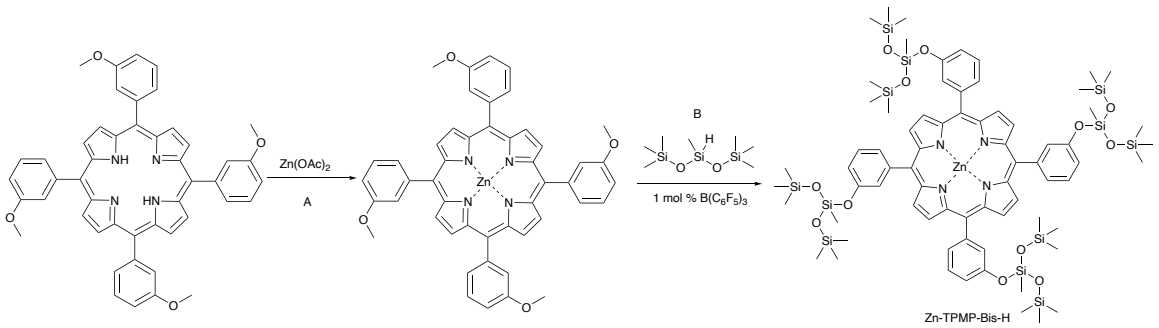

Figure 2.1: A) Synthesis of Zn-TPMP. B) Synthesis of Zn-TPMP-Bis-H

The metalation of TPMP was determined to be a necessary step in the synthesis of silylated TPMP, as previous attempts to directly react TPMP via the PR reaction were unsuccessful. With the metalated porphyrin, by contrast, the synthesis of the silylated derivative, Zn-TPMP-Bis-H, could be achieved readily at room temperature in a yield of 91% provided sufficient $B(C_6F_5)_3$ catalyst (~1 mol%) was used (Figure 2.1B). Concentrations below this value resulted in no reaction even under reflux in toluene. Unlike the starting material, which is a solid, Zn-TPMP-Bis-H is a liquid at room temperature and is soluble in a wide array of polar and non-polar solvents including hexanes, pentane, toluene, and dichloromethane.

2.4.2 Preparation of Elastomers: Physical Dispersion of Porphyrins

2.4.2.1 Zn-TPMP

Elastomers were synthesized using a platinum cure system composed of HMS-301 (multifunctional hydride PDMS crosslinker) and DMS-V22 (telechelic vinyl functional PDMS). This system was selected to evaluate the potential of Zn-TPMP as a dielectric filler

without the additives and fillers commonly found in commercial formulations. Initially, Zn-TPMP was physically dispersed in various weight percentages into the formulation and cured into elastomers ~1 mm thick. This technique resulted in elastomers with inhomogeneous dispersions of porphyrin. While samples containing 2-10% initially appeared to be homogenous (Figure 2.2A), agglomeration of porphyrin could be readily observed in the 10% sample when observed under an optical microscope (Figure 2.2B) or by eye in the samples containing 0.5-1% porphyrin, as the low concentrations of porphyrin in these cases produced transparent elastomers in which agglomeration could be observed.

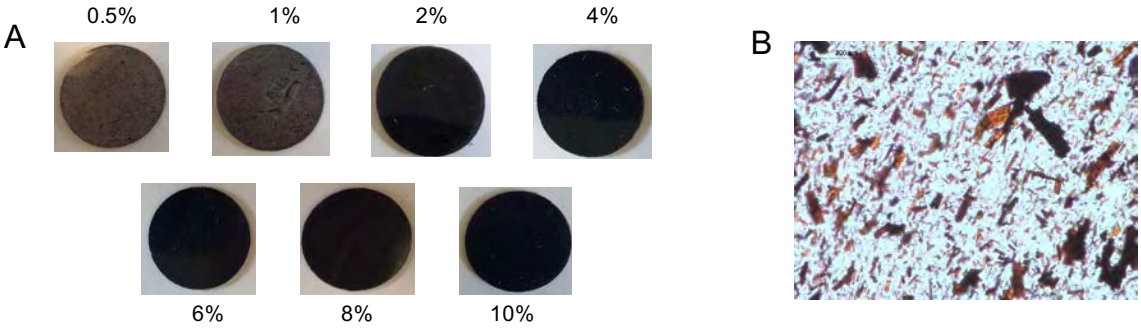

Figure 2.2: A) Elastomers with increasing weight percentages of Zn-TPMP, 1mm thick. B) Optical microscope image of a 10% Zn-TPMP elastomer, 100 μm thick

Attempts to improve the dispersions by increasing the mixing time or speed ultimately proved unsuccessful, as did pre-dissolving the porphyrin in DCM prior to dispersal. The latter technique resulted in elastomers with defects (voids) due to evaporation of the solvent during the curing process. When evaluated for their dielectric properties, little deviation from the control could be observed, the measured relative permittivities are all within the range generally accepted for unmodified silicone elastomers (2.5-3) and are similar to that of the permittivity measured for the control.[1] Additionally,

the conductivity of the elastomers remained unchanged regardless of the amount of additive used.

However, while the relative dielectric loss (tanδ) of the Zn-TPMP samples were similar, they were all slightly lower than the control (Table 2.3). The poor performance of Zn-TPMP as a dielectric filler is not surprising, as it is well known that the potential of a dielectric filler is directly related to its miscibility in the silicone elastomer, with the highest performance achieved with fillers that are fully miscible in the elastomer formulation.30 Mechanical characterization of these elastomers was hindered by the tendency of the PDMS system to tear during handling, a common problem for silicone elastomers that don't contain reinforcing agents.31 As a consequence, mechanical characterization could not be performed to determine the Young's moduli of the materials. In place of Young's moduli, the Shore OO hardnesses, a measurement of a materials resistance to indentation, were measured to determine the impact of Zn-TPMP on the mechanical properties of the elastomers. It was observed that at the highest loadings, 8 and 10%, the Shore OO hardness increased while, at lower loadings 0.5-6%, the Shore OO hardness was only one unit higher than the control (

Table 2.3 2.3). Given the sensitivity of the Shore OO durometer, these values can all be considered equal within error.

Analysis of the storage moduli of the materials confirmed that increasing the loading of Zn-TPMP resulted in harder materials with the storage moduli increasing as the loading of Zn-TPMP increased. While the effect of Zn-TPMP at low loadings is minimal, and within the accepted error window of 10% for rheological data, at higher loadings (6-

10%), the effect on storage modulus can be clearly observed. In this case it is believed that at higher loadings the Zn-TPMP is acting as a very weak reinforcing agent (Figure 2.3).

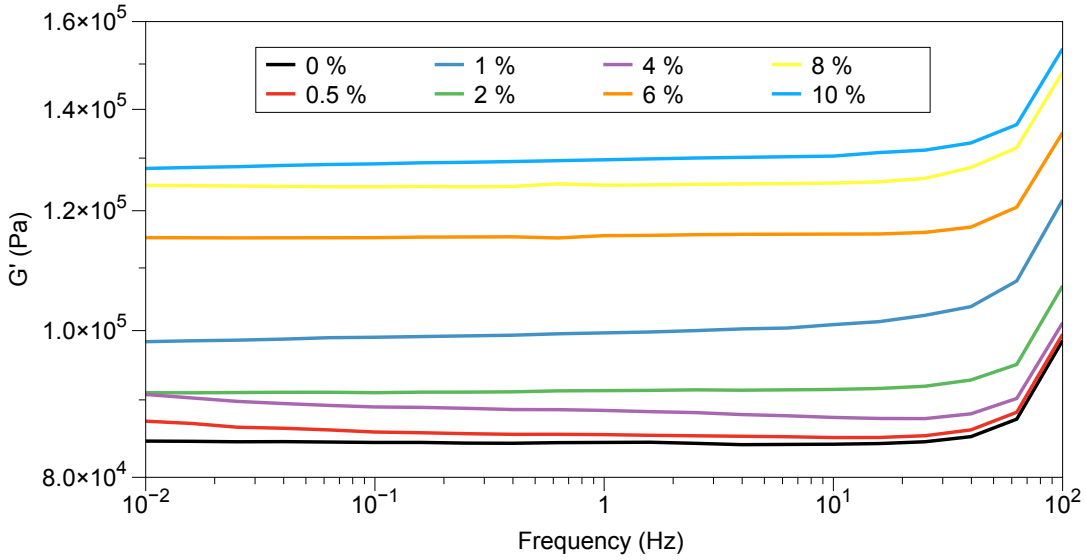

Figure 2.3: Storage modulus (G') of Zn-TPMP homemade elastomers @ 25°C.

Table 2.3: Summary of dielectric properties and shore oo hardness of elastomers with varying weight percentages of Zn-TPMP.

Weight % Zn-TPMP	Permittivity @ 0.1 Hz	Tanδ@ 0.1 Hz	Conductivity (S/cm) @ 0.1 Hz	Shore OO
0	3.08	0.018	1.16×10^{-13}	65
0.5	3.08	0.042	1.16×10^{-13}	65
1	3.03	0.086	1.14×10^{-13}	65
2	3.1	0.046	1.17×10^{-13}	66
4	2.99	0.031	1.11×10^{-13}	66
6	3.03	0.042	1.22×10^{-13}	66
8	3.03	0.050	1.13×10^{-13}	67
10	3.18	0.046	1.21×10^{-13}	69

2.4.2.2 Zn-TPMP-Bis-H

The same procedure as described for Zn-TPMP was adapted for the synthesis of elastomers containing Zn-TPMP-Bis-H. Unlike Zn-TPMP, Zn-TPMP-Bis-H readily dispersed in the HMS-301+DMS-V22 pre-elastomer mixture because, it is inferred, the bis(trimethylsiloxy) groups on the porphyrin help to facilitate its incorporation into the pre-elastomer mixture. Once dispersed, homogenous elastomers were produced at loadings of 0.5-4%; at loadings above this phase separation of the Zn-TPMP-Bis-H could be seen in the optical micrographs, presenting as dark regions (Figure 2.4). This suggests that 4% is the upper loading limit that can be achieved before the porphyrin oil begins to phase separate from the elastomer mixture.

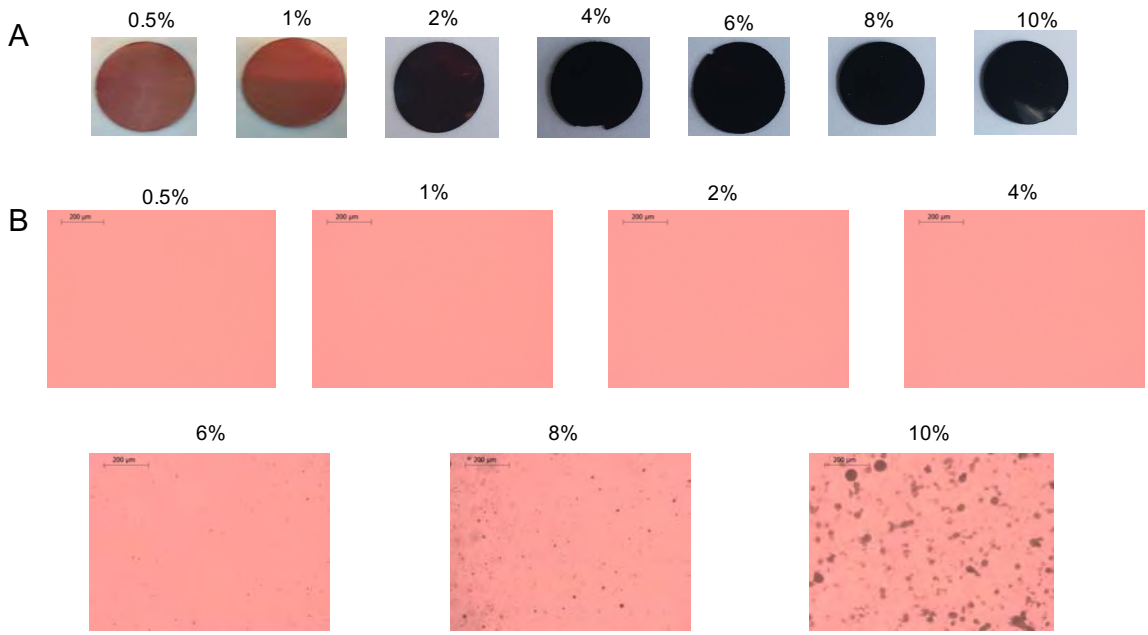

Figure 2.4: A) Elastomers with increasing weight percentages of Zn-TPMP-Bis-H, 1mm thick. B) Optical images of elastomers, 100 µm thick.

In the extreme cases of the 8 and 10% porphyrin-containing elastomers, purple Zn-TPMP-Bis-H would readily transfer to filter paper from the elastomer if a force greater than gravity (e.g., a weight) was applied (Figure 6.23). That is, at these loadings the phase separated siliconized porphyrin was able to migrate to the air interface, a well-known property of silicone oils,[32] after which point it could easily transfer from the elastomer.

The dielectric behavior of these samples was evaluated. Dielectric permittivity at 0.1 Hz increased with the percentage of Zn-TPMP-Bis-H present in the samples (Table 2.4). Unlike the Zn-TPMP samples, improvements in the permittivity could be noted even at the lowest loading, 0.5%, which had a permittivity of 4.15, well outside the generally accepted range for unmodified silicone elastomers.[1]

Table 2.4: Summary of dielectric properties and shore oo hardness of elastomers with varying weight percentages of Zn-TPMP-Bis-H elastomers.

Weight % Zn-TPMP-Bis-H	Permittivity @ 0.1 Hz	Tanδ @ 0.1 Hz	Conductivity (S/cm) @ 0.1 Hz	Shore OO
0	3.08	0.018	1.16×10^{-13}	65
0.5	4.15	70.8	3.48×10^{-11}	66
1	4.62	98.9	3.00×10^{-11}	65
2	5.04	125	3.54×10^{-11}	65
4	5.51	194	4.67×10^{-11}	63
6	6.75	221	7.28×10^{-11}	62
8	7.60	170	9.36×10^{-11}	59
10	15.9	150	1.51×10^{-10}	59

The elastomers all exhibited conductive behavior with a plateau in the conductivity in the region of 10^{-1}-10^{1} Hz. Furthermore, in this region the conductivity increased linearly as a function of entrained porphyrin concentration. While the permittivity and conductivity increased in line with loading of Zn-TPMP-Bis-H, changes in the tanδ were not linear; an

increase in tanδ was observed as the loading was increased to 6%, but the 8 and 10% samples had lower relative dielectric losses than those of the 4 and 6% samples (Table 2.4). This changeover in response coincides with the point at which gross phase separation was observed in the sample. Unsurprisingly, then, the tanδ was significantly affected once gross phase separation arose; the relaxation behavior in the two phases is different due to localized conduction in the phases with high concentrations of porphyrin within the elastomer.[33]

2.4.2.3 Zn-TPMP-Bis-H at higher loadings

As was the case with the Zn-TPMP system, the Young's moduli of these materials could not be measured due to their relatively poor mechanical properties. Therefore, Shore OO hardness was used to obtain a general idea of the impact of Zn-TPMP-Bis-H on the mechanical properties of the elastomers. Surprisingly, as the loading increased, the Shore OO hardness decreased. The rheological behaviour, specifically the storage moduli of the elastomers exhibited the same trend suggesting that Zn-TPMP-Bis-H has a softening/plasticizing effect on the elastomers (Figure 2.5).

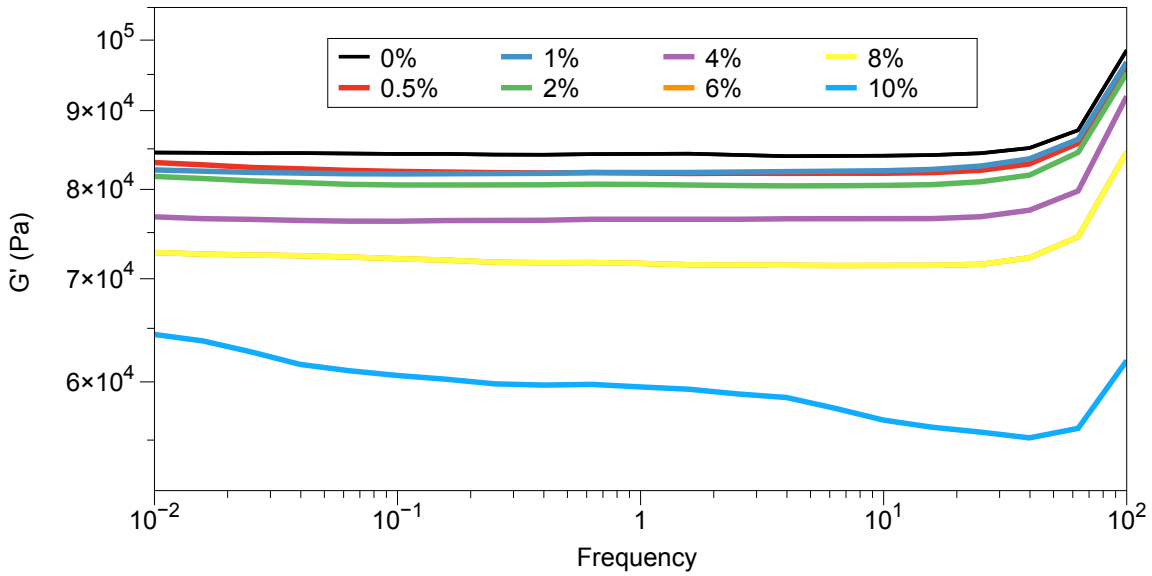

Figure 2.5: Storage moduli (G') of Zn-TPMP-Bis-H homemade formulation elastomers @ 25°C.

This outcome is reminiscent of the impact that silicone oils have on elastomers when they are incorporated as an additive; diluting the network with an oil leads to a softer gel.[34] All elastomers, aside from that formed with 10% Zn-TPMP-Bis-H behave like classical, well-crosslinked networks, exhibiting solely high-frequency relaxation. The storage modulus of the 10% elastomer shows clear indications of much more complex relaxation behavior. It showed a strong frequency-dependent behavior indicating the emergence and disappearance of transient structures, which may include stacked configurations in the areas with high aromatic content and dangling structures that arise from high content porphyrin phases within the elastomer, which is in agreement with the dielectric properties.

Given the tendency of the self-designed, unfilled model PDMS network to tear, it was deemed to be unsuitable for further testing. Therefore, a more resilient commercial

silicone formulation, Elastosil 625, a filled elastomer, was used for all further tests with Zn-TPMP-Bis-H as a dielectric filler.

2.4.2.4 Elastosil 625 Samples

Elastosil 625 was selected as an alternative for the HMS-301/ DMS-V22 system due to its superior mechanical properties, as well as previous performance when used in dielectric applications.[1] Zn-TPMP-Bis-H was dispersed in the two-part Elastosil formulation using the process described above in concentrations of 2, 6 and 10 wt% Zn-TPMP-Bis-H, respectively; these loadings were selected in order to provide a comparison with the homemade system. It was noted that the commercial formulations containing 6 and 10% Zn-TPMP-Bis-H did not cure unless additional catalyst was added (otherwise the product appeared to be a soft gel). To ensure consistency, the same higher catalyst loadings were used with all Elastosil 625 samples containing Zn-TPMP-Bis-H; the amount of additional catalyst added matched the concentration used for the homemade elastomer formulations. IR spectroscopy was used to confirm complete consumption of Si-H groups (Figure 6.21).

The dispersion behaviour of Zn-TPMP-Bis-H in Elastosil 625 was slightly different than in the homemade PDMS system; phase separation at high loadings was not observed (Figure 2.6). It is believed that the additives present in Elastosil 625 help to improve the incorporation of Zn-TPMP-Bis-H in the elastomer.[15] However, gross phase separation was still observed in the 10% sample (Figure 6.23).

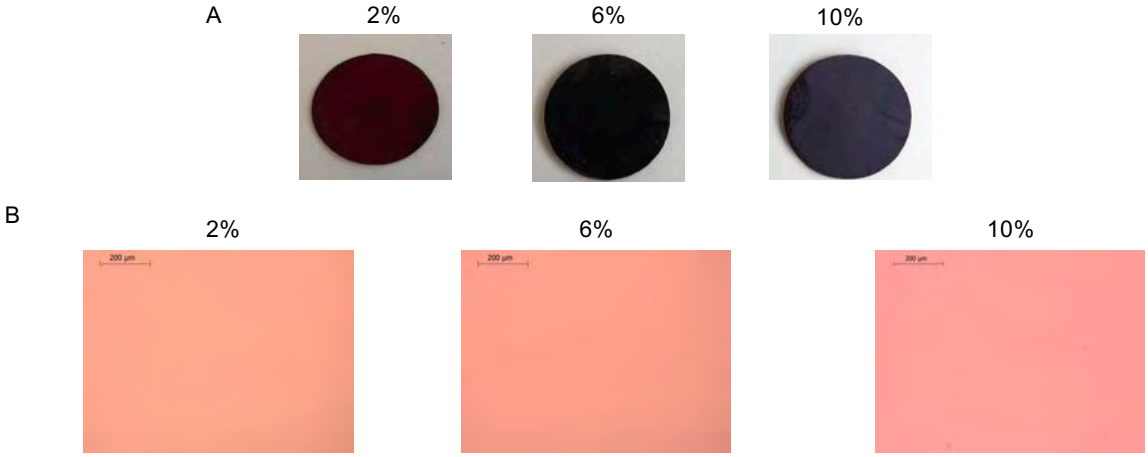

Figure 2.6: A) Elastosil 625 elastomers with increasing weight percentages of Zn-TPMP-Bis-H, 1mm thick. B) Optical microscope images, 100 μm thick.

2.4.2.5 Young's Moduli / Rheological Properties

Unlike the elastomers made from the homemade PDMS formulation, Elastosil 625 elastomers were not prone to tearing and could be cast as robust thin films. Tensile tests revealed that the Young's moduli decreased as the percentage of porphyrin increased (Table 2.5). This was surprising, as previous work has shown that increasing the loading of aromatic groups in silicone elastomers results in higher Young's moduli, via π– π interactions.[35] In this case, it is inferred that the large bis(trimethylsiloxy) group impede aromatic association, such that the porphyrin acts as a plasticizer rather than a reinforcing agent.[34] With Zn-TPMP-Bis-H, the Young's moduli of the elastomers could be reduced even in the presence of the silica reinforcing agents contained within the Elastosil formulation. This is advantageous for dielectric elastomer actuators, as softer materials have better actuation performance.

Table 2.5: Mechanical properties of Elastosil 625 properties.

Sample	Young's Modulus @ 10% Strain (MPa)	Tensile Strength (MPa)	Tensile Strain (%)
0%	0.65±0.07	6.22±2.07	519±89
2%	0.60±0.06	3.20±0.55	418±33
6%	0.40±0.05	3.77±0.62	538±40
10%	0.16±0.02	1.96±0.35	510±67
10%*	0.08±0.01	1.20±0.07	435±19

Rheological studies of the samples showed that the trend observed in the pure PDMS system - increased loading lowers storage modulus - held for the Elastosil samples as well (Figure 2.7). Noticeably absent in the storage moduli results were any characteristics that would indicate phase separation was occurring in the samples, consistent with the lack of phase separation observed in the optical micrographs of the Elastosil elastomers.

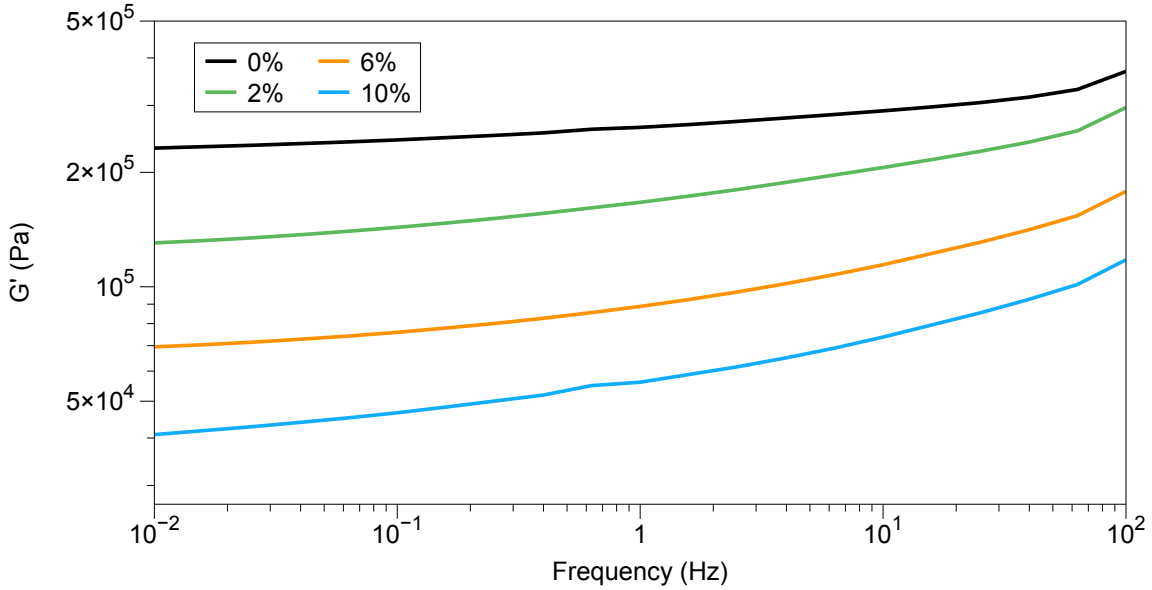

Figure 2.7: Storage moduli (G') of Zn-TPMP-Bis-H Elastosil 625 samples @ 25°C.

2.5 Dielectric Properties of Elastosil 625 Samples

The dielectric performance of the porphyrin in commercial formulations closely resembled those of the HMS-301+DMS-V22 system; the permittivities increased with increasing Zn-TPMP-Bis-H concentration (Table 2.6). However, the permittivities in commercial silicone were slightly lower than those measured for the unfilled PDMS samples. The permittivity at the lowest loading level of 2% Zn-TPMP-Bis-H is higher than that usually obtained when using inorganic fillers. For example, elastomers containing TiO_2, $BaTiO_3$ or ZnO typically require loadings >10% to obtain permittivities greater than 3.[1] The use of inorganic fillers also required specialized mixing techniques where Zn-TPMP-Bis-H can be easily mixed in by hand or, for better consistency, using a speedmixer. Zn-TPMP-Bis-H also performed favorably when compared to other organic additives; elastomers using only a 10% loading gave permittivities ~13 comparable to those achieved by Zhang et al. using CPO, but in the latter case 40% CPO loading was required.[22, 23] It compares favorably when compared to other highly conjugated organic systems such poly(hexylthiophene) and polyaniline. In the case of polyaniline, permittivities greater than 8 could not be achieved even at loadings greater than 30%.[20] Poly(hexylthiophene) exhibited very similar permittivity; a loading of 6% poly(hexylthiophene) in silicone had a permittivity of ~14, whereas a 10% loading of Zn-TPMP-Bis-H resulted in a permittivity of ~13.[21]

The Elastosil 625 samples also exhibited a conductive region from 10^{-1}-10^{1} Hz and, like the homemade system, the conductivity in this region increased with the amount of porphyrin added. The dielectric loss (tanδ) values @ 0.1 Hz also increased in line with

increased loading of porphyrin, reflecting the more homogenous dispersions achieved in the Elastosil samples compared to the initial self-designed elastomers without any additives for e.g. improved stability and miscibility.

To assess the performance of the DEs a figure of merit (F_{OM}), described by equation 2 was calculated, where ε' is the permittivity of the elastomer, ε_o is the permittivity in a vacuum, E_b is the dielectric breakdown strength and Y is the Young's modulus.[36]

$$F_{om} = \frac{3\varepsilon' \varepsilon_o {E_b}^2}{Y} \quad (2)$$

The F_{OM} of Elastosil 625 in the absence of additives was calculated and normalized to 1, the results of these calculations are shown Table 2.6. From these relative F_{OM} we can see that the samples containing porphyrin have higher F_{OM}s than that of the control with the 10% sample having a F_{OM} 6 times greater than that of the control. The increase in the F_{OM} values is due to the increase in permittivity as well as the reduction in Young's moduli imparted by the porphyrin additive.

Table 2.6: Summary of dielectric properties for Elastosil 625 elastomers in comparison to homemade cure systems.

Silicone Formulation	% Zn-TPMP-Bis-H	Permittivity @ 0.1 Hz	Tanδ @ 0.1 Hz	Conductivity (S/cm) @ 0.1 Hz	F_{OM}
Homemade	0%	3.08	0.018	1.16×10^{-13}	-
	2%	5.04	125	3.48×10^{-11}	-
	6%	6.75	221	7.28×10^{-11}	-
	10%	15.9	150	1.51×10^{-10}	-
Elastosil 625	0%	2.32	0.004	7.36×10^{-14}	1.00
	2%	8.67	199	4.28×10^{-11}	1.33
	6%	9.68	267	2.70×10^{-11}	1.93
	10%	12.7	262	4.21×10^{-11}	5.80

2.5.1 Dielectric Breakdown

The dielectric breakdown strength of elastomers was found to have an inverse relationship with the percentage of Zn-TPMP-Bis-H found therein. That is, as the percentage of porphyrin increased the dielectric breakdown strength decreased. This is commonly observed in silicone elastomers when an additive is added; the permittivity increases but the dielectric breakdown strength decreases.[1] However, it is well known that the dielectric breakdown strength of silicone elastomers is affected by the Young's moduli of the materials.[37] In order to ascertain whether the reduction in dielectric breakdown strength is due to a property of the porphyrin or the reduction in Young's modulus, a previously described model (shown in equation 3), was applied, where E_{BD} and $E_{BD,o}$ refer to the dielectric breakdown strength of the modified and unmodified elastomer (control),

respectively, k^*_{BD} represents the proportionality constant between the Young's modulus and dielectric breakdown strength, and Y and Y_o represent the Young's moduli of the modified and unmodified elastomers, respectively.[15]

$$E_{BD} = E_{BD,o}\,(1 + k^*_{BD}\left(\frac{Y}{Y_o} - 1\right) \quad (3)$$

A positive k^*_{BD} value indicates the filler increases the dielectric breakdown strength and that the reduction in dielectric breakdown strength is mainly due to the decreased Young's moduli. The calculated k^*_{BD} values for the porphyrin elastomers are shown in Table 6 and are positive, suggesting the porphyrin additive serves to increase the dielectric breakdown strength. However, its ability to simultaneously act as a plasticizer, causing decreases in the Young's moduli leads to corresponding reductions in the dielectric breakdown strength despite its role as a voltage stabilizing filler. Further analysis of the dielectric breakdown strengths was conducted using Weibull statistical analysis. Analysis of this data showed that the shape parameter, an indicator of microscopic homogeneity, remained relatively constant for all samples except for the 6% sample that exhibited slightly elevated shape parameter when compared with the other samples (Table 2.7). This suggests that the 6 % sample has the most uniform electrical breakdown, indicating that the sample does consist of a homogenous dispersion of the Zn-TPMP-Bis-H dielectric filler that is also able to act as a voltage stabilizer.[19,33] In other words, the 6% sample exhibits a lower dielectric breakdown strength due to its softness but its electrical properties are enhanced compared to the reference. For large-scale production of dielectric elastomer films the

shape parameter is the most crucial parameter, since it as measure of the homogeneity of the materials.[19]

Table 2.7: Dielectric breakdown strength and Young's modulus for Elastosil 625 samples.

Sample	E_b (V/μm)	β	η (V/μm)	r^2 of Weibull fit	Y (MPa)	k^*_{BD}
0%	98.4±4.1	26.6	100	0.89	0.65±0.07	-
2%	60.0±2.4	27.9	61.0	0.90	0.60±0.06	5.07
6%	57.3±2.1	32.0	58.0	0.94	0.40±0.05	1.08
10%	50.3±0.8	22.0	52.7	0.91	0.16±0.02	0.65

2.5.2 Actuation Tests

The elastomer containing 0% porphyrin was actuated to establish a base line performance for the elastomers. The sample exhibited minimal actuation at low voltages and achieved a maximum area strain of 12% before undergoing dielectric breakdown at 60 V/μm. As expected, the elastomers containing 2, 6 and 10% porphyrin performed better than the control (Figure 2.8). Unsurprisingly, given the trend observed in the experimentally measured dielectric breakdown strengths, the 10% sample underwent dielectric breakdown at the lowest electrical field strength of 36 V/ μm, while the 2 and 6% sample exhibited nearly identical breakdown voltages 51 V/μm and 52 V/ μm, respectively. The elastomer with the highest concentration (6%) of well-dispersed Zn-TPMP-Bis-H, confirmed through microscopy and Weibull analysis, exhibited the best performance of the samples tested. Significant actuation, up to ~ 8%, could be achieved at voltages below 1 kV and at 1 kV an actuation of ~10% could be achieved. The 6% sample also continued to actuate as the driving voltage was increased, ultimately achieving

a maximum strain of ~ 43% before undergoing dielectric breakdown. By comparison, the 2% sample only achieved 1% actuation at 1 kV, the same as the control and the 2% sample was only able to achieve a maximum 12% strain before undergoing dielectric breakdown. The inhomogeneous 10% sample had an almost identical performance to the 6% sample at low voltages, 9% area actuation at 1 kV but, as previously mentioned, suffered from a low dielectric breakdown strength, limiting it to a maximum strain of 22%.

The strains achieved by these materials are an improvement on those achieved by most dielectric elastomer materials; to our knowledge the actuation strains were greater than any inorganic filler previously evaluated.[1] In the case of the most closely related system, which used a 20% loading of organic copper-phthalocyanine oligomers, actuation strains of ~ 11% at ~ 25 V/ μm were measured before the sample underwent dielectric breakdown. This compares with the 6 % sample tested in this study was able to achieve the same actuation (~ 11%) at 25 V/μM at a significantly lower loading of additive. Additionally, the siliconized porphyrin was able to continue to actuate at higher field strengths. This can be attributed to the ability to make homogeneous dispersions in the silicone elastomer carrier; that is, the absence of agglomeration contributes to the reduced actuation performance.

When compared to other known organic fillers the Zn-TPMP-Bis-H elastomers also had excellent performance. Elastomers containing poly(hexylthiophene) outperformed the Zn-TPMP-Bis-H elastomers at low fields, as they were able to actuate up to ~8% at 6 V/μm at a 1 % loading vs ~3% actuation for 6 % Zn-TPMP-Bis-H. However,

the use of organic solvents were required to achieve dispersion in the former case. In addition, the samples containing poly(hexylthiophene) were pre-strained by 100 % while our samples were only pre-strained by 5%. Finally, 6 V/μm represents the maximum electrical field that can be applied in the case of the poly(hexylthiophene), significantly lower than the maximum field that can be applied to any of the samples used in this study.21 At 50 V/μm an elastomer containing 15% polyaniline encapsulated in divinylbenzene had an actuation strain of ~12%, 68% lower than that achieved in the 6% Zn-TPMP-Bis-H sample at the same electrical field.[20]

The actuation performance of the samples evaluated in this study, when compared to literature examples, highlights the promise of macrocycles like porphyrins such as Zn-TPMP-Bis-H as high-permittivity dielectric additives. We are currently examining further modification of the Zn-TPMP core to improve its dispersibility at higher loadings which could lead to even better performing material, eventually allowing for devices that could achieve high strains at low electrical fields removing a potential barrier to commercialization.

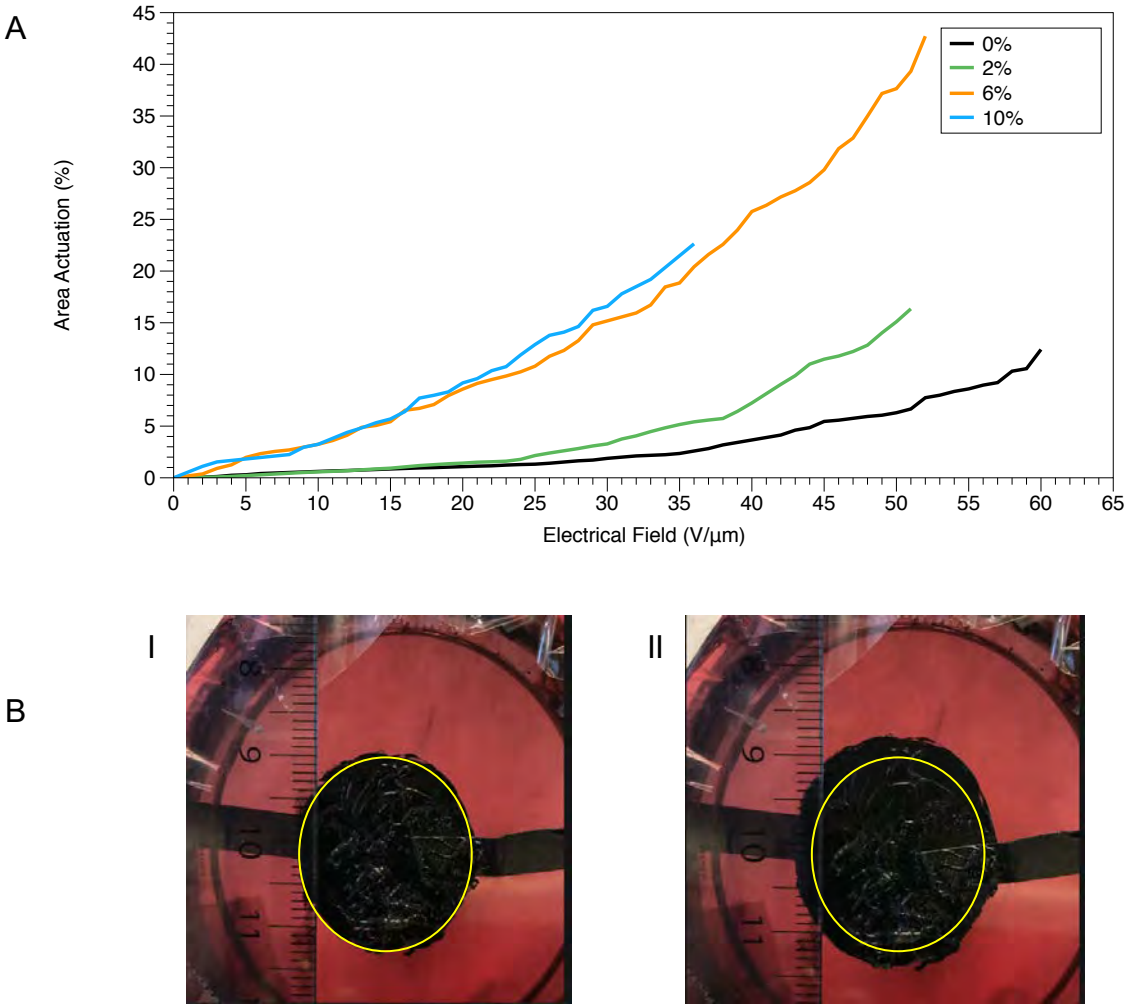

Figure 2.8: A) Actuation performance of 50 µm Elastosil 625 films. B) i) 6% elastomer with 0 V applied. ii) 6% elastomer with 2.55 kV applied (yellow circle indicated unexpanded dimension).

2.6 Conclusions

The blending of small quantities, up to 10 %, of the modified porphyrin Zn-TPMP-Bis-H served to increase the relative permittivity of silicone elastomers while simultaneously reducing their Young's moduli. Elastomers exhibited homogenous dispersions not previously encountered due to the compatibilization of the porphyrin with silicone elastomers via the Piers-Rubinsztajn reaction. Dielectric losses remained low due to the homogeneity of the blends. These factors led to the synthesis of silicone elastomers that could achieve large actuations, >40 % in response to applied electrical fields in the case of a 6 % loading of permittivity-enhancing filler. These elastomers represent a step forward towards the realization of devices that can be commercialized due to their ability to actuate at low electrical fields and at the same time with limited modifications of the commercial elastomers.

2.7 Acknowledgements

CBG and MAB acknowledge with gratitude financial support from the National Sciences and Research Council of Canada. CBG thanks Mitacs for a Mitacs Globalink Research Award.

2.8 References

1 F. B. Madsen, A. E. Daugaard, S. Hvilsted and A. L. Skov, *Macromol. Rapid Commun.*, 2016, **37**, 378–413.

2 R. Pelrine, R. D. Kornbluh, J. Eckerle, P. Jeuck, S. Oh, Q. Pei and S. Stanford, in *Smart Structures and Materials 2001: Electroactive Polymer Actuators and Devices*, International Society for Optics and Photonics, 2001, vol. 4329, pp. 148–156.

3 Y. Qiu, E. Zhang, R. Plamthottam and Q. Pei, *Acc. Chem. Res.*, 2019, **52**, 316–325.

4 L. J. Romasanta, M. A. Lopez-Manchado and R. Verdejo, *Prog. Polym. Sci.*, 2015, **51**, 188–211.

5 R. E. Pelrine, R. D. Kornbluh and J. P. Joseph, *Sens. Actuators Phys.*, 1998, **64**, 77–85.

6 D. M. Opris, *Adv. Mater.*, 2018, **30**, 1703678.

7 F. Carpi, G. Gallone, F. Galantini and D. De Rossi, in *Dielectric Elastomers as Electromechanical Transducers*, eds. F. Carpi, D. De Rossi, R. Kornbluh, R. Pelrine and P. Sommer-Larsen, Elsevier, Amsterdam, 2008, pp. 51–68.

8 G. Gallone, F. Carpi, D. De Rossi, G. Levita and A. Marchetti, *Mater. Sci. Eng. C*, 2007, **27**, 110–116.

9 L. Yu and A. L. Skov, *Int. J. Smart Nano Mater.*, 2015, **6**, 268–289.

10 H. Zhao, D.-R. Wang, J.-W. Zha, J. Zhao and Z.-M. Dang, *J. Mater. Chem. A*, 2013, **1**, 3140–3145.

11 H. Stoyanov, P. Brochu, X. Niu, E. Della Gaspera and Q. Pei, *Appl. Phys. Lett.*, 2012, **100**, 262902.

12 L. Yu, F. B. Madsen, S. Hvilsted and A. L. Skov, *RSC Adv.*, 2015, **5**, 49739–49747.

13 H. Zhao, L. Zhang, M.-H. Yang, Z.-M. Dang and J. Bai, *Appl. Phys. Lett.*, 2015, **1 06**, 092904.

14 H. Böse, D. Uhl, K. Flittner and H. Schlaak, in *Electroactive Polymer Actuators and Devices (EAPAD) 2011*, International Society for Optics and Photonics, 2011, vol. 7976, p. 79762J.

15 A. L. Skov and L. Yu, *Adv. Eng. Mater.*, 2018, **20**, 1700762.

16 H. Zhao, Y.-J. Xia, Z.-M. Dang, J.-W. Zha and G.-H. Hu, *J. Appl. Polym. Sci.*, 2013, **127**, 4440–4445.

17 M. Wåhlander, F. Nilsson, R. L. Andersson, C. Cobo Sanchez, N. Taylor, A. Carlmark, H. Hillborg and E. Malmström, *J. Mater. Chem. A*, 2017, **5**, 14241–14258.

18 L. C. Sim, S. R. Ramanan, H. Ismail, K. N. Seetharamu and T. J. Goh, *Thermochim. Acta*, 2005, **430**, 155–165.

19 H. Silau, N. B. Stabell, F. R. Petersen, M. Pham, L. Yu and A. L. Skov, *Adv. Eng. Mater.*, 2018, **20**, 1800241.

20 M. Molberg, D. Crespy, P. Rupper, F. Nüesch, J.-A. E. Månson, C. Löwe and D. M. Opris, *Adv. Funct. Mater.*, 2010, **20**, 3280–3291.

21 F. Carpi, G. Gallone, F. Galantini and D. De Rossi, *Adv. Funct. Mater.*, 2008, **18**, 235–241.

22 C. Löwe, X. Zhang and G. Kovacs, *Adv. Eng. Mater.*, 2005, **7**, 361–367.

23 Q. M. Zhang, H. Li, M. Poh, F. Xia, Z.-Y. Cheng, H. Xu and C. Huang, *Nature*, 2002, **419**, 284–287.

24 E. A. Ough, M. J. Stillman and K. A. M. Creber, *Can. J. Chem.*, 1993, **71**, 1898–1909.

25 F. Ghani, J. Kristen and H. Riegler, *J. Chem. Eng. Data*, 2012, **57**, 439–449.

26 B. A. Kamino, B. Mills, C. Reali, M. J. Gretton, M. A. Brook and T. P. Bender, *J. Org. Chem.*, 2012, **77**, 1663–1674.

27 B. A. Kamino, J. B. Grande, M. A. Brook and T. P. Bender, *Org. Lett.*, 2011, **13**, 154–157.

28 M. J. Gretton, B. A. Kamino, M. A. Brook and T. P. Bender, *Macromolecules*, 2012, **45**, 723–728.

29 K. M. Smith, D. A. Goff, R. J. Abraham and J. E. Plant, *Org. Magn. Reson.*, 1983, **21**, 505–511.

30 F. B. Madsen, I. Dimitrov, A. E. Daugaard, S. Hvilsted and A. L. Skov, *Polym. Chem.*, 2013, **4**, 1700–1707.

31 P. Mazurek, S. Vudayagiri and A. Ladegaard Skov, *Chem. Soc. Rev.*, 2019, **48**, 1448–1464.

32 M. A. Brook, *Silicon in Organic, Organometallic, and Polymer Chemistry*, Wiley, 1999, pp. 256-308.

33 A. H. A. Razak and A. L. Skov, *RSC Adv.*, 2016, **7**, 468–477.

34 F. B. Madsen, S. Zakaria, L. Yu and A. L. Skov, *Adv. Eng. Mater.*, 2016, **18**, 1154–1165.

35 A. Fatona, J. Moran-Mirabal and M. A. Brook, *Polym. Chem.*, 2018, **10**, 219–227.

36 P. Sommer-Larsen and A. L. Larsen, in *Smart Structures and Materials 2004: Electroactive Polymer Actuators and Devices (EAPAD)*, International Society for Optics and Photonics, 2004, vol. 5385, pp. 68–77.

37 L. Yu and A. L. Skov, *Macromol. Rapid Commun.*, 2018, **39**, 1800383.

Chapter 3 Synthesis of Siliconized Photosensitizers for use in $^1O_2$ Generating Silicone Elastomers: An EPR Study

3.1 Abstract

Biomedical devices based on silicone are essential tools in modern healthcare, but can be compromised by development of device acquired infections (DAIs). Unfortunately, the continued rise of antibiotic-resistant organisms makes current strategies to combat DAIs insufficient. Recently, the use of photoactive coatings that produce reactive oxygen species (ROS), specifically singlet oxygen ($^1O_2$), has attracted attention as a potential alternative to traditional strategies to prevent DAIs. However, the synthesis and characterization of silicone devices capable of $^1O_2$ production are not trivial. Development is hindered by the incompatibility of photosensitizers with the silicone matrix and an incomplete understanding of how the method of incorporation impacts $^1O_2$ production. Using the Piers-Rubinsztajn reaction**,** the photosensitizer 5,10,15,20-(tetra-3-methoxyphenyl)porphyrin (TPMP) was derivatized to be compatible with silicone matrices without the assistance of solvents and could be incorporated either covalently or physically within silicone elastomers. EPR measurements indicated that $^1O_2$ was more efficiently generated from elastomers containing a covalently crosslinked TPMP derivative than their physically dispersed counterparts, due to the minimization of aggregates.

3.2 Introduction

Biomedical devices, such as Foley catheters, have become critical tools in modern healthcare, temporarily restoring function during medical procedures and extended hospital stays.[1–3] Unfortunately, as with any implanted medical device, their prolonged use (allowed use up to 30 days) is associated with an increased risk of device-acquired infections (DAIs).[4] The Centers for Disease Control and Prevention (CDC) estimates that 13,000 deaths are due to catheter-associated urinary tract infections each year in the United States alone.[5] These infections occur due to the colonization of the catheter surface, leading to pathogenic biofilms.[6] There is an unmet need to reduce biofilm formation on polymeric devices.

Two strategies are typically used to decrease biofilm formation on implanted biomaterials, thus reducing the risk of DAIs: modification with hydrophilic polymers to prevent adhesion[7] or impregnation of the polymer with an antibacterial agent such as silver nanoparticles or antibiotics. These two strategies are often used in combination to maximize their impact.[8] However, the continued rise of antibiotic-resistant bacteria and concerns over silver nanoparticle toxicity[9] necessitates developing alternative strategies for biofilm disruption.

Recently, the use of reactive oxygen species (ROS) as an antimicrobial strategy, particularly singlet oxygen ($^1O_2$), has received considerable attention.[10–14] Applications that exploit $^1O_2$ depend on reliably incorporating a photosensitizer into the desired device material and subsequently exciting it to the triplet state with the correct wavelength of light. The excited photosensitizer reacts with $^3O_2$ to produce singlet oxygen, which then migrates

to the interface to kill bacteria. This method is highly tunable and additionally advantageous because the antibacterial activity can be controlled externally by applying a photostimulus and is effective against gram-positive bacteria.[15] This method was used with great success by Felgenträger et al., who incorporated 5-(4-hydroxyphenyl)-10,15,20-triphenylporphyrin into a polystyrene matrix coated on a PMMA sheet.[16] These materials showed minimal leaching of porphyrin into biological media and killed *S. aureus* at the polymer interface. Polystyrene is unfortunately subject to oxidation, which could potentially limit its application in ROS-producing materials, as the indiscriminate oxidizing capabilities of singlet oxygen will ultimately compromise the device.[17,18]

Silicone elastomers are widely used in biomedical applications. Unlike polystyrene, they are very resistant to oxidation and are well known to be highly permeable to gases, particularly oxygen.[19] Coupled with their high biocompatibility,[20] these properties make them well suited to the exploitation of ROS production in medical devices. Despite this, there are very few reports on the development of ROS-producing silicones. In an early paper, van Laar et al. incorporated the photosensitizer thionine into silicone elastomers.[21]

Similarly, Noimark et al. doped the photosensitizers acridine orange, methylene blue, and toluidine blue O, crystal violet, and malachite green into silicone elastomers.[22] These groups utilized a swell-encapsulation method to incorporate the dyes into the matrices. In both cases, the elastomers produced singlet oxygen, but the technique that was utilized to introduce the dyes has crucial drawbacks. The systems created by van Laar et al. were susceptible to leaching of the photosensitizer into surrounding media; the same issues are likely to exist for the systems produced by Noimark et al.[21,22]

van Laar et al. attempted to overcome the issue of leaching by utilizing swell encapsulation to incorporate the dye 5,15-(2,6-dichlorophenyl)-10,20-(4-allyloxyphenyl)porphyrin, and then covalently tethered the dye to the matrix by hydrosilylation using a hydride-terminated polydimethylsiloxane.[21] In a similar manner, Peveler et al. covalently attached BODIPY dyes to silicone elastomer surfaces. The $^1O_2$ produced by the BODIPY system was able to kill *S. aureus* and *E. coli*, highlighting the potential of $^1O_2$ generating silicone systems.[23] Unfortunately, these methods both require multistep syntheses to first make the photosensitizer and then graft it onto the elastomer surface.

Additionally, due to the incompatibility of the photosensitizers with silicone, a swell encapsulation step was needed to introduce the dyes before they could be covalently grafted into the matrix.[21,23] The system developed by Peveler et al. required an additional step, washing with copious amounts of solvent for 96 h to remove residual untethered dye. Although the untethered dye could be recycled, this ultimately challenges reproducibility of the method.

Two significant roadblocks remain in the development of $^1O_2$-releasing silicones: efficient incorporation of the photosensitizer, and reliable detection of $^1O_2$ at their air interfaces. Reliance on the swell-encapsulation technique is problematic, as this technique leads to defects in the material and irreproducible dispersions that lead to reduced performance in its intended application. The former challenge can easily be addressed by first derivatizing the photosensitizer with siloxane groups, such that it can be dispersed in

the silicone matrix simply by mechanical mixing; this technique was used effectively to create dielectric silicone elastomers.[24]

The direct detection of $^1O_2$ via phosphorescence has been the primary method for quantifying $^1O_2$ near material interfaces,[16,22,23] a technique that possesses several issues: the emission intensities of $^1O_2$ are weak; and, reliable detection requires sophisticated equipment.[25] A variety of indirect detection techniques reliant on absorbance or fluorescence of $^1O_2$ traps have been developed, including singlet oxygen sensor green (SOSG), 1,3-diphenylisobenzofuran (DPBF), anthracene dyes, uric acid and potassium iodide. These widely applied methods are incredibly powerful for entirely solution based systems[25,26] but have disadvantages that make them poorly suited to detecting $^1O_2$ from an interface. DPBF is photosensitive and rapidly degrades at the wavelengths necessary to activate porphyrins[27] and, in addition to acting as a trap for $^1O_2$, SOSG is independently able to produce $^1O_2$.[28] Uric acid has a host of issues associated with its use that can often lead to misinterpretation of the data and is most notably not a selective probe for singlet oxygen.[29] The detection of $^1O_2$ via reaction with KI to produce I_3^- has been successfully used to detect migration of singlet oxygen from polystyrene interfaces. Unfortunately this reaction simultaneously produces hydroxide anions which could damage silicone materials.[16,19]

An alternative $^1O_2$ detection system is electron paramagnetic resonance (EPR) spectroscopy. EPR is highly sensitive towards unpaired electrons, and has been widely used to identify paramagnetic substances and free radicals in technical sectors including mineralogy and the cosmetics industry.[30–33] EPR can be utilized to reliably evaluate $^1O_2$

production through an indirect method. EPR relies on using a spin trap such as 2,2,6,6-tetramethyl-4-piperidone, which reacts with $^1O_2$ to produce a persistent free radical that can then be detected and quantified using EPR. This technique has been applied extensively in solution systems. EPR detection of $^1O_2$ has several associated advantages over other methods. Provided the correct spin trap is selected it is selective for $^1O_2$.[34] EPR is far more sensitive than any absorbance-based technique and has been determined to be second only to the fluorescent assay SOSG in terms of sensitivity.[35,36] Additionally, unlike SOSG, the spin traps used in EPR do not produce their own singlet oxygen and are not themselves subject to photodegradation like absorption-based assays, which eliminates potential sources of error.[28,34] Previously, van Laar et al. successfully utilized EPR non-quantitatively for $^1O_2$ detection in silicone elastomers highlighting its potential for the detection of $^1O_2$ in silicone environments.[21]

The challenges associated with incorporating photosensitizers, including establishing how the incorporation method impacts $^1O_2$ generation, continue to impede the rational design of silicone ROS-generating antimicrobial coatings. Presented herein are the syntheses of two novel photosensitizers, via the Piers-Rubinsztajn (PR) reaction, that are compatible with silicone networks without the need of any solvent during processing and which can be incorporated either covalently or physically. A detailed quantitative investigation into their $^1O_2$ generating capabilities was performed using EPR. Both materials exhibit excellent $^1O_2$ generating abilities. However, a notable difference in capabilities exist between materials containing physically dispersed vs covalently incorporated dyes.

3.3 Experimental

3.3.1 Materials

5,10,15,20-(Tetra-3-methoxyphenyl)porphyrin (TPMP) was purchased from Porphychem, France. Zinc acetate 99.99% trace metal basis, tetraethyl orthosilicate (TEOS), activated Brockmann Activity I neutral aluminum oxide, Karstedt's catalyst (platinum(0) 1,3-divinyl-1,1,3,3-tetramethyldisiloxane complex solution (0.05 M in vinyl-terminated poly(dimethylsiloxane)), 2,2,6,6-tetramethyl-4-piperidone (4-oxo-TEMP), trimethoxybenzene, activated granular carbon, 4-14 mesh and deuterated chloroform ($CDCl_3$) were purchased from Sigma-Aldrich. Tris(pentaflurophenyl)borane ($B(C_6F_5)_3$, BCF) was purchased from Alfa-Aesar and was dissolved in dichloromethane to provide a stock solution of 10 mg mL^{-1}. Vinyl-1,1,3,3-tetramethyldisiloxane, pentamethyldisiloxane, α-monovinyl-ω-monohydride-terminated polydimethylsiloxane (DMS-HV15, 2000-3000 g/mol, 40-60 cSt) and hydride-terminated polydimethylsiloxane (DMS-H31, 28,000g mol^{-1}, 1000 cSt) and octamethylcyclotetrasiloxane (D_4) were purchased from Gelest. 4-oxo-TEMP was purified as previously described before use.[37] All other reagents were used without further purification. Solvents were purchased from Fischer Scientific. The Dual Asymmetric Centrifuge (DAC) Model DAC 150.1 FV7-K and FlackTek cups were purchased from FlackTek Inc. The four-sided 50, 100, 150 200 μm, 50 mm wide film applicator (3540 Bird Film Applicator: 50-100-150-200 μm) was purchased from Elcometer. The PR160-427nm lamp was purchased from Kessil.

3.3.2 NMR

^{1}H, ^{13}C, and ^{29}Si nuclear magnetic resonance (NMR) spectra were recorded on a Bruker NEO 600 magnet. In addition, multinuclear heteronuclear single quantum coherence (HSQC) and heteronuclear multiple bond correlation (HMBC) experiments were performed. $CDCl_3$ was used as the solvent in each case (δ ^{13}C = 77 ppm, δ ^{1}H = 7.26 ppm). Quantitative NMR analysis was performed using trimethoxybenzene as an internal standard.

3.3.3 Electrospray Ionization Mass Spectrometry

Electrospray ionization mass spectrometry (ESI-MS) was performed using an Agilent 6340 Ion Trap mass spectrometer. Sample concentrations were 50-100 μM.

3.3.4 MALDI-ESI

The molecular mass was determined using MALDI-TOF mass spectrometry (UltrafleXtreme, Bruker Daltonics, Billerica, MA, USA) in positive ion mode (linear detection). Dithranol was used as a matrix.

3.3.5 AFM

Atomic force microscopy (AFM) images were obtained using a Bruker Multimode AFM using ScanAsyst operating in PeakFore Tapping method. Scans were done at 0.2 Hz with 512 samples per line and a 25 μm square sample area.

3.3.6 UV-Vis and Fluorescence

UV-Vis spectra were obtained on a BioTek Syngery LX multi-mode reader. Fluorescence intensity measurements were obtained on a Biotek Cytation 5.

3.3.7 EPR

EPR measurements were conducted at room temperature on a Bruker EMXNano benchtop EPR spectrometer. The acquisition parameters were: microwave frequency = 9.62 GHz; modulation amplitude = 2.0 G; sweep width = 200 G; microwave power = 6.31 mW; number of scans = 10; and time constant = 20.5 ms. The resultant 4-oxo-TEMPO product concentration was obtained by utilizing the built-in SpinFit module in the Xenon software (by Bruker), where the experimental spectrum was fitted based on the pre-set 4-oxo-TEMPO simulation model. Triplicate measurements were performed (Figure 3.3).

3.3.8 Synthesis of $Si(Si_2O_2C_6H_{15})_4$ 1

TEOS (2.00 g, 9.60 mmol) and vinyl-1,1,3,3-tetramethyldisiloxane (9.24 g, 57.6 mmol) were added to a 500 mL uncapped round-bottomed flask and dissolved in toluene (100 mL). Tris(pentafluorophenyl)borane solution (0.01 mol%, 295 mL) was added and the reaction was stirred for 4 h. The solvent was removed in *vacuo*, and the resultant light-yellow oil was purified via FCC (flash chromatography) on alumina with hexanes to yield a colorless oil **1** (6.79 g, 9.31 mmol, 97%). ^{1}H NMR (600 MHz, $CDCl_3$) δ 6.13 (dd, 4H, J = 20.4, 14.8 Hz), 5.92 (dd, 4H, J = 14.8, 3.8 Hz), 5.74 (dd, 4H, J = 20.4 3.8 Hz), 0.16 (s, 24H), 0.09 (s, 24H). ^{13}C NMR (151 MHz, $CDCl_3$) δ 139.55, 131.18, 1.22, 0.49. ^{29}Si (119 MHz, $CDCl_3$) δ -3.93, -20.54, -109.75 ppm. ESI-MS: calc for $C_{24}H_{60}O_8Si_9NH_4$ $[M+NH_4]^+$, 746.2550; found 746.2547.

3.3.9 Synthesis of Zinc 5,10,15,20-(Tetra-3-methoxyphenyl)porphyrin (Zn-TPMP)

TPMP (5.00 g, 6.80 mmol) was added to a 2 L round-bottomed flask and dissolved in 1 L of chloroform:methanol mixture (1:1). Zinc acetate (2.50 g, 14.0 mmol) was added, and the

reaction mixture was stirred vigorously for 5 h. The solvent was removed in *vacuo* to yield a purple solid that was suspended in methanol and collected via vacuum filtration. The product was rinsed with water (3x100 mL) to remove excess zinc acetate and dried overnight to yield a purple solid (5.15, 6.45 mmol, 95%). ^{1}H NMR (600 MHz, $CDCl_3$) δ 8.99 (s, 8H), 7.82-7.77 (m, 8H), 7.63 (t, *J* = 7.7 Hz, 4H), 7.32-7.31 (m, 4H), 3.96 (s, 12H). ^{13}C NMR (151 MHz, $CDCl_3$) δ 157.94, 150.29, 144.28, 132.17, 127.76, 127.48, 121.04, 120.50, 113.60, 55.64 ppm. ESI-MS: calc. for $C_{48}H_{36}N_4O_4Zn$, 796.2028 $[M]^+$; found, 796.2026. λ_{max} (DCM)= 420 nm

3.3.10 Synthesis of Zn-TPMP-HV15 2

Zn-TPMP (3.50 g, 4.40 mmol) was added to a 500 mL round-bottomed flask and dissolved in toluene (100 mL), DMS-HV15 (75.0 g, 17.7 mmol) was added. Tris(pentaflurophenyl)borane solution (2 mol%, 18 mL) was added dropwise. The reaction was stirred for 4 h and the solvent was removed in *vacuo* to yield a purple oil **2**, the oil was purified by FCC on alumina with hexanes to yield a purple oil (20 g, M_n (NMR) = ~18,000 g mol^{-1}). ^{1}H NMR (600 MHz, $CDCl_3$) δ 8.98 (s, 8H), 7.83-7.79 (m, 8H), 7.36-7.35 (m, 8H), 6.13 (dd, 4H, *J* = 20.4, 14.8 Hz), 5.94 (dd, 4H, *J* = 14.8, 3.8 Hz), 5.74 (dd, 4H, *J* = 20.4, 3.8 Hz), 0.36-0.35 (m, 24H), 0.18-0.01 (m, 1380H). ^{13}C NMR (151 MHz, $CDCl_3$) δ 153.04, 150.31, 144.37, 139.56, 132.11, 131.82, 128.67, 127.46, 126.78, 120.87, 120.88, 1.49, 1.35, 1.24, 0.99, 0.46, 0.11. ^{29}Si (119 MHz, $CDCl_3$) -4.12, -13.08, -20.57, -20.92, -21.65 -21.96 ppm. λ_{max} (DCM)= 420 nm, λ_{max} (D_4)= 415 nm

3.3.11 Synthesis of Zn-TPMP-Penta 3

Zn-TPMP-HV15 (2.00 g, 0.110 mmol) was added to a 50 mL round-bottomed flask and dissolved in toluene (25 mL). Pentamethyldisiloxane (100 mg, 0.7 mmol) and Karstedt's catalyst (2.0 mL, 0.10 mmol) was added. The reaction was stirred overnight, after which activated charcoal (0.5 g) was added and the reaction was stirred for an additional 12 h. The reaction was filtered through Celite and the solvent was removed in *vacuo* to yield a purple oil **3** (1.95 g, M_n (NMR)= 18,000 g/mol). ^{1}H NMR (600 MHz, $CDCl_3$) δ 8.97 (s, 8H), 7.82-7.78 (m, 8H), 7.57 (t, 4H, *J* = 7.9Hz), 7.35-7.35 (m, 4H), 0.42 (s, 16H), 0.35-0.34 (m, 24H), 0.17-0.09 (m, 1516H). ^{13}C NMR (151 MHz, $CDCl_3$) δ 153.01, 150.29, 144.36, 132.09, 128.64, 127.43, 126,76, 120.86, 119.28, 9.81, 9.72, 2.16, 1.57,1.37, 1.27, 0.98, 0.12, 0.21, 0.366. ^{29}Si (119 MHz, $CDCl_3$) 8.37, 8.34, 6.99, -13.08, -20.58, -21.66 ppm. λ_{max} (DCM)= 420 nm, λ_{max} (D_4)= 415 nm

3.3.12 General Procedure for Preparation of Silicone Elastomers

The appropriate amounts of DMS-H31, $Si(Si_2O_2C_6H_{15})_4$, Zn-TPMP-HV15, or Zn-TPMP-Penta, as detailed in Tables S1 and S2, were added to 40 mL FlackTek cups and mixed at 3500 rpm for 5 min in a DAC to provide stock elastomer solutions with concentrations of 1×10^{-3}, 1×10^{-4}, and 1×10^{-5} M, respectively. Stock elastomer solutions (10 g) were transferred to 10 mL FlackTek cups to which Karstedt's catalyst (0.5-1 mL, 2.5×10^{-2}- 5.0 $x10^{-2}$ mmol) was added before the solutions were mixed at 3500 rpm for an additional 1 min. After mixing, a four-sided bird film applicator was used to prepare thin films (~200 μm) for $^{1}O_2$ studies. Thin films were placed in an oven to cure for 5 h at 50 °C. After curing, thin films were punched from the film with a 16 mm (5/8") diameter cutting dye and

transferred to 12-well black-walled plates, before being used in $^1O_2$ EPR studies. Additional samples, ~1 mm thick, were prepared using the same procedure but were cured in 10 mL FlackTek cups.

3.3.13 Leaching Studies

Elastomers – were placed in 20 mL scintillation vials and 2 mL of ethanol or PBS buffer was added. The supernatant was analyzed at 10 min and 12 h by UV-Vis for the presence of Zn-TPMP-HV15 or Zn-TPMP-Penta.

3.3.14 Preparation of Spin-Trap Solution for Detection of 1O2 via EPR

4-oxo-TEMP (7.76 g, 0.5 mol) was dissolved in 95% ethanol (500 mL) to provide a 100 mM stock solution.

3.3.15 Detection of $^1O_2$ via EPR

Elastomer surfaces in 12-well plates were rinsed with IPA (3x3 mL) to remove unbound porphyrin and dried before being covered with fresh 4-oxo-TEMP solution in (1 mL) and irradiated with a Kessil PR160-427 nm lamp tuned to 25% intensity, 3 cm above the surface of the sample, for an average intensity of 55.5 mW/cm^2. Measurements were taken at predetermined time intervals (2, 4, 6, and 8 and 10 min), then turning off lamp and transferring 100 mL of the solution to an EPR tube (4 mm outer diameter)

3.4 Results and Discussion

3.4.1 Synthesis of Zn-TPMP-Penta 3

The synthesis of $Si(Si_2O_2C_6H_{15})_4$ proceeded cleanly at room temperature via the Piers-Rubinsztajn reaction[38] in an excellent yield of 97% (Figure 3.1). It was necessary to

perform the reaction in a large volume flask left uncapped to accommodate the generation of ethane.

It was noted that a slight excess (1.5 eq.) of vinyl-1,1,3,3-tetramethyldisiloxane was needed to consume TEOS entirely. Residual vinyl-1,1,3,3-tetramethyldisiloxane was easily removed via FCC on alumina and was not observed in the final product. Analysis of the spectral data obtained for the product was consistent with the structure shown in Figure 3.1. Peaks corresponding to the ethoxy groups of TEOS were absent from both the ^{1}H and ^{13}C NMR, confirming 100% conversion of the TEOS, while signals present at 6.13-5.74 ppm in ^{1}H NMR and 139.55 and 131.18 ppm in ^{13}C NMR are consistent with the presence of vinyl groups. Finally, ^{29}Si NMR showed three peaks at -3.93, -20.54, and -109.25, corresponding to the M (Me_3SiO), D ($Me_2SiO_{2/2}$), and Q ($SiO_{4/2}$) units, respectively, of the product.

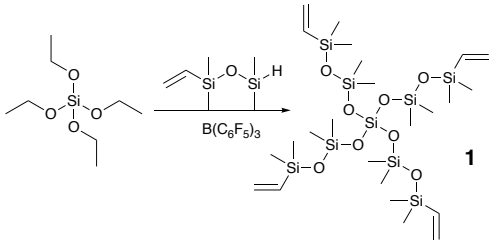

Figure 3.1: Synthesis of $Si(Si_2O_2C_6H_{15})_4$ 1 via the PR reaction.

3.4.2 Syntheses and Characterization of Zn-TPMP-HV15 and Zn-TPMP-Penta

3.4.2.1 Zn-TPMP-HV15 2

Zn-TPMP-HV15 **2** was synthesized using the PR reaction in a similar manner to the previously described Zn-TPMP-Bis-H.[24] Unlike simpler aromatic molecules such as eugenol[39] and dimethoxybenzene,[40] which require as little as 0.01 mol% catalyst, the PR

reaction of Zn-TPMP to produce Zn-TPMP-HV15 **2** required a significantly higher catalyst loading – 2 mol% – before the reaction occurred (Figure 3.2B). At this catalyst loading, the reaction proceeded in a manner typical of all PR reactions; bubbling of the solution was noted after a brief induction period, 5-10 min, accompanied by an exotherm followed by the rapid release of methane. Residual, DMS-HV15 polymer was noted in the ^{1}H NMR and removed using FCC on alumina with 100% hexanes; 20 g of a purple oil was retrieved after removing the solvent.

Analysis of the product with ^{1}H NMR indicated 100% loss of the methoxy groups, as well as the presence of signals in the region of 6.13-5.74 ppm, indicating the presence of vinylic protons, signals at 139.56 and 131.82 ppm consistent with vinylic carbons, as well as the absence of a peak at 55.64 ppm in the ^{13}C NMR spectrum corresponding to the methoxy carbon in the starting material. However, in both the ^{13}C and ^{29}Si NMR results, additional peaks not consistent with the reported structure were observed. Five additional signals at 1.49, 1.35, 0.99, 0.46, and -0.11 ppm were noted in the ^{13}C NMR spectrum, while three additional signals at -20.57, -20.92, and -21.65 were noted in the ^{29}Si NMR data (Figure 6.31-6.33). Further investigation using ^{1}H-^{13}C HSQC/HMBC and ^{1}H-^{29}Si HMBC methods confirmed that these signals represent carbon and silicon atoms in slightly different environments on the polymer chain, as these signals only showed interactions with the signal at 0.18-0.01 ppm corresponding to the Si-CH_3 protons of the polymer chain (Figure 6.34-6.36). Analysis of the starting polymer, DMS-HV15 confirmed that these peaks are present prior to the reaction and do not arise due to unidentified side reactions (Figure 6.45-6.47).

End group analysis by NMR of Zn-TPMP-HV15 provided an M_n of 17,690 g mol^{-1}. Further analysis of the product by MALDI-ESI (Figure 6.37) indicated a molecular weight consistent with that calculated by end group analysis, as a broad signal centered around 15,000 g mol^{-1} was detected.[41] Quantitative NMR using trimethoxybenzene as an internal standard was used as a tertiary method for the calculation of the molecular weight and provided a molecular weight of 17,740 g mol^{-1}, in close agreement with that calculated by end group analysis and MALDI.

3.4.2.2 Zn-TPMP-Penta 3

Zn-TPMP-Penta **3** was synthesized via the hydrosilylation of Zn-TPMP-HV15 with pentamethyldisiloxane (Figure 3.2C). Careful purification of Zn-TPMP-Penta was essential to remove as much residual Pt catalyst as possible, as trace amounts of catalyst dramatically impacted the cure time of the elastomer formulations using Zn-TPMP-Penta. Similar to Zn-TPMP-HV15, additional signals not consistent with the reported structure were observed in the ^{13}C and ^{29}Si NMR. Further spectroscopic analysis using ^{1}H-^{13}C HSQC/HMBC and ^{1}H-^{29}Si HMBC confirmed that these peaks represent carbon and silicon atoms in slightly different environments on the polymer chains, originating from the starting polymer. A broad signal centered around 15,000 g mol^{-1} was detected using MALDI; quantitative NMR placed the molecular weight ~18,255 g mol^{-1}.

3.4.3 Preparation of Elastomers

Preliminary studies allowed the optimization of crosslink density for the silicone films, which were chosen to provide materials that were sufficiently robust to be cast as thin films or, for example, as tubes. Silicone elastomers are typically strengthened with

reinforcing silica fillers, but these were avoided here to ensure that the filler did not scatter the blue light used to activate the porphyrin. Desirable properties were obtained using platinum-catalyzed hydrosilylation cure of commercially available hydride-terminated PDMS (28,000 g mol^{-1}) and the crosslinker $Si(Si_2O_2C_6H_{15})_4$ **1** in a 1:1 stochiometric ratio of vinyl:Si-H. These materials were chosen because: the vinyl groups in **1** are not sterically encumbered and react at similar rates to vinyl groups in **2**; both thin and thick films were readily prepared and were easily handled.

This system allowed for precise control over the photosensitizer concentration. The crosslink density was fixed by controlling the quantities **1** and **2** added, both of which are tetrafunctional crosslinkers, without changing the final ratio of vinyl/Si-H. The photosensitizer concentration was then controlled by the net quantity of **2** or **3** placed in the pre-elastomer and then cured (Figure 3.2D and E,Table 6.6-6.7). Zn-TPMP-HV15 **2** and Zn-TPMP-Penta **3** showed excellent compatibility with the silicone pre-elastomer formulation and required no additional solvent to facilitate their incorporation. Preliminary tests indicated mixing by hand was sufficient to incorporate the photosensitizers. However, to ensure consistency between batches, a speed-mixer was used. Using this methodology, elastomers containing 1×10^{-3}, 1×10^{-4}, and 1×10^{-5} M were prepared. Note that, by contrast, all previous photosensitizers evaluated required the assistance of solvent to be incorporated into silicone formulations.[21–23]

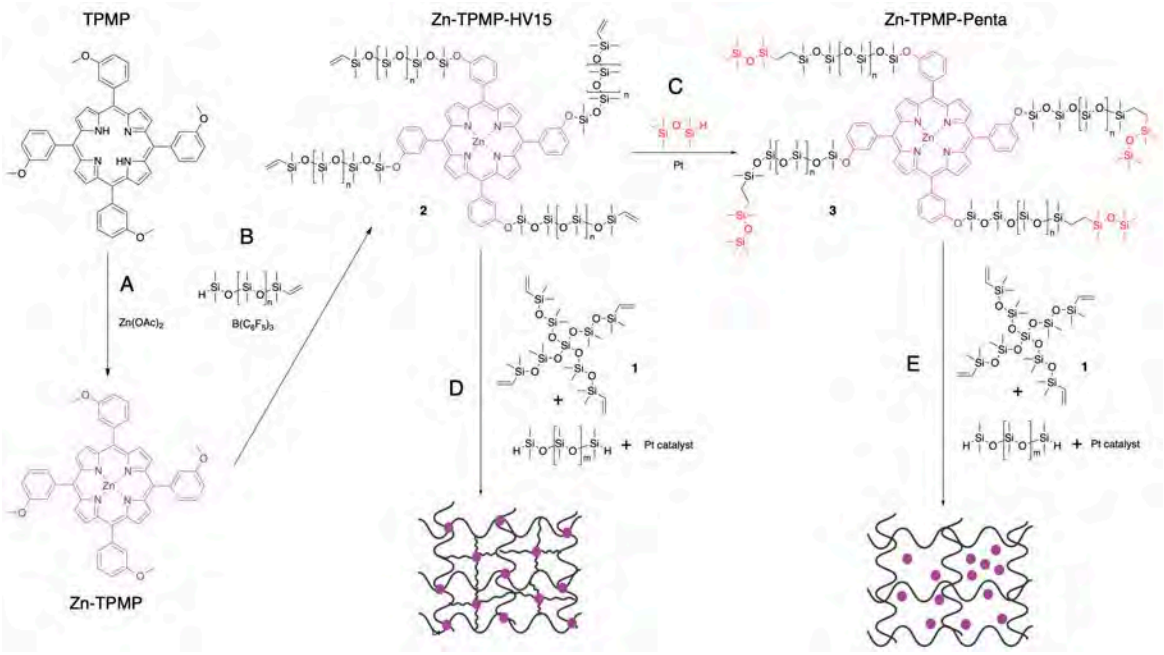

Figure 3.2: :A) Synthesis of Zn-TPMP. B) Synthesis of Zn-TPMP-HV15. C) Synthesis of Zn-TPMP-Penta. D) Synthesis of Zn-TPMP-HV15 covalent elastomers. E) Synthesis of Zn-TPMP-Penta physically dispersed elastomers. Pt=Karstedt's catalyst.

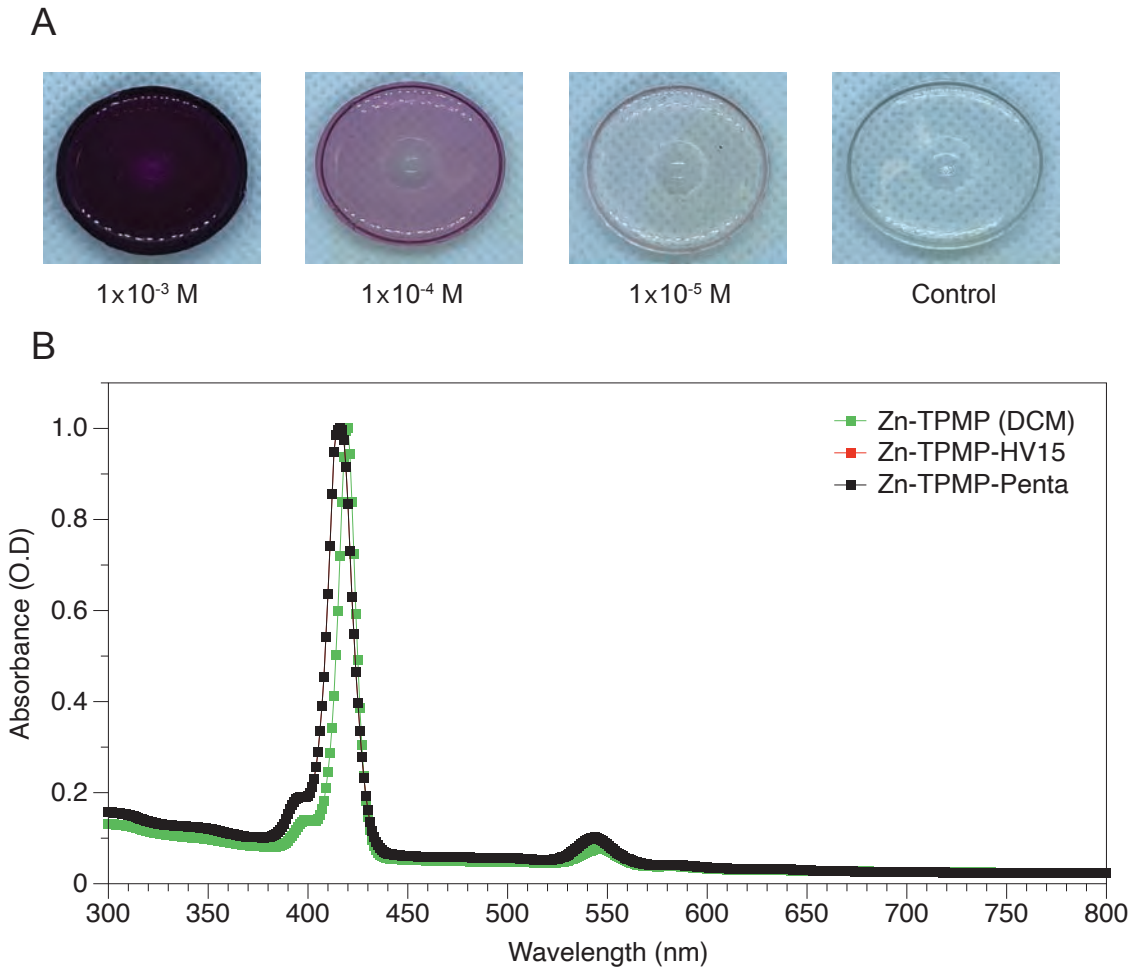

Figure 3.3: A) Representative images of elastomers prepared (~ 1 mm thick x 3 cm diameter). B) UV-Vis of HV15 and HV15-Penta when incorporated into elastomers and Zn-TPMP in DCM.

Following catalyst addition, surface cure was noted within 1 h with complete cure achieved after 2-3 h. To maintain consistency, all samples were cured at 50 °C for 5 h. Elastomers possessed a characteristic purple color (Figure 3.3A). UV-Vis of the elastomers showed a Soret band at 416 nm. This represents a 4 nm shift from the Soret band of the porphyrins in DCM, but is consistent with the UV-Vis of Zn-TPMP-HV15 in D_4. These data are consistent with previous studies which indicate that only modifications of the

porphyrin periphery by groups that extend the conjugation result in significant changes to the UV-Vis (Figure 3.3B).[42]

It is well established that, even with its short lifetime, $^1O_2$ can migrate ~100 nm in polymer systems.[16,43] Therefore, films should be as thin as possible to maximize the quantity of $^1O_2$ able to migrate to the interface where pathogen killing can occur. Materials thicker than 100 nm are still capable of generating $^1O_2$ but only the first 100 nm can be considered active to external media. The need for thin samples must also be balanced with the mechanical integrity of the film. Attempts to cast thin films below 200 μm were not successful; the films were easily torn during the preparation process necessary to measure the $^1O_2$ production. Therefore, elastomers were prepared using a casting blade set to 200 μm. When fully cured, the average elastomer thicknesses were between 100-125 μm, except for the control, which was slightly thicker at 170 μm (Table 6.8). These samples could be handled and transferred to 24 black-walled plates after curing.

Using the same formulations, elastomers were prepared at 1 mm thicknesses for extraction. These samples were immersed for 12 hours in PBS buffer to mimic a biological environment. This cycle was repeated three times with fresh PBS buffer between each cycle. No mass loss was observed after these extraction cycles and no porphyrin could be detected by UV-Vis in the aqueous supernatant at either 10 minutes or 12 h. The same procedure was used for samples immersed in ethanol. In this case, UV-Vis of the supernatants showed no signs of Zn- TPMP-HV15 or Zn-TPMP-Penta after 10 minutes. After 12 hours only trace amounts could be detected by UV-Vis, and only in the first extraction cycle. As a precaution all samples were rinsed with ethanol before being utilized

in $^1O_2$ generation studies. The use of an organic solvent such as DCM could extract almost all of the porphyrin from Zn-TPMP-Penta elastomers but. Zn-TPMP-HV15 showed no leaching.

3.4.4 $^1O_2$ Generation

The conversion of 4-oxo-TEMP to 4-oxo-TEMPO was used to indirectly monitor $^1O_2$ delivery at elastomer interfaces using EPR. Elastomers in 24-well plates were covered in 0.5 mL of 0.1 M 4-oxo-TEMP in 95% ethanol and exposed to a 427 nm light source for 2, 4, 6, 8, and 10 min. A portion of the solution (100 μL) was then transferred to an EPR tube and analyzed for the presence of 4-oxo-TEMPO.

As expected, control samples containing no photosensitizer failed to produce any $^1O_2$, as indicated by the absence of an observable 4-oxo-TEMPO signal in the EPR spectra. All samples containing the photosensitizers Zn-TPMP-HV15 and Zn-TPMP-Penta produced $^1O_2$ (Figure 3.3). The $^1O_2$ generation capabilities were shown to depend on three criteria: irradiation time; photosensitizer concentration; and method of incorporation of photosensitizer into the elastomer.

Elastomers with three porphyrin concentrations were evaluated: 1×10^{-3}; 1×10^{-4}; and 1×10^{-5} M. Films prepared using Zn-TPMP-HV15 generally produced more 4-oxo-TEMPO at higher photosensitizer concentrations. When HV15 silicone elastomer samples were irradiated for 6 min, subsequent analysis of the 4-oxo TEMP/4-oxo-TEMPO solution by EPR showed photosensitizer conc. of 1×10^{-3} M → 6.8×10^{-7} M 4-oxo-TEMPO; 1×10^{-4} → 4.3×10^{-7} 4-oxo-TEMPO, and 1×10^{-5} M → 1.3×10^{-7} M, 4-oxo-TEMPO, respectively. These differences reflect higher $^1O_2$ production at higher photosensitizer concentrations.[44]

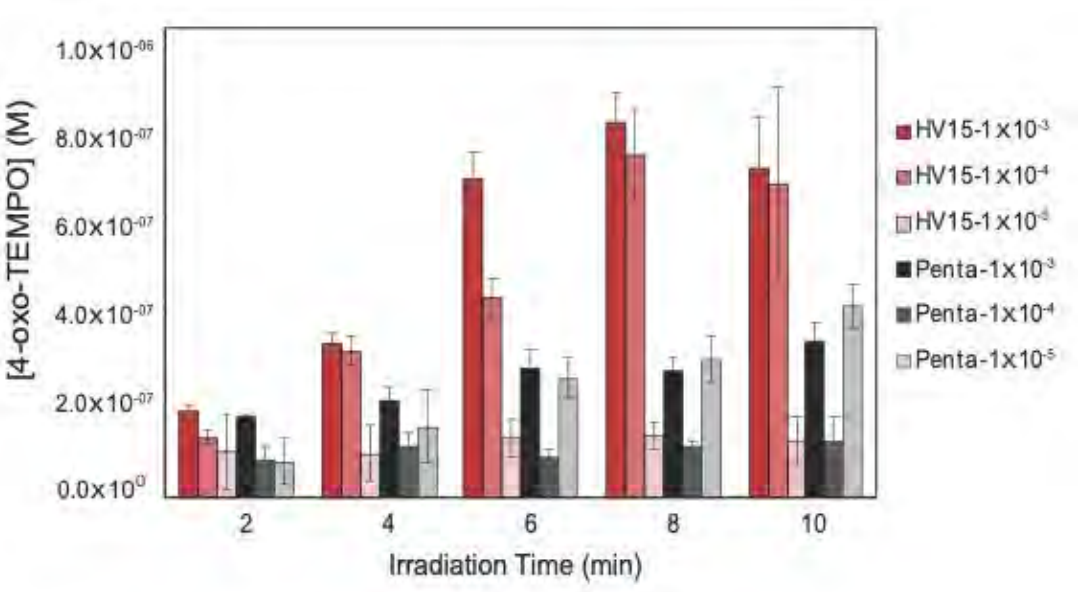

Figure 3.4: Production of 4-oxo-TEMPO by Zn-TPMP-HV15 (red series – labelled as HV15) and Zn-TPMP-Penta (black series – labelled as Penta) elastomers.

The 4-oxo-TEMPO production for 1×10^{-5} M samples plateaued immediately after 2 min due to photobleaching of the porphyrin, which resulted in complete degradation of the porphyrin after 2 minutes at this concentration, as indicated by the absence of a Soret band at 416 nm (Figure 6.55). Eventually, a plateau in 4-oxo-TEMPO production for 1×10^{-3} and 1×10^{-4} M films was also reached at 8 and 10 min, respectively, but complete photodegradation of the porphyrin was not observed (Figure 6.53-6.54). In these cases, a decrease in the Soret band at 416 nm was noted along with the appearance of a new peak at 490 nm. This is consistent with the porphyrin undergoing photomodification, as opposed to true photobleaching that results in complete loss of absorbance in the visible region.[45] Rather, in this case the plateau likely reflects the finite amount of oxygen in the elastomers available to react with the excited photosensitizer.[46]

Unlike Zn-TPMP-HV15, the influence of Zn-TPMP-Penta concentration on $^1O_2$ production was not readily apparent. Initially, it was hypothesized that Zn-TPMP-Penta samples would perform better than Zn-TPMP-HV15 samples. This theory was based on previous observations which indicated that siloxane-modified porphyrins that are not covalently incorporated into the network have a tendency to migrate to the air interface.[24] It was expected that this tendency would result in a greater initial concentration of photosensitizer at the interface, minimizing the distance produced $^1O_2$ would have to migrate, and maximizing $^1O_2$ release. Additionally, this should serve as a method to replenish photodegraded porphyrin.

All Zn-TPMP-Penta films produced *lower* amounts of 4-oxo-TEMPO than their Zn-TPMP-HV15 counterparts (Figure 3.3). Unlike Zn-TPMP-HV15 samples, a clear trend between 4-oxo-TEMPO and photosensitizer concentrations could not be observed. In fact, 1×10^{-3} and 1×10^{-5} M Zn-TPMP-Penta films had comparable $^1O_2$ production capabilities, as evidenced by the almost identical 4-oxo-TEMPO concentrations in the reactive solution, while 1×10^{-4} Zn-TPMP-Penta films, like the films prepared with a concentration of 1×10^{-5} Zn-TPMP-HV15, quickly reached a plateau in 4-oxo-TEMPO concentration after 2 min.

These trends are not be explained by photobleaching of the photosensitizer. After 10 min, 1×10^{-3} and 1×10^{-5} M films still showed a Soret band, with a reduced intensity, at 416 nm in the UV-Vis spectra along with a new peak at 490 nm, while 1×10^{-5} M films showed no porphyrin after 2 min. Instead, the reduced $^1O_2$ production and conflicting concentration trends between Zn-TPMP-HV15 and Zn-TPMP-Penta were determined to be due to aggregation of Zn-TPMP-Penta in the elastomer.

Aggregation of porphyrins in solution leads to quenching of the excited state and is known to cause decreased $^1O_2$ production. Typically, aggregation is readily detected by UV-Vis spectroscopy, as H and J-aggregates cause blue and red shifts, respectively.[47] However, neither Zn-TPMP-HV15 or Zn-TPMP-Penta elastomers exhibited a red or blue shift when compared to one another (Figure 3.3B). We attribute this to the fact that the measurements are being made in a polymeric elastomer; detection of aggregates is more complicated because the polymer plays a critical role in facilitating aggregation.

Kalachyova et al. extensively studied the aggregation behavior of *meso*-tetraphenylporphyrin physically dispersed in poly(methyl methacrylate) and provided an excellent framework for monitoring aggregation in polymer matrices.[48] They determined that the PMMA matrix played a critical role in causing porphyrin aggregation, proposing that the polymer chains extruded the unmodified porphyrin from the bulk to the surface of the polymer where they aggregated. This behavior was only induced above a certain activation energy, which could be provided by sintering the samples at elevated temperatures above the T_g of PMMA. In these cases, UV-Vis was still a powerful tool for initially detecting aggregation, but as aggregates become larger the technique failed and a combination of AFM and fluorescence spectroscopy was needed to monitor aggregation.[48]

The challenges associated with using UV-Vis to detect aggregation in polymer matrices are exacerbated in the case of silicone elastomers due to their unique physicochemical properties. As a consequence of the large Si-O-Si bond angle (~145°), silicone backbones are highly flexible and have low T_gs, typically <-120 °C.[19] The modification of Zn-TPMP with polysiloxanes imparted these unique properties of silicones

to the porphyrin, as evidenced by their liquid state at room temperature and readily dissolution in silicone formulations. The high mobility imparted by the silicone chains at room temperature facilitates the aggregation process such that small aggregates are never detected by UV-Vis – they become too large. We previously observed aggregation of a similar physically dispersed siliconized photosensitizer using optical microscopy, but at much higher concentrations (5.0×10^{-2} - 7.0×10^{-2} M).[24] In the case of Zn-TPMP-HV15 and Zn-TPMP-Penta, optical microscopy was not sensitive enough due to the low concentrations used. Instead, a combination of microscopy and fluorescence intensity measurements were utilized here.

Fluorescence intensity measurements confirmed the presence of aggregates in Zn-TPMP-Penta. Films containing Zn-TPMP-Penta suffered from fluorescence quenching when compared to Zn-TPMP-HV15 films of equivalent concentrations. The film containing 1×10^{-3} M of Zn-TPMP-Penta had only a marginal decrease in intensity relative to its Zn-TPMP-HV15 counterpart, the films containing 1×10^{-4} and 1×10^{-5} M of Zn-TPMP-Penta showed significant fluorescence quenching when compared to their counterparts (Figure 3.5). This is in line with previous observations which suggest that above a porphyrin concentration of 10 μ M the type and extent of aggregation becomes difficult to detect via fluorescence.[49] In our case this concentration coincides with the point at which the fluorescence response is no longer linear (Figure 6.51). Instead, AFM was successfully used to probe for aggregates; films with the highest photosensitizer concentration were used. A largely featureless surface for Zn-TPMP-HV15 was observed. By comparison, the Zn-TPMP-Penta film had unique features – aggregates ~ 80 nm high and – that were not

present in Zn-TPMP-HV15 but are similar to those previously observed under optical microscopy (Figure 6.52).

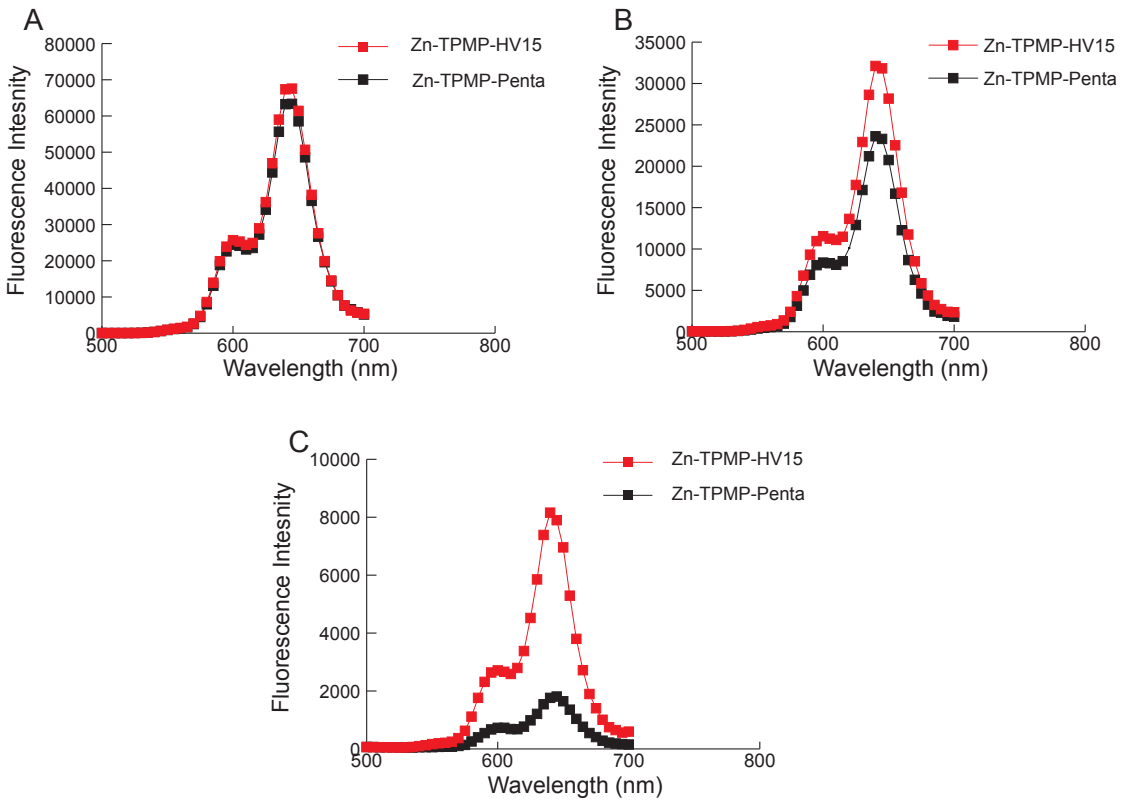

Figure 3.5: Fluorescence scans of two porphyrins with different concentration in cast films A) 1×10^{-3} B) 1×10^{-4} C) 1×10^{-5}.

These aggregates quenched $^1O_2$ production and resulted in the reduced 4-oxo-TEMPO concentrations observed (Figure 3.3). Since the formation of the aggregates cannot be controlled, this helps to explain the lack of a trend between Zn-TPMP-Penta concentration and $^1O_2$ production. It is conceivable that different areas of the film had different degrees of aggregation, leading to the poor reproducibility observed with the Zn-TPMP-Penta samples.

Tethered Zn-TPMP-HV15 samples do not suffer from these issues, as the aggregation of the porphyrin is avoided or minimized by covalently immobilizing the photocatalyst in the elastomer, which fixes it in space. A similar effect has been observed when photosensitizers have been immobilized on solid supports such as SiO_2 and aggregation has been proposed to play a role in elastomeric systems, although this has not yet been definitively proven.

The results obtained in this study provide a base for the rational design of $^1O_2$-producing silicones for use in biomedical devices. Singlet oxygen generated from tethered photosensitizers is able to migrate through the silicone elastomer, which itself is highly resistant to oxidation. The concentrations of $^1O_2$ released from the Zn-TPMP-HV15 series of materials exceed those of surfaces known to be able to destroy surface-bound pathogens. It will now be necessary to demonstrate that the $^1O_2$ released from these materials can kill bacteria in biological media.

3.5 Conclusions

The derivatization of the porphyrin Zn-TPMP via the Piers-Rubinsztajn reaction with DMS-HV15 provides a photosensitizer that can either be covalently incorporated or, with an additional synthetic step, physically dispersed in silicone elastomers. These photosensitizers can be incorporated without the assistance of solvent, creating a reproducible alternative to the previously used swell-encapsulation technique. Covalent immobilization of the photosensitizer minimizes aggregation-induced $^1O_2$ quenching, leading to higher efficiency of $^1O_2$ release. These materials and the investigation of their singlet oxygen-generating capabilities via EPR advance a step further towards the rational design of $^1O_2$ generating silicone antimicrobial coatings.

3.6 Acknowledgments

The authors acknowledge with gratitude the financial support of the National Sciences and Engineering Research Council of Canada and Suncor Energy. We thank Dr. Kalina Ranguelova (Bruker) for her useful discussions on EPR, and Hamza Khattak and Dr. Kari Dalnoki-Veress (McMaster University) for their assistance with AFM.

3.7 References

1 J. Elvy and A. Colville, *J. Infect. Prev.*, 2009, **10**, 36–41.

2 R. C. L. Feneley, I. B. Hopley and P. N. T. Wells, *J. Med. Eng. Technol.*, 2015, **39**, 459–470.

3 F. Abbasi, H. Mirzadeh and A.-A. Katbab, *Polym. Int.*, 2001, **50**, 1279–1287.

4 G. Garg, N. Chawla, A. Gogia and A. Kakar, *J. Fam. Med. Prim. Care*, 2016, **5**, 539–542.

5 R. M. Klevens, J. R. Edwards, C. L. Richards, T. C. Horan, R. P. Gaynes, D. A. Pollock and D. M. Cardo, *Public Health Rep.*, 2007, **122**, 160–166.

6 B. W. Trautner and R. O. Darouiche, *Am. J. Infect. Control*, 2004, **32**, 177–183.

7 R. Roy, M. Tiwari, G. Donelli and V. Tiwari, *Virulence*, 2018, **9**, 522–554.

8 P. Ramritu, K. Halton, P. Collignon, D. Cook, D. Fraenkel, D. Battistutta, M. Whitby and N. Graves, *Am. J. Infect. Control*, 2008, **36**, 104–117.

9 N. Poulter, K. Vasilev, S. S. Griesser and H. J. Griesser, in *Biomaterials Associated Infection: Immunological Aspects and Antimicrobial Strategies*, eds. T. F. Moriarty, S. A. J. Zaat and H. J. Busscher, Springer, New York, NY, 2013, pp. 355–378.

10 M. R. Hamblin and T. Hasan, *Photochem. Photobiol. Sci.*, 2004, **3**, 436–450.

11 F. Cieplik, D. Deng, W. Crielaard, W. Buchalla, E. Hellwig, A. Al-Ahmad and T. Maisch, *Crit. Rev. Microbiol.*, 2018, **44**, 571–589.

12 F. Vatansever, W. C. M. A. de Melo, P. Avci, D. Vecchio, M. Sadasivam, A. Gupta, R. Chandran, M. Karimi, N. A. Parizotto, R. Yin, G. P. Tegos and M. R. Hamblin, *FEMS Microbiol. Rev.*, 2013, **37**, 955–989.

13 H. Mahmoudi, A. Bahador, M. Pourhajibagher and M. Y. Alikhani, *J. Lasers Med. Sci.*, 2018, **9**, 154–160.

14 A. Lanzilotto, M. Kyropoulou, E. C. Constable, C. E. Housecroft, W. P. Meier and C. G. Palivan, *JBIC J. Biol. Inorg. Chem.*, 2018, **23**, 109–122.

15 T. Maisch, J. Baier, B. Franz, M. Maier, M. Landthaler, R.-M. Szeimies and W. Bäumler, *Proc. Natl. Acad. Sci.*, 2007, **104**, 7223–7228.

16 A. Felgenträger, T. Maisch, A. Späth, J. A. Schröder and W. Bäumler, *Phys. Chem. Chem. Phys.*, 2014, **16**, 20598–20607.

17 M. C. DeRosa and R. J. Crutchley, *Coord. Chem. Rev.*, 2002, **233–234**, 351–371.

18 J. Shang, M. Chai and Y. Zhu, *Environ. Sci. Technol.*, 2003, **37**, 4494–4499.

19 M. A. Brook, *Silicon in Organic, Organometallic, and Polymer Chemistry*, Wiley, 1999.

20 J. Curtis and A. Colas, in *Biomaterials Science (Third Edition)*, eds. B. D. Ratner, A. S. Hoffman, F. J. Schoen and J. E. Lemons, Academic Press, 2013, pp. 1106–1116.

21 F. M. P. R. van Laar, F. Holsteyns, I. F. J. Vankelecom, S. Smeets, W. Dehaen and P. A. Jacobs, *J. Photochem. Photobiol. Chem.*, 2001, **144**, 141–151.

22 S. Noimark, E. Salvadori, R. Gómez-Bombarelli, A. J. MacRobert, I. P. Parkin and C. W. M. Kay, *Phys. Chem. Chem. Phys.*, 2016, **18**, 28101–28109.

23 W. J. Peveler, S. Noimark, H. Al-Azawi, G. B. Hwang, C. R. Crick, E. Allan, J. B. Edel, A. P. Ivanov, A. J. MacRobert and I. P. Parkin, *ACS Appl. Mater. Interfaces*, 2018, **10**, 98–104.

24 C. B. Gale, M. A. Brook and A. L. Skov, *RSC Adv.*, 2020, **10**, 18477–18486.

25 Y. You, *Org. Biomol. Chem.*, 2018, **16**, 4044–4060.

26 Y. Zhao, Y. Liu, Q. Xu, M. Barahman, D. Bartusik, A. Greer and A. M. Lyons, *J. Phys. Chem. A*, 2014, **118**, 10364–10371.

27 X.-F. Zhang and X. Li, *J. Lumin.*, 2011, **131**, 2263–2266.

28 X. Ragàs, A. Jiménez-Banzo, D. Sánchez-García, X. Batllori and S. Nonell, *Chem. Commun.*, 2009, 2920–2922.

29 M. Bregnhøj, L. Dichmann, C. K. McLoughlin, M. Westberg and P. R. Ogilby, *Photochem. Photobiol.*, 2019, **95**, 202–210.

30 J. Götze, M. Plötze, H. Fuchs and D. Habermann, *Mineral. Mag.*, 1999, **63**, 149–163.

31 S. B. Lohan, A.-C. Lauer, S. Arndt, A. Friedrich, K. Tscherch, S. F. Haag, M. E. Darvin, H. Vollert, A. Kleemann, I. Gersonde, and others, *Cosmetics*, 2015, **2**, 286–301.

32 N. V. Blough, *Environ. Sci. Technol.*, 1988, **22**, 77–82.

33 A. B. dos Santos, D. H. S. Silva, V. da S. Bolzani, L. Ã. Santos, T. M. Schmidt and O. Baffa, *J. Braz. Chem. Soc.*, 2009, **20**, 1483–1492.

34 B. Li, H. Lin, D. Chen, B. C. Wilson and Y. Gu, *J. Innov. Opt. Health Sci.*, 2012, **06**, 1330002.

35 K. Nakamura, K. Ishiyama, H. Ikai, T. Kanno, K. Sasaki, Y. Niwano and M. Kohno, *J. Clin. Biochem. Nutr.*, 2011, **49**, 87–95.

36 H. Wu, Q. Song, G. Ran, X. Lu and B. Xu, *TrAC Trends Anal. Chem.*, 2011, **30**, 133–141.

37 W. C. Dunlap, Y. Yamamoto, M. Inoue, M. Kashiba-Iwatsuki, M. Yamaguchi and K. Tomita, *Int. J. Cosmet. Sci.*, 1998, **20**, 1–18.

38 M. A. Brook, *Chem. – Eur. J.*, 2018, **24**, 8458–8469.

39 S. E. Laengert, A. F. Schneider, E. Lovinger, Y. Chen and M. A. Brook, *Chem. – Asian J.*, 2017, **12**, 1208–1212.

40 A. F. Schneider, E. K. Lu, G. Lu and M. A. Brook, *J. Polym. Sci.*, 2020, **58**, 3095–3106.

41 S. Servaty, W. Köhler, W. H. Meyer, C. Rosenauer, J. Spickermann, H. J. Räder, G. Wegner and A. Weier, *Macromolecules*, 1998, **31**, 2468–2474.

42 Q. Arooj, G. J. Wilson and F. Wang, *RSC Adv.*, 2016, **6**, 15345–15353.

43 M. Bregnhøj, M. Westberg, F. Jensen and P. R. Ogilby, *Phys. Chem. Chem. Phys.*, 2016, **18**, 22946–22961.

44 A. G. Griesbeck, M. A. Miranda and J. Uhlig, *Photochem. Photobiol. Sci.*, 2011, **10**, 1431–1435.

45 R. Bonnett and G. Martı´nez, *Tetrahedron*, 2001, **57**, 9513–9547.

46 J.-W. Hwang, S.-J. Jung, I. Heo, H.-A. Son, J.-H. Kim, K.-K. Wang and Y.-R. Kim, *J. Anal. Methods Chem.*, 2019, **2019**, 2584686.

47 B. Long, O. Bakr and F. Stellacci, *J. Exp. Nanosci.*, 2008, **3**, 53–60.

48 Y. Kalachyova, O. Lyutakov, V. Prajzler, J. Tuma, J. Siegel and V. Švorčík, *Polym. Compos.*, 2014, **35**, 665–670.

49 Z. Yang, G. Pu, X. Ning, Y. Wu, Z. Zhang, D. Shan and X. Lu, *Phys. Chem. Chem. Phys.*, 2019, **21**, 10614–10620.

Chapter 4 Hemin-doped, Ionically Crosslinked Silicone Elastomers with Peroxidase-like Reactivity

4.1 Abstract

The encapsulation of hemin in polymer systems represents a powerful tool for the preparation of synthetic enzymes. Reported systems largely focus on the creation of hydrogels or microreactors that require a degree of modification to the hemin molecule itself. We describe the straightforward synthesis of hydrophobic hemin-aminosilicone crosslinked silicone elastomers with peroxidase-like reactivity. Elastomers are formed from purely ionic interactions between commercial silicones and native hemin, which acts as a crosslinker. Elastomers prepared from ethylene diamine-based silicones are robust elastomers in which hemin is retained, while monoamine analogues can leach hemin into the environment. The system is easily tunable allowing for precise control of the hemin concentration and the physical properties of the elastomer. Upon exposure to peroxide-containing solutions, elastomers oxidize the substrate 3',3',5',5'-tetramethylbenzidine at the interface. Elastomers containing excess amine show greater catalytic efficiency due to the coordination of the amines to the iron center of hemin. The reaction can be followed using UV-visible spectroscopy; rates of reaction and Michaelis-Menten parameters were derived.

4.2 Introduction

Peroxidases are a diverse class of enzymes found in both mammals and plants that play critical and diverse roles in numerous biological processes.[1,2] In these processes, they are responsible for the oxidation of biological and inorganic substrates by catalyzing the reduction of hydrogen peroxide.[3] Generally, they can be broadly divided into two classes: hemeperoxidases and non-heme peroxidases.[2] In plants, heme-peroxidases comprise >80% of the known peroxidases and contain the porphyrin heme that is responsible for the catalytic activity of the enzyme.[2]

Recently, peroxidases, in particular horseradish peroxidase, have become powerful tools in organic synthesis, as they are capable of catalyzing a variety of organic reactions.[4] Due to their oxidative transformation capabilities, they have also been utilized in water remediation to remove phenolic contaminants.[5–7] Unfortunately, like all enzymes, the use of peroxidases in industrial and synthetic applications is limited by the stability of the enzymes. While great strides have been made by immobilizing of enzymes on solid substrates to improve their longevity, this strategy is not without its disadvantages, including leaching of the enzyme, loss of enzymatic activity over time, and increased costs for production.[8–12]

An alternative to utilizing natural peroxidases is the development of artificial enzymes, for example, the utilization of hemin as a peroxidase mimic.[13] Hemin serves as a replacement for the catalytic center in natural peroxidases and has been shown to be biologically active on its own. It represents a cost-effective alternative to traditional

enzymes, as it can be collected as a byproduct of the meat processing industry.[14–17] However, hemin is notoriously insoluble in aqueous solutions and forms catalytically inactive dimers at both acidic and basic pHs.[18] Therefore, the development of artificial enzymes that minimize hemin dimerization, allowing it to serve as a peroxidase mimic, has become a significant area of interest.[13]

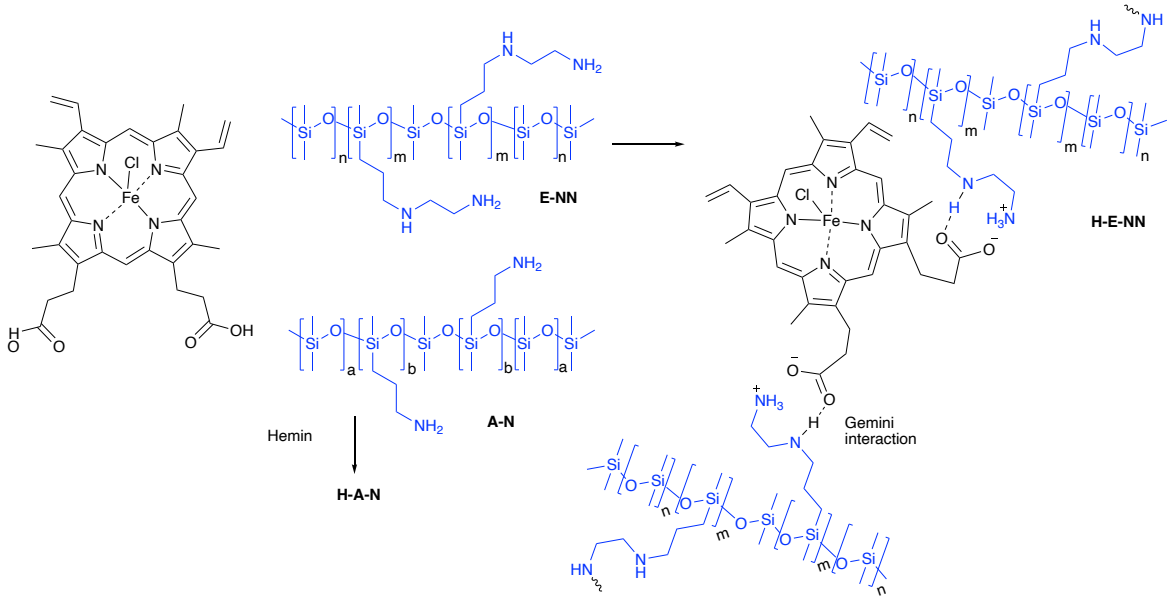

Figure 4.1: Structure of hemin and conversion to elastomers by mixing with suitable aminoalkylsilicones, shown in detail for 1:1 COOH/NH_2 **H-E-NN**.

The immobilization of hemin on substrates such as graphene or carbon nanotubes is a well-known, powerful strategy to produce artificial peroxidases.[13,19,20] The supports provide the artificial enzymes with high surface areas leading to materials that are capable of catalyzing the oxidation of a variety of substrates. Unfortunately, the preparation of the substrates and subsequent immobilization of the hemin are complex processes. An alternative to surface immobilized enzymes is the development of hemin-polymer materials

that serve as artificial enzymes.[21,22] These materials can be advantageous over supported enzymes when, as is normally the case, they use simple synthetic protocols and, after production, more closely mimic the protein environment of the native enzyme in its normal environment.

An excellent example of this strategy to create hemin-polymer materials exploited the carboxylic acids present on hemin to install synthetically useful functional groups that could be utilized to form nanozymes.[22] By first modifying the carboxylic acid groups present on hemin with *N*-(3-aminopropyl)methacrylamide hydrochloride (APMA), a monomer or crosslinker could be produced that could be copolymerized with acrylamide or *N,N'*-methylenebisacrylamide, respectively, to produce hydrogel nanozymes. These nanozymes were capable of oxidizing 3',3',5',5'-tetramethylbenzidine (TMB) or methylene blue over multiple cycles in aqueous solutions containing hydrogen peroxide. However, the pre-derivatization required to form these nanozymes is a limitation of their utility, and 100% conversion of the starting material was not achieved, resulting in a mixture of modified and unmodified hemins being used in subsequent reactions. In a simpler and very elegant approach, Wang et al. formed supramolecular hydrogels via self-assembly by combining hemin and amino acid derivatives, relying entirely on ionic interactions.[21] Utilizing this method, a mixture of monomeric and dimeric hemin could be obtained in the hydrogels. They showed excellent catalytic activity when evaluated against a variety of substrates in both aqueous and organic environments.

Ionic crosslinking takes advantage of the naturally occurring carboxylic acid groups present on hemin (Figure 4.1), thereby minimizing the number of steps required to

synthesize these artificial enzymes. This is a powerful strategy that could be utilized to dramatically expand the number and types of polymer-based artificial enzymes. One class of polymers that could potentially be used to create artificial enzymes are silicones. They have previously been demonstrated to be excellent polymers for the encapsulation of naturally occurring enzymes but have yet to be utilized in the synthesis of artificial enzymes.[23–27] Silicones would be particularly advantageous as constituents of synthetic peroxidases, as they are highly resistant to oxidation.[28] One would not, therefore, expect competitive reactions, including polymer degradation, during the catalyzed reactions. However, silicones are exceptionally hydrophobic and hemin is essentially insoluble in hydrophobic media.

We have previously shown that the reliable incorporation of porphyrins, which are typically insoluble in hydrophobic media, can be modified with silicone sidechains, using the Piers-Rubinsztajn reaction, such that the products are readily dispersible in silicone elastomers; the properties of the porphyrin were retained.[29] That methodology requires aromatic alcohols or ethers on the porphyrin that, unfortunately, hemin does not possess.[30,31] Thermoplastic silicone networks that are ionically crosslinked through the interactions between amino-silicones and carboxylic acids have been reported;[32–34] the use of ethylenediamino-modified silicones leads to particularly robust elastomers through 'gemini' interactions.[32] Based on the reports of ionically crosslinked hemins noted above,[21] we reasoned this strategy could also be adopted for silicone/hemin elastomers. Herein, we report the synthesis of silicone elastomers where hemin plays the role of both crosslinker and catalytic center. Elastomers were formed by mixing pendant amino-

silicones with varying equivalents of hemin in a solvent to facilitate mixing. Ionically crosslinked elastomers were formed following removal of the solvent and annealing. The resulting robust elastomers exhibited excellent peroxidase activity at the interface when evaluated using the TMB assay and show excellent stability to solvents.

4.3 Experimental Section

4.3.1 Materials and Methods

Hemin from bovine ≥ 90%, 3',3',5',5'-tetramethylbenzidine ≥ 99%, phosphate citrate buffer tablets, luminol and potassium hydroxide were purchased from Sigma-Aldrich. Aminopropylmethylsiloxane (4-5%)-dimethylsiloxane copolymer **A-N** (AMS-152, 100-300 cSt; the unit molecular weight calculated by NMR $[(OSiMe_2)_x(OSiMeCH_2CH_2CH_2NH_2)_1]_y$, x~27 was 2100 g mol^{-1}), aminoethylamino-propylmethylsiloxane (2-4%)-dimethylsiloxane copolymer **E-NN** (AMS-233, 900-1200 cSt; the unit molecular weight calculated by NMR $[(OSiMe_2)_x(OSiMeCH_2CH_2CH_2NHCH_2CH_2NH_2)_1]_y$, x~ 49, was 3800 g mol^{-1}) and octamethylcyclotetrasiloxane D_4 were purchased from Gelest. Hydrogen peroxide (30%), Falcon® 24-well polystyrene clear flat bottom untreated cell culture plates, and solvents were purchased from Fischer-Scientific. Ethanol (96%) was degassed using ultrasonication before use. All other reagents were used without further purification unless specified. Thin films were cast using an Elcometer 3540/1 Four-Sided Film Applicator set to the 200 μm edge. UV-Vis measurements were obtained on a BioTek Synergy LX plate reader reading in a kinetic mode. Centrifugation was performed in a Thermo Electron Corporation Durafuge Model No: 51231202.

4.3.2 Standard Solutions:

4.3.2.1 Preparation of Phosphate Citrate Buffer

A phosphate-citrate buffer tablet was dissolved in 100 mL of 18 MΩ water to provide 0.05 M pH 5 buffer. The buffer was adjusted to pH 4 using HCl (1M).

4.3.2.2 Preparation of 10 mM TMB Stock Solution

TMB (48 mg, 0.20 mmol) was dissolved in 96% ethanol (20 mL) to provide a 10 mM stock solution.

4.3.2.3 Preparation of Active TMB Solutions with Varying TMB Concentrations

The appropriate volumes of 10 mM TMB stock solution and 30% H_2O_2 were added to 10 mL volumetric flasks (Table 4.1). The volume was adjusted to 10 mL with the pH 4 phosphate-citrate buffer and solutions were used immediately after preparation and stored no longer than 1 h.

Table 4.1: Reagent volumes for preparation of TMB solutions utilized in kinetics studies.

Final TMB Concentration [mM]	Volume 10 mM TMB Solution [mL]	Volume 30% H_2O_2 [mL]	Volume 0.05 M PC Buffer [mL]	Final Volume [mL]
0.1	100	41	9.86	10
0.2	200	41	9.76	10
0.3	300	41	9.66	10
0.4	400	41	9.56	10
0.6	600	41	9.36	10
0.8	800	41	9.16	10
1	1000	41	8.96	10

4.3.2.4 General Procedure for the Preparation of Hemin-Silicone Elastomers

Hemin and **A-N** or **E-NN** (Table 4.2) were placed in a 20 mL scintillation vial to which a toluene:IPA mixture (15 mL) was added. The mixture was sonicated at 45 °C for 35-45 min or until a homogenous solution was obtained. The reactions were centrifuged to remove impurities in the hemin and undissolved hemin (4000 rpm, 30 min), and the volume of the supernatant was reduced *in vacuo* to ~2.0 mL. The silicone-hemin mixture was dispensed onto a poly(vinyl acetate) film using a 3 mL syringe and cast into thin films using

a casting blade set to 200 μm. Films were cured at room temperature for 12 h before being placed in an oven at 80 °C for 6 h. This process was necessary to anneal the polymers and allow them to reach maximum modulus.

Table 4.2: Masses of reagents utilized in preparation of elastomers.

H-A-N					
$COOH:NH_2$	**A-N** [g, mmol][a)]	Hemin [mg, mmol] [a)]	Volume Toluene [mL]	Volume IPA [mL]	Total Hemin Concentration [mM]
1:1	2.0, 0.94	305, 0.936	5	10	234
1:2	2.0, 0.94	152, 0.466	5	10	116
1:4	2.0, 0.94	76.0, 0.240	5	10	58.0
H-E-NN					
$COOH:NH_2$	**E-NN** [g, mmol][a)]	Hemin [mg, mmol] [a)]	Volume Toluene [mL]	Volume IPA [mL]	Total Hemin Concentration [mM]
1:1	2.0, 0.52	170., 0.521	5	10	130
1:2	2.0, 0.52	85.0, 0.261	5	10	65
1:4	2.0, 0.52	43.0, 0.132	5	10	33

a) Refers to mmol primary NH_2 and COOH.

4.3.3 Oxidation of Luminol

Luminol (2.0 g, 11 mmol) and KOH (15 g, 260 mmol) were dissolved in 250 mL of distilled water. An **E-NN**-hemin elastomer (1:1 COOH:amine) was placed in the bottom of a 20 mL scintillation vial. The luminol solution (5 mL) was poured into the vial and the solution was monitored for a change in color (Figure 4.4C,D).

4.3.4 Preparation of Elastomers for TMB Assay

Using an 8 mm metal punch, samples were cut from the ~ 200 μm thick parent elastomer film (~50 mm^2 surface area, only the top surface and sides were exposed) and transferred to 24-well plates containing 100 μL of methanol. The process helps properly seat the coupons within the well such that only the top surface is exposed to the reaction solution. The plates were placed in the oven at 50 °C for 30 min to evaporate the methanol (Figure 6.64).

4.3.5 General Procedure for TMB Assay

TMB active solutions (400 μL) were added to the surface of elastomers in 24-well plates. Absorbance readings @ 650 nm were taken every 15 s for 5 min. The background absorbance of the elastomer @ 650 nm was subtracted and a pathlength correction was manually applied using a K-factor of 0.173. Elastomers were rinsed with distilled (3 x 10mL) and placed in the oven at 50 °C between cycles.

4.4 Results and Discussion

4.4.1 Preparation of Elastomers

The synthesis of hemin-containing silicone elastomers was accomplished in a four-step process that exploited the existing functional groups on hemin. The elastomers had a characteristic dark red to light orange color depending on the amount of hemin present, which could be controlled by simply varying the ratio of amines to carboxylic acids in the formulation (Figure 4.2). Reproducibly achieving robust elastomers required optimization of five parameters: solvent; amino-silicone; curing time and temperature; and amount of hemin.

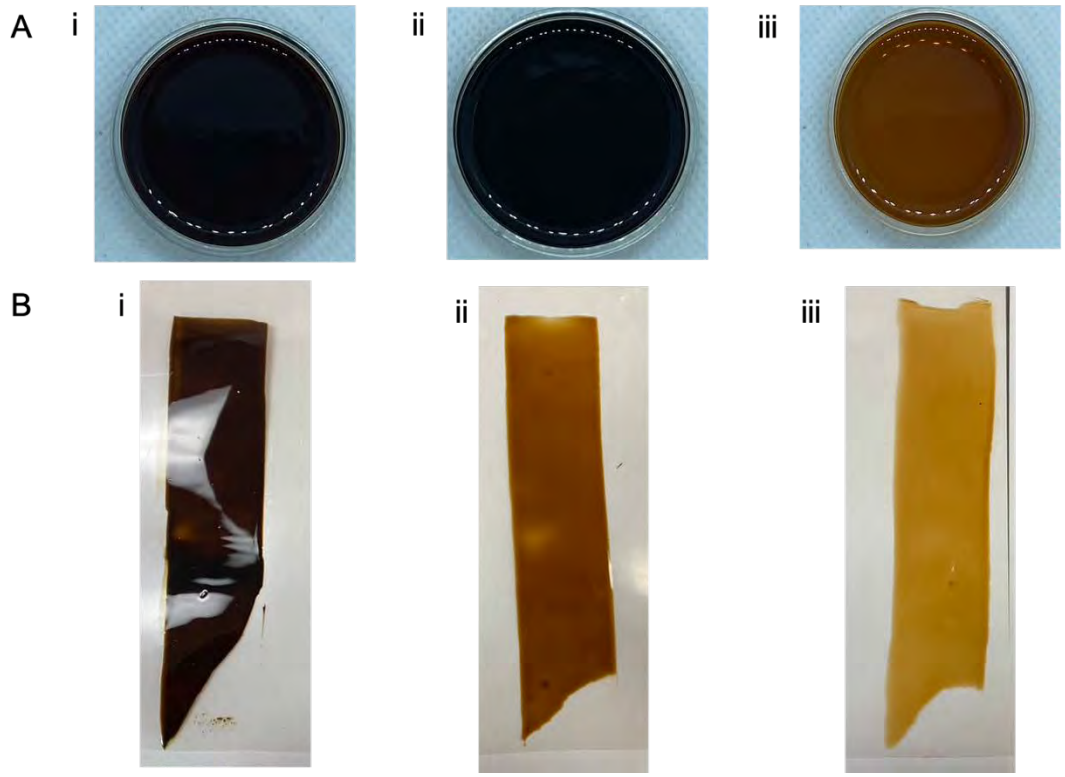

Figure 4.2: A) Bulk **H-E-NN** elastomers (~1 mm thick). i) 1:1 COOH:NH_2. ii) 1:2 COOH:NH_2. iii) 1:4 COOH:NH_2 B) Elastomer hemin films (~ 200 μm thick). i) 1:1 COOH : NH_2. ii) 1:2 COOH:NH_2 iii) 1:4 COOH:NH_2. **H-E-NN**.

4.4.1.1 Impact of Solvents

The general incompatibility of porphyrins with silicones (hydrophilic vs hydrophobic) initially posed a challenge to the development of the hemin-silicone materials. If porphyrins are not compatibilized with silicones to permit dispersion throughout the matrix, avoiding aggregation, little to none of their unique optoelectronic or catalytic properties are observed in silicone environments.[29] Although ionically crosslinked silicone elastomers could be prepared by combining linear silicone polymers containing carboxylic acids and amines,[32] respectively, without the assistance of any solvents, hemin proved to be completely insoluble in the commercial aminosilicones used in the study. Therefore, a solvent was necessary to facilitate the synthesis of the elastomers.

Finding a solvent in which hemin and silicones are both soluble proved difficult. While hemin is soluble in basic media (0.1 M NaOH), silicones are known for their hydrophobicity, which precluded the use of any aqueous media for the synthesis of the elastomers (and silicones can undergo depolymerization processes in contact with base[28]). Hemin is readily soluble in DMSO, but attempts to use this solvent were unsuccessful, as the aminoalkylsilicones exhibited minimal solubility and two immiscible phases formed even after extensive sonication. Hemin is sparingly soluble in alcoholic solvents such as methanol, ethanol and isopropanol (IPA). It was, however, noted that the direct addition of aminoalkylsilicones to hemin-isopropanol (IPA) dispersions dramatically enhanced the solubility of the hemin (Figure 4.3A,B). It is inferred that the amines present on the silicone served as organic bases, deprotonating the hemin for form carboxylates, helping to pull hemin into IPA solution.

4.4.1.2 Influence of the type of Amino Silicone on the Preparation and Stability of Elastomers

Two pendant amino-silicones were investigated, aminopropylmethylsiloxane-dimethylsiloxane copolymer (**A-N**) or aminoethylaminopropylmethylsiloxane-dimethylsiloxane copolymer (**E-NN**, Figure 4.1). Immediate differences were noted between the use of **A-N** and **E-NN** during the first step of the elastomer synthesis. When forming **H-A-N**, the solution became homogenous within 15-20 minutes, with the aminosilicone rapidly pulling hemin into solution. However, the use of **A-N** was not without its drawbacks. Almost immediately after solubilization to give homogeneous mixtures crosslinking was observed via the formation of gels in the vials. This made subsequent steps in the elastomer synthesis very difficult. Casting films or even forming bulk elastomers with these higher viscosity materials resulted in elastomers with large structural defects (Figure 6.63). Unless these formulations were rapidly processed once homogenous, the product elastomers always had defects. Attempts to control the gelation by doubling the volume of solvent were unsuccessful and, further, this strategy led to longer processing times in subsequent steps and the final elastomers exhibited poor stability to solvents.

Solutions of hemin made from **E-NN** slowly formed over the course of 2 hours, but full solubilization could be achieved more rapidly by sonicating the mixtures at 45 °C for 30-45 min and adding 33% (v/v) toluene as a cosolvent. Centrifugation of these samples resulted in the removal of a precipitate, likely a mixture of unreacted hemin and the 10% impurities that were present in the starting material (as reported by the supplier). If this step was ignored, the final quality of the elastomers was poor and zones containing precipitates

could be seen in the final elastomers. Unlike **A-N**, formulations containing **E-NN** never exhibited gelation or premature crosslinking and ultimately were more reliable for the production of elastomers. In all cases, viscous oils were retrieved once the IPA-toluene mixture was removed (Figure 4.3C). We were surprised to discover that these oils – prior to curing into elastomers – were highly soluble in low viscosity silicone oil (D_4, $(Me_2SiO)_4$) and showed an intense Soret band at ~400 nm which matches the UV-Vis spectrum of hemin in DMSO (Figure 4.3D). The solubility of hemin/aminosilicone materials in D_4 demonstrates the efficacy of the process to form monomeric hemin species. Note that the different behavior of aminosilicones to solvents was also manifested once elastomers had formed – see below.

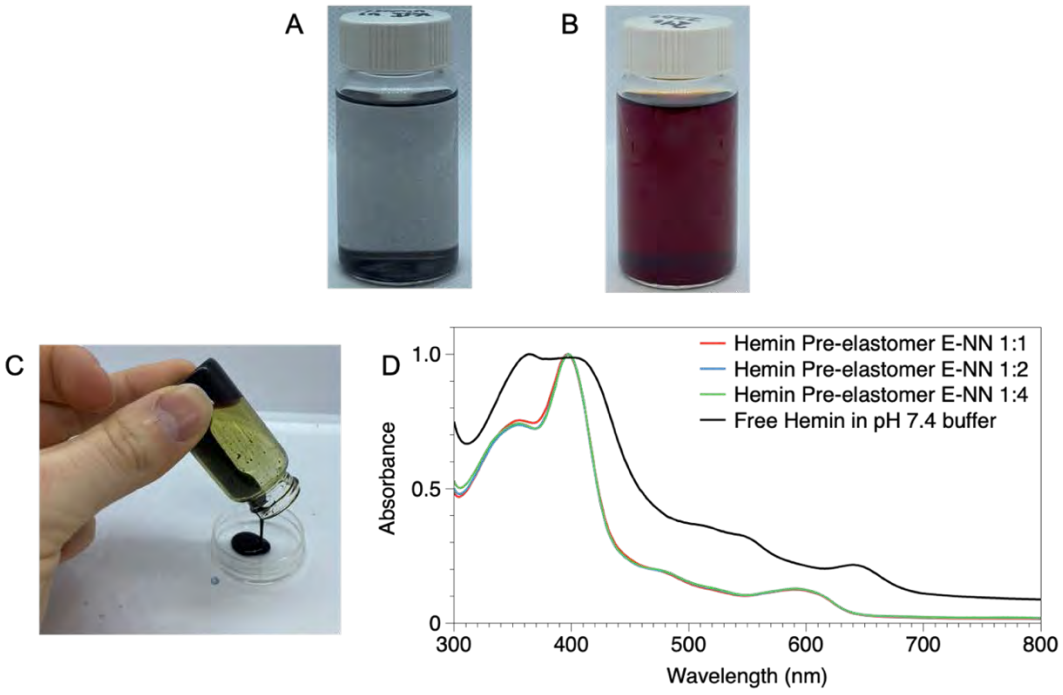

Figure 4.3: A) Hemin in IPA/toluene prior to and, B) Hemin in IPA/toluene after addition of **E-NN** and sonication. C) Image of **H-E-NN** 1:1 NH_2:COOH oil prior to heating to remove vestiges of solvent and annealing. D) UV-Vis of **H-E-NN** pre-elastomer oils diluted in D_4.

4.4.1.3 Impact of Curing Time and Temperature

Utilizing the silicone-hemin oils, two conditions for curing elastomers were tested: room and elevated temperature (80 °C). Full cure was determined to be the point at which the surfaces of the elastomers were no longer tacky and films could be easily peeled from the poly(vinyl acetate) substrate (Figure 4.2). When **H-E-NN** elastomers were cured exclusively at room temperature the process was slow and inconsistent, and surfaces remained tacky for prolonged periods >4 days. However, full cure was readily achieved if the pre-elastomers were cured first at room temperature for 12 hours, allowing the material to set, and then placed in an oven set to 80 °C for 6 hours to anneal. The necessity for the extended cure times is consistent with previous observations which suggest that elevated temperatures are needed to achieve full cure for silicone ionic elastomers.[32] It should be noted that placing the elastomers immediately in the oven was not beneficial as some regions of the film appeared to flow creating areas of variable thickness; the initial room temperature cure was necessary to achieve reproduceable results.

4.4.1.4 Effect of [COOH]/[NH2] on Elastomer Preparation

Initially, attempts were made to make elastomers from **A-N** and **E-NN** (Figure 4.1) at five [COOH]/[NH_2] ratios, where NH_2 refers only to the primary amines present on the polymer: 4:1; 2:1; 1:1; 1:2; and 1:4. The formulations containing stoichiometric excesses of carboxylic acid (excess hemin) were rapidly eliminated from the study, after preliminary results indicated that the excess hemin never went into solution. However, the three formulations containing equal or excess NH_2 to COOH groups all showed promise in the sense that homogenous fluids and then elastomers formed. Moreover, with these

formulations it was straightforward to control the amount of hemin present in the resulting elastomers.

4.4.1.5 Resilience of the Hemin-containing Elastomers

Understanding the stability of the elastomers, once formed, to various solvents was critical in determining the conditions under which the materials could operate as synthetic peroxidases. It was necessary to avoid solvents, like acetone, that could react with the amines in the elastomer. The resilience to hemin leaching from elastomers – a key characteristic for utility – depended on specific solvents and on the nature of the aminosilicone constituent. **A-N** 1:2 and **E-NN** 1:1 formulations contain almost equivalent concentrations of hemin, 116 mM and 130 mM, respectively, assuming a homogenous dispersion hemin within the elastomers (Table 3). When directly comparing these materials, it was observed that the **A-N** formulations exhibited significantly more leaching of hemin into toluene despite containing a slightly lower loading of hemin. The difference could be observed even by eye when looking at the supernatant used in the extractions (Figure 4.4A,B).

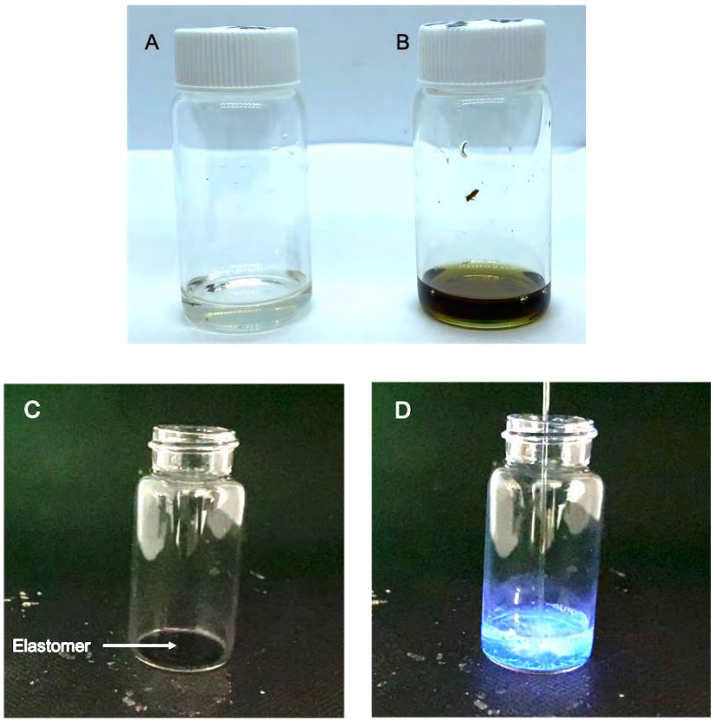

Figure 4.4: A) Supernatant following extraction of **H-E-NN** 1:1 elastomer in toluene. B) Supernatant following extraction of **H-A-N** 1:2 in toluene. C) 1:1 **H-E-NN** elastomer in 20 mL vial prior to addition of luminol. D) After addition of luminol+H_2O_2.

These differences in stability can be attributed to the nature of the amino-silicone utilized in the elastomer. The use of amino-silicones capable of forming gemini ionic bonds such as in **H-E-NN** (Figure 4.1) led to more mechanically robust and solvent stable materials than the **H-A-N** analogues.[32] Based on the much lower stability of **H-A-N** elastomers to solvents, the focus shifted exclusively to formulations utilizing **H-E-NN**. **H-E-NN** elastomers showed continued, slow leaching into excellent solvents for silicone like toluene and IPA. However, no detectable leaching by UV-Vis could be observed in methanol, pH 4 0.05 M phosphate-citrate buffer or 90:10 water:ethanol indicating the membranes could be utilized in aqueous solvents without concerns about leaching.

4.4.2 Characterization of Elastomers

UV-Vis spectroscopic analysis of the pre-elastomer oils suggested that the ionic incorporation of hemin in silicones is an effective way to isolate monomeric hemin, compared to dimers or aggregates. The presence of monomeric hemin was established by UV-Vis spectroscopy. **H-A-N** and **H-E-NN** elastomers (~200 μm thick) containing 1:1 and 1:2 COOH:NH_2 ratios possessed large quantities of hemin. This impacted the ability to follow processes using UV-Vis spectroscopy, as at a thickness of 200 μm wavelengths less than 450 nm could not be read due to the high intensity of the hemin absorbance. The mechanical properties were such that elastomers could not be cast at lower thicknesses, as the materials tore while trying to transfer them to well plates. Fortunately, a full spectrum ranging from 300-800 nm could be read for **H-E-NN** at a 1:4 ratio due to the lower quantity of hemin present (Figure 4.2B, Figure 4.5A). In this spectrum a Soret band at 410 nm could be observed, similar to that observed when the pre-elastomers were diluted in D_4 indicating the monomeric hemin is retained when the pre-elastomer oil is fully cured.

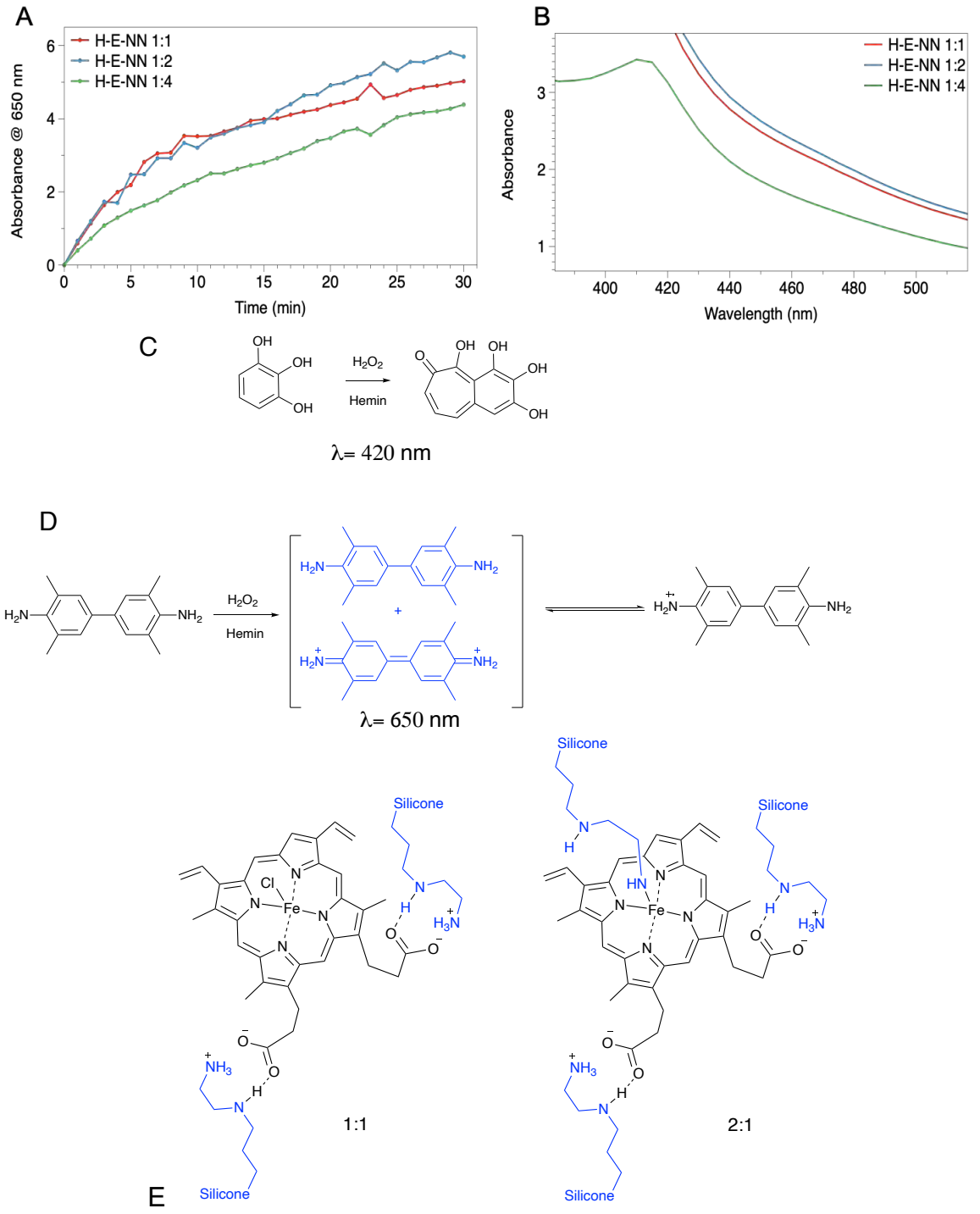

Figure 4.5: A) UV-Vis of **H-E-NN** elastomers. B) Reaction progress of hemin elastomers **H-E-NN** 1:1, 1:2 and 1:4 reacting with TMB H_2O_2. Hemin-mediated oxidation of C) pyrogallol and D) TMB. E) **H-E-NN** 1:1 and1:2 porphyrin complexes showing the activating axial amine ligand in the latter case.

4.4.3 Peroxidase Activity of Elastomers

4.4.3.1 Hemin Elastomers with Luminol

Basic luminol solutions containing hydrogen peroxide are known to react with the iron of heme in blood to produce a bright chemiluminescence.[35] The peroxidase activity of the exposed surface of elastomers was, therefore, initially probed using the luminol assay. Exposure of a ~200 μm thick elastomer 1:1 **H-E-NN** coupon (surface area ~ 50 mm^2) to a solution of luminol resulted in the rapid production of a bright chemiluminescence (Figure 4.4C,D) providing a positive indicator that the hemin in the elastomers both remained accessible to the aqueous luminol solution and had retained the peroxidase activity of the porphyrin.

4.4.3.2 Peroxidase Activity of Elastomers-TMB

Typically, the enzyme activity of synthetic peroxidases is quantitatively described using Michaelis-Menten kinetics by evaluating the conversion of pyrogallol to purpurogallin (λ=420 nm) or TMB to the charge transfer complex (λ=650 nm, Figure 4.5C,D). These assays were utilized to evaluate the catalytic activity at the elastomer interface.

Elastomers cut from ~200 μm thick films were placed in 24-well plates and their upper surfaces were covered by solutions containing the substrate and H_2O_2. It was rapidly seen that evaluating the catalytic activity of the elastomers by use of the pyrogallol assay was not possible, as the absorbance wavelength overlapped significantly with that of hemin present in the elastomer. However, TMB could be easily used as a substrate to follow

peroxidase activity, as the charge transfer complex absorbs at 650 nm and the signal for hemin at this wavelength could be subtracted to obtain the signal for TMB.

Although it is well known that the hydrophobicity of silicones prevents the ingress of water into silicone elastomers, we were pleased to discover that there was sufficient hemin presenting at the elastomer surface to catalyze the production of the charge transfer complex (Figure 4.5D). The progress of the reaction between TMB, H_2O_2 and hemin-containing elastomers was initially monitored over 30 minutes with measurements taken every minute using a 1 mM solution of TMB (Figure 4.5B). A linear region was observed from 1-5 minutes for all elastomers. To determine initial rates of reactions, elastomers were again placed in 24-well plates and the surface of the elastomers were covered with solutions (400 μL) containing varying substrate concentrations (0.1-1 mM) with a consistent H_2O_2 concentration (40 mM). The evolution of the product was monitored kinetically over the first 5 minutes of reaction, with a reading every 15 s. Preliminary tests necessitated the elimination of 0.1 mM and 0.2 mM substrate concentrations as the change in absorbance at these concentrations could not be distinguished from the background of the elastomer. Utilizing, 0.3, 0.4, 0.6, 0.8 and 1 mM substrate concentrations initial rates of reactions were determined and used to construct Lineweaver-Burke plots (Figures S1-S3) from which the important parameters k_{cat} and K_m were derived (Table 4.3).

To do these calculations, it was necessary to calculate the 'concentration' of available hemin to which the substrate was exposed. A method commonly used to quantify water penetration in hydrophobic nanoparticles is drop penetration, which follows changes in water droplet size shape as water is taken into a mostly hydrophobic surface.[36] It was

hoped that this method would provide the thickness of the hemin-containing elastomer layer that was accessible to substrate. The sensitivity of the method was insufficient, as the changes in volume of the water drop over the first five minutes were smaller than what could be accurately measured using ImageJ. That is, it was not possible to measure any water ingress into the silicone. We are currently exploring the use of fluorescent microscopy techniques to provide a better estimate of the penetration depth of TMB. Since there was no evidence of swelling by water gravimetrically or via use of the observed drop method we somewhat arbitrarily, but conservatively, based the kinetic calculations on the quantity of hemin that would be found in the 250 nm of elastomer closest to the substrate solution; it is likely far less.

Free hemin is known to have a k_{cat} of 2.4 min^{-1}.[37] Based on calculations using the 250 nm thickness, all formulations evaluated in this study possessed k_{cat} values higher than that of hemin and had comparable values to those reported for other synthetic polymer peroxidases, which range from 19-246 (Table 4.3).[19,21] The absolute efficiency of the peroxidase activity will thus require further analytical experiments to measure the available fraction of hemin bound in the silicone elastomer.

Table 4.3: Michaelis-Menten parameters for first reaction cycle of elastomers and comparison of k_{cat} values over multiple reaction cycles.

Formulation **H-E-NN**	Available Hemin [mmol]	V_{max} [μM min ^{1}]	k_{cat} [min^{-1}]	K_M [mM]
1:1	5.74×10^{-3}	53.2	3.70	3.22
1:2	2.87×10^{-3}	120.	17.0	8.34
1:4	1.45×10^{-3}	70.4	19.2	5.36
Repetitions				
Formulation **H-E-NN**	Available Hemin [mmol]	k_{cat} [min^{-1}] Initial trial	2^{nd} trial	3^{rd} trial
1:1	5.74×10^{-3}	3.70	1.43	2.40
1:2	2.87×10^{-3}	17.0	8.34	24.4
1:4	1.45×10^{-3}	19.2	2.90	2.33

Distinct differences in the kinetic parameters were noted (Table 4.3). Elastomers containing excess amine exhibited better performance during the initial catalytic cycle, with **H-E-NN 1:4** possessing the highest k_{cat} value while **H-E-NN 1:1** possessed the lowest. This was expected, as it is well known that the catalytic activity of natural peroxidases such as HRP are dependent on the availability of amino acids that serve as axial ligands assisting in the cleavage of O-O bonds and stabilizing transition states during catalytic cycles.[38–40]

Synthetic peroxidases utilizing simple aliphatic or aromatic amines exhibit similar behavior.[21,22,37,38]

In the silicone systems, amines present in the elastomers are thus playing two critical roles, providing ionic crosslinking interactions, and acting as axial ligands for hemin. **H-E-NN** elastomers containing 1:1 ratio have theoretically only enough primary amines to titrate the carboxylic acids and therefore the number of hemin molecules containing coordinated amines is anticipated to be very low; we suspect the involvement of the secondary amine in gemini interactions minimizes its participation in coordination to iron. As the ratio of amines in the formulations increases, so too does the number of hemin molecules containing axially coordinated amines resulting in improved catalytic performance (Figure 4.5E). In the amine rich **H-E-NN** 1:2 and 1:4, there is sufficient amine to both titrate the carboxylic acids and coordinate to the iron. Initially, it was expected that **H-E-NN** 1:2 would have the best performance as it precisely contains the right amount of amine to titrate the carboxylic acids and coordinate to the iron.[41] However, **H-E-NN** 1:4 exhibited comparable activity in the first cycle. It is likely that in this case the additional free amine available in **H-E-NN** 1:4 plays a similar role to arginine in HRP facilitating the cleavage of the peroxide bond through hydrogen bond formation.[18,38]

An important consideration when developing synthetic peroxidases is their recyclability. Ideally, a synthetic peroxidase should be active for multiple cycles with minimal to no loss in catalytic activity. To examine their recyclability, the silicone elastomers used in the initial kinetic studies were rinsed with water, and dried in a 50 °C oven for 30 min (less than the temperature for the initial silicone cure, such that hemin

stability should not be affected) and then subjected to two additional reaction cycles. As indicated in Table 4.3, all elastomers showed reduction in their catalytic efficiency, as indicated by reduced k_{cat} after first usage, but not irreversibly. The 1:2 and 1:1 samples in the 3rd trial recovered activity on the third trial, with 1:2 showing complete recovery. However, 1:4 did not recover activity between the second and third cycles. This data suggests that changes in activity may have more to do with efficient cleaning of the elastomer surface rather than loss of activity of the immobilized hemin per se. This is supported by visual changes observed in the elastomers after each catalytic cycle. Despite immediate and extensive rinsing between each cycle, changes in color were noticed in elastomers exposed to TMB with a blue-purple color forming on the surface of the elastomers, particularly at higher TMB concentrations (Figure 6.62). This suggests that between each cycle some TMB deposits on the elastomer passivating the surface and lowering the catalytic activity. Unfortunately, exposure to solvents which could more effectively remove TMB, such as acetone or toluene, also result in leaching of the hemin from the elastomer. This prevents precise characterization of recyclability by changing the effective concentration of hemin through leaching.

Previous work to immobilize hemin in polymers has logically focused on the exploitation of water compatible/swellable polymers. In addition to hydrogels created from acrylamides that required modification of hemin,[22] there is the key precedent work of Wang et al. that simply used ionic bonds to lock the hemin in place.[21] These strategies both achieved the desired goal of immobilized peroxidase activity.

The current system borrows from the work of Wang et al.,[21] in the sense that ionic bonds are all that is required to crosslink silicones. However, it differs in that we use systems that rely on ionic bonds to give silicone elastomers that do not swell with water to a significant degree. It was necessary to exploit the stronger crosslinks provided by gemini interactions to achieve structurally viable elastomers **H-E-NN** (Figure 4.1); elastomers based on simple amines **H-A-N** did not anchor the hemin molecules sufficiently well, and problematic leaching of hemin was observed. The efficiency of the peroxidase reaction did not track with the total hemin concentration within the elastomers, but rather with the amount of available amine indicating the amine is critical to the catalytic efficiency (Table 4.3). The catalytic elastomers, once washed and dried, could be reused. The subtleties of the process are not currently optimized, as shown by the lower activity after 1 cycle.

There are several attractive features that are associated with immobilized, surface active peroxidase catalysts, hemin in this case, that reside in a hydrophobic silicone environment. The slow leaching of hemin from **H-E-NN** elastomers into the good solvents suggests it will be possible to recover and reuse the silicone oils in new elastomers using hemin or other crosslinkers, an attribute consistent with the principles of Green Chemistry. Currently, we have utilized self-standing silicone elastomer films to develop these materials. However, it should be straightforward to utilize thin coatings of the materials on other substrates that provide physical stability. The utilization of the peroxidase catalysts with silicone-based microfluidics is of particular interest. Most interesting, in our view, is the ability to have the locus of reaction at an aqueous interface, rather than requiring the material to swell in water. In this case, the needs of the immobilized catalyst are met by the

contents of the aqueous reaction solution and issues of transport to the catalyst are avoided. This is reminiscent of the behavior of lipase enzymes, which similarly operate at water/oil interfaces.[27]

4.5 Conclusion

Hemin acts as a crosslinking agent for diaminoalkylsilicones via ionic interactions. Optimization of the parameters allowed for the reproduceable production of silicone elastomers in which the hemin concentration can be precisely controlled. The hemin presenting at the water-elastomer interface exhibited peroxidase reactivity consistent with Michaelis-Menten enzyme kinetics. The materials exhibited the optimal peroxidase like reactivity when the ratio of hemin to amine was 1:2 due to the coordination of amines to iron center. The materials maintain peroxidase activity over three cycles, with some loss of activity. The synthetic approach thus constitutes a simple, recyclable strategy to create hydrophobic films with peroxidase activity.

4.6 Acknowledgements

We acknowledge with gratitude the financial support of the Natural Sciences and Engineering Research Council of Canada (NSERC).

4.7 References

1 H. R. Hallingbäck, R. R. Gabdoulline and R. C. Wade, *Biochemistry*, 2006, **45**, 2940–2950.

2 Pandey, Veda, Awasthi, Manika, Singh, Swati, Tiwari, Sameeksah, and Dwivedi, Upendra, *Biochem Anal Biochem*, 2017, **6**, 1–16.

3 J. Everse, in *Encyclopedia of Biological Chemistry*, eds. W. J. Lennarz and M. D. Lane, Elsevier, New York, 2004, pp. 354–361.

4 G. R. Lopes, D. C. G. A. Pinto and A. M. S. Silva, *RSC Adv.*, 2014, **4**, 37244–37265.

5 Q. Husain, *Rev Environ Sci Biotechnol*, 2010, **9**, 117–140.

6 V. A. Cooper and J. A. Nicell, *Water Res*, 1996, **30**, 954–964.

7 S. Preethi, A. Anumary, M. Ashokkumar and P. Thanikaivelan, *SpringerPlus*, 2013, **2**, 341.

8 M. P. Conte, K. H. A. Lau and R. V. Ulijn, *ACS Appl. Mater. Interfaces*, 2017, **9**, 3266–3271.

9 U. Hanefeld, L. Gardossi and E. Magner, *Chem. Soc. Rev.*, 2009, **38**, 453–468.

10 J. J. Damnjanović, M. G. Žuža, J. K. Savanović, D. I. Bezbradica, D. Ž. Mijin, N. Bošković-Vragolović and Z. D. Knežević-Jugović, *J. Mol. Catal. B Enzym.*, 2012, **75**, 50–59.

11 E. Yilmaz, K. Can, M. Sezgin and M. Yilmaz, *Bioresour. Technol.*, 2011, **102**, 499–506.

12 R. C. Rodrigues, C. Ortiz, Á. Berenguer-Murcia, R. Torres and R. Fernández-Lafuente, *Chem. Soc. Rev.*, 2013, **42**, 6290–6307.

13 A. M. Alsharabasy, A. Pandit and P. Farràs, *Adv. Mater.*, 2021, **33**, 2003883.

14 C. S. F. Bah, A. E.-D. A. Bekhit, A. Carne and M. A. McConnell, *Compr. Rev. in Food Sci. Food Saf.*, 2013, **12**, 314–331.

15 H. Cheng, L. Zhang, J. He, W. Guo, Z. Zhou, X. Zhang, S. Nie and H. Wei, *Anal. Chem.*, 2016, **88**, 5489–5497.

16 R. Qu, L. Shen, Z. Chai, C. Jing, Y. Zhang, Y. An and L. Shi, *ACS Appl. Mater. Interfaces*, 2014, **6**, 19207–19216.

17 Y. Lin, J. Ren and X. Qu, *Acc. Chem. Res.*, 2014, **47**, 1097–1105.

18 E. S. Ryabova, A. Dikiy, A. E. Hesslein, M. J. Bjerrum, S. Ciurli and E. Nordlander, *J Biol Inorg Chem*, 2004, **9**, 385–395.

19 T. Xue, S. Jiang, Y. Qu, Q. Su, R. Cheng, S. Dubin, C.-Y. Chiu, R. Kaner, Y. Huang and X. Duan, *Angew. Chem. Int. Ed.*, 2012, **51**, 3822–3825.

20 Y. Zhang, C. Xu and B. Li, *RSC Adv.*, 2013, **3**, 6044–6050.

21 Q. Wang, Z. Yang, X. Zhang, X. Xiao, C. K. Chang and B. Xu, *Angew. Chem. Int. Ed.*, 2007, **46**, 4285–4289.

22 J. Guo, Y. Liu, J. Zha, H. Han, Y. Chen and Z. Jia, *Polym. Chem.*, 2021, **12**, 858–866.

23 P. Mazurek, P. M. Zelisko, A. L. Skov and M. A. Brook, *ACS Appl. Polym. Mater.*, 2020, **2**, 1203–1212.

24 C. A. Malpass, K. W. Millsap, H. Sidhu and L. B. Gower, *J. Biomed. Mater. Res.*, 2002, **63**, 822–829.

25 A. M. Ragheb, O. E. Hileman and M. Brook, *Biomaterials*, 2005, **26**, 6973–6983.

26 Y. Poojari, A. S. Palsule, S. J. Clarson and R. A. Gross, *Silicon*, 2009, **1**, 37–45.

27 A. Ragheb, M. A. Brook and M. Hrynyk, *Chem. Commun.*, 2003, 2314–2315.

28 M. A. Brook, in *Silicon in Organic, Organometallic, and Polymer Chemistry*, Wiley, 1999, pp. 256–308.

29 C. B. Gale, M. A. Brook and A. L. Skov, *RSC Adv.*, 2020, **10**, 18477–18486.

30 J. B. Grande, D. B. Thompson, F. Gonzaga and M. A. Brook, *Chem. Commun.*, 2010, **46**, 4988–4990.

31 M. A. Brook, *Chem. Eur. J.*, 2018, **24**, 8458–8469.

32 S. Zheng, Y. Chen and M. A. Brook, *Polym. Chem.*, 2020, **11**, 7382–7392.

33 A. Genest, D. Portinha, E. Pouget, K. Lamnawar, F. Ganachaud and E. Fleury, *Macromol. Rapid Commun.*, 2021, **42**, 2000372.

34 H. Lu and S. Feng, *J. Polym. Sci. A. Polym Chem*, 2017, **55**, 903–911.

35 A. Karabchevsky, A. Mosayyebi and A. V. Kavokin, *Light Sci. Appl*, 2016, **5**, e16164–e16164.

36 Z. Liu, Y. Wang, F. J. Muzzio, G. Callegari and G. Drazer, *Langmuir*, 2017, **33**, 56–65.

37 Q. Wang, Z. Yang, M. Ma, C. K. Chang and B. Xu, *Chem. Eur. J.*, 2008, **14**, 5073–5078.

38 W. Wu, Q. Wang, J. Chen, L. Huang, H. Zhang, K. Rong and S. Dong, *Nanoscale*, 2019, **11**, 12603–12609.

39 M. Gajhede, D. J. Schuller, A. Henriksen, A. T. Smith and T. L. Poulos, *Nat. Struct. Biol*, 1997, **4**, 1032–1038.

40 J. H. Dawson, *Science*, 1988, **240**, 433–439.

41 E. Reguera, J. Balmaseda, J. Fernández-Bertrán, A. Paneque and H. Yee-Madeira, *Transit. Met. Chem.*, 2004, **29**, 451–456.

Chapter 5 Conclusions and Future Outlook

5.1 General Conclusions

The synthesis of siloxane- or polysiloxane-modified porphyrins opens the field to the development of new and interesting silicone materials with diverse applications. Applications include those that take advantage of the interesting optoelectronic and chemical properties of porphyrins, which remain unaltered by the presence of silicones.

To date, two types of porphyrins have been investigated 5,10,15,20-(tetra-3-methoxyphenyl)porphyrin and hemin. The synthetic porphyrin 5,10,15,20-(tetra-3-methoxyphenyl)porphyrin can be easily modified via the Piers-Rubinsztajn reaction and incorporated into elastomers. Modified porphyrins show unique liquid like properties, due to the low T_g of the silicones. Careful selection of the siloxane or polysiloxane allows derivatives to be synthesized that can be either covalently incorporated or physically dispersed in elastomers. Each method has distinct advantages and disadvantages. Physical dispersion is simple and compatible with pre-existing commercial silicone elastomer kits but is load limited, due to the natural tendency of silicone oils to migrate to air interfaces. Covalent incorporation prevents leaching and migration by fixing the porphyrin within the elastomer body but requires additional synthetic considerations during elastomer formation.

Hemin can be easily incorporated into silicone elastomers without functional group modification. Instead, the carboxylic acids present on the porphyrin ring are utilized in acid-base chemistry with pendant aminosilicones. Initially, viscous oils can be isolated that

show excellent solubility in silicone oil. These same oils can be used to create ionically crosslinked elastomers.

A consistent observation across all projects is the need to control the natural tendency of porphyrins to aggregate. Aggregation of the porphyrins inside silicone matrices prevents optimal performance of subsequent materials but remains challenging to control.

5.2 Chapter 2 Conclusions and Future Work

Modifying Zn-TPMP with methylbis(trimethylsiloxy)silane allows for the production of a silicone soluble porphyrin. Utilizing a physical dispersion technique, the modified porphyrin can be dispersed into both homemade and commercially available platinum cure silicone elastomers. The high polarizability of the aromatic electrons leads to increases in permittivities from 3 to 13. Materials exhibit excellent actuations at relatively low voltages for DEs but suffer from low dielectric breakdown strengths and migration of the oil, ultimately limiting the operating conditions of elastomers.

Future work should aim to address three shortcomings: the migration of the oil from the bulk; phase separation at high loadings; and the dielectric breakdown strength. Migration of the oil and phase separation could be limited or eliminated entirely by covalently linking the porphyrin into the elastomer. It should be noted that this could have implications on other important parameters such as the Young's modulus, and dielectric breakdown. Therefore, a systematic study should be performed to determine the influence of crosslinked porphyrins on the mechanical and dielectric breakdown properties of the elastomers. It is possible that covalent incorporation may serve to simultaneously improve dielectric breakdown by limiting imperfections in the elastomers that could arise due to

physical dispersion, or through the covalent incorporation of aromatic groups that are known to act as voltage stabilizers.

5.3 Chapter 3 Conclusions and Future Work

The PR reaction was successfully utilized to create a derivative of TPMP that could be covalently incorporated into elastomers or further modified to create a new derivative that can be physically dispersed. The method of incorporation proved to be critical for optimizing singlet oxygen generation. Elastomers containing physically dispersed photosensitizer universally exhibited poor performance when evaluated using EPR spectroscopy. Aggregation shut down singlet oxygen production in elastomers with physically dispersed derivatives. Covalent incorporation, by contrast, resulted in materials with excellent singlet oxygen generating capabilities. It was determined that covalent incorporation limited aggregation of the porphyrin.

While the films have been shown to be capable of singlet oxygen generation, their efficacy against bacteria still needs to be established. These investigations are on-going, and the films are being tested against a variety of gram-negative and positive bacteria. Future work should focus on improving the stability of the elastomers or alternative photosensitizers. Additional photosensitizers to be investigated must be compatible with the PR reaction. Strategies to improve the mechanical stability of the films should also be explored, possibly by the addition of inorganic fillers.

An alternative strategy would involve the construction of porphyrin-silicone dendrimers. If properly synthesized, these materials could act in an analogous manner to MDTQ resins and provide mechanical reinforcement without the need for inorganic

fillers.[1,2] This could be accomplished using sequential reactions including the PR reaction and hydrosilylation techniques that have been successfully utilized in the construction of silicone dendrimers.[2,3] Improving the mechanical properties could allow elastomers to be cast thinner this maximizing singlet oxygen migration.

5.4 Chapter 4 Conclusions and Future Directions.

Hemin is a promising peroxidase mimic that can be used in the development of synthetic polymer enzymes. Hemin can be incorporated through acid-base chemistry into pendant aminosilicones. The amines that present on the silicone serve as a base deprotonating carboxylic acid on hemin, facilitating its incorporation into the elastomer body. Initially, viscous oils can be isolated that slowly at room temperature cure or more rapidly at elevated temperatures. When evaluated against an aqueous peroxidase assay, the elastomer exhibits peroxidase reactivity at the interface due to redox chemistry associated with the iron centre of hemin. The behaviour of peroxidase reactivity can be described using Michaelis-Menten kinetics.

The calculation of Michaelis-Menten parameters requires a precise description of the hemin concentration. The interfacial nature of the reaction suggests that not all the hemin present in the elastomer will be available for reaction. Future work will aim to determine the depth of TMB (tetramethylbenzidine) penetration into the elastomer. Fluorescence microscopy techniques will be utilized. Elastomers will be exposed to fluorophores and the penetration depth of the fluorophores will be monitored. This will provide information about the quantity of hemin that is available to react at the interface, which can be used in more precise calculations.

5.5 Future Research Areas

5.5.1 Investigating Aggregation

Across the three research projects investigated in this thesis, the aggregation of porphyrins was suspected to be a source of decreasing overall quality of the materials. While a level of control over the aggregation was exhibited using the strategies described above, achieving a greater level of control is critical to the advancement of the field.

A comprehensive study should be performed to determine under what conditions porphyrins aggregate in silicone matrices. This could be accomplished by synthesizing a series of porphyrin-polysiloxane copolymers via the PR reaction in which the spacing between porphyrins is precisely controlled. This could provide a way to control the proximity of porphyrins to one another and determine the spacing required to prevent aggregation. This would provide important information for the design of future materials.

Equally important is the ability to reliably detect aggregation in the silicone materials, which was not always straightforward. UV-Visible spectroscopy, while reliable for the detection of aggregates in solution, was less so within silicone elastomers especially at high concentrations. AFM and fluorescence spectroscopy offered greater reliability and any precision materials synthesized should be characterized using these techniques to provide a basis for the comprehensive detection of aggregates in silicones.

5.6 References

1 P. Mazurek, S. Vudayagiri and A. Ladegaard Skov, *Chem. Soc. Rev.*, 2019, **48**, 1448–1464.

2 S. Zheng, S. Liang, Y. Chen and M. A. Brook, *Molecules*, 2019, **24**, 4133.

3 J. B. Grande, T. Urlich, T. Dickie and M. A. Brook, *Polym. Chem.*, 2014, **5**, 6 728–6739.

Chapter 6 Appendix

6.1 Appendix I: Supporting Information for Chapter 2

6.1.1 Synthesis of Zn-TPMP

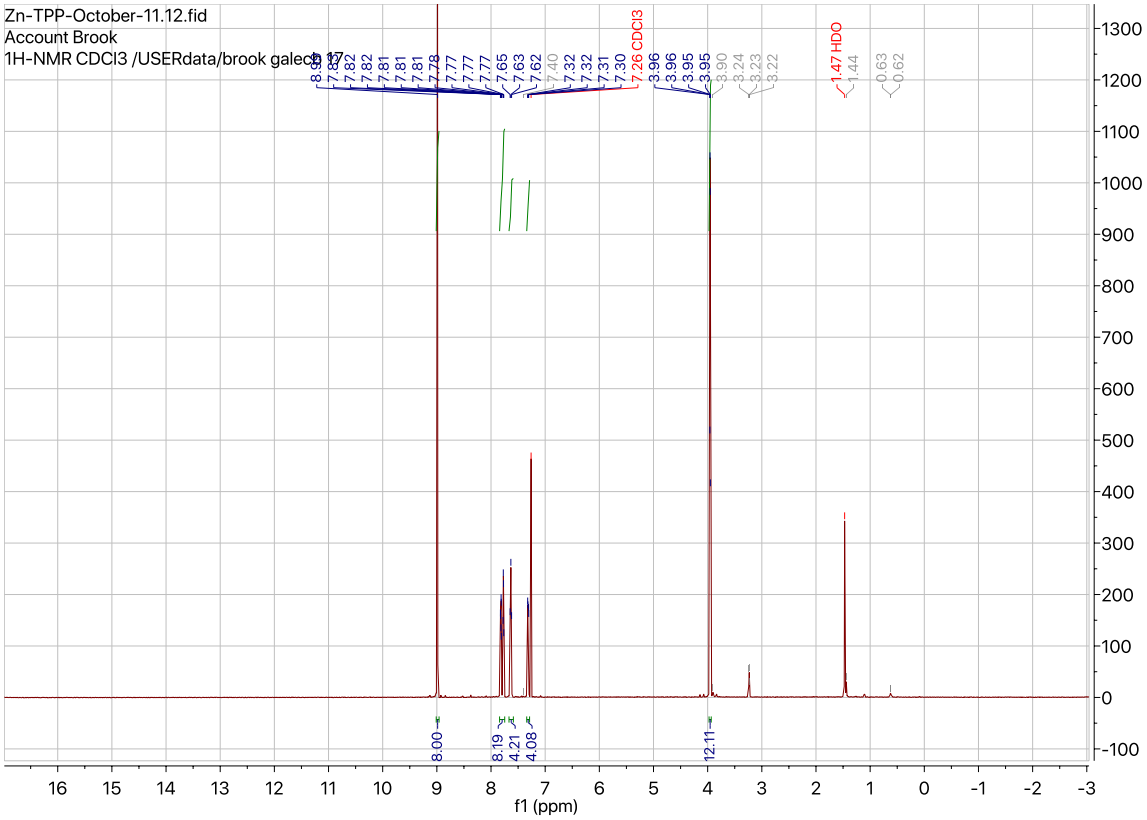

Figure 6.1: ^{1}H-NMR of Zn-TPMP.

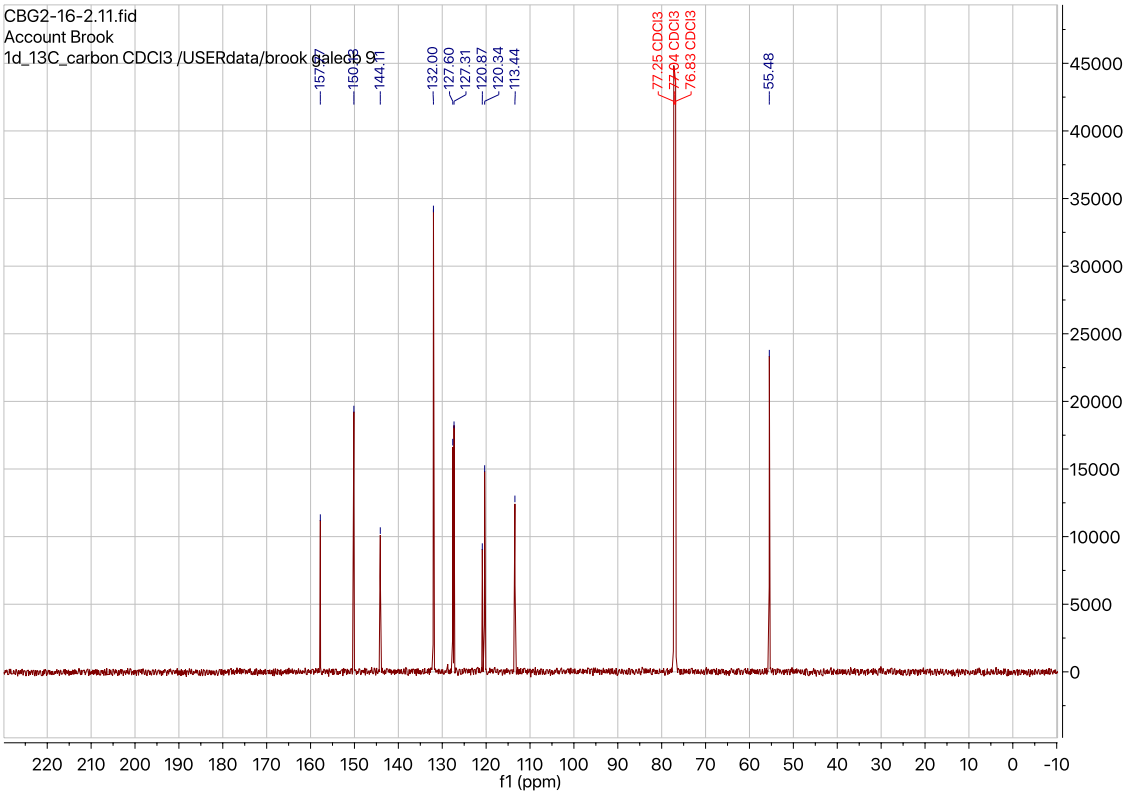

Figure 6.2: ^{13}C-NMR of Zn-TPMP.

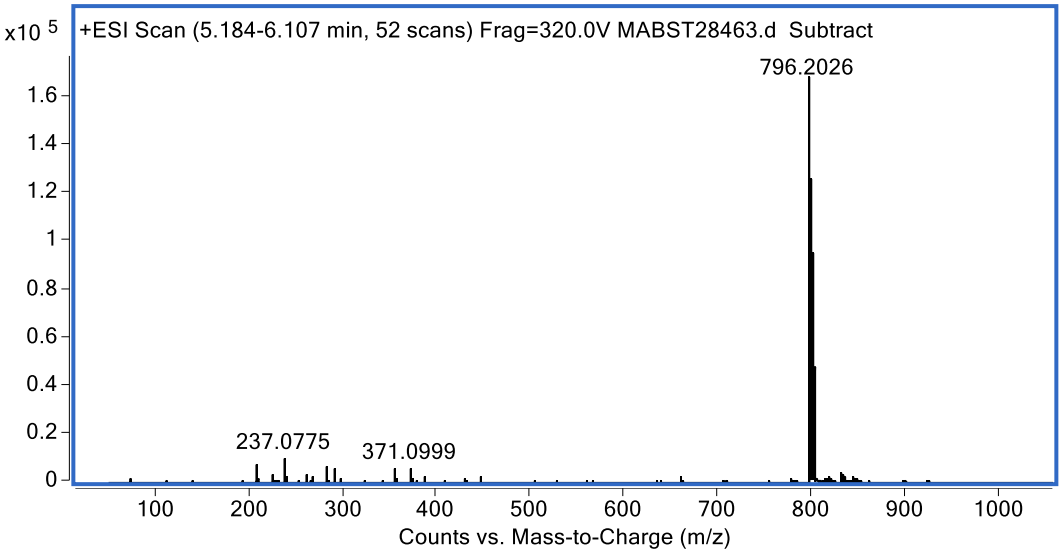

Figure 6.3: ESI-MS of Zn-TPMP.

6.1.2 Synthesis of Zn-TPMP-Bis-H

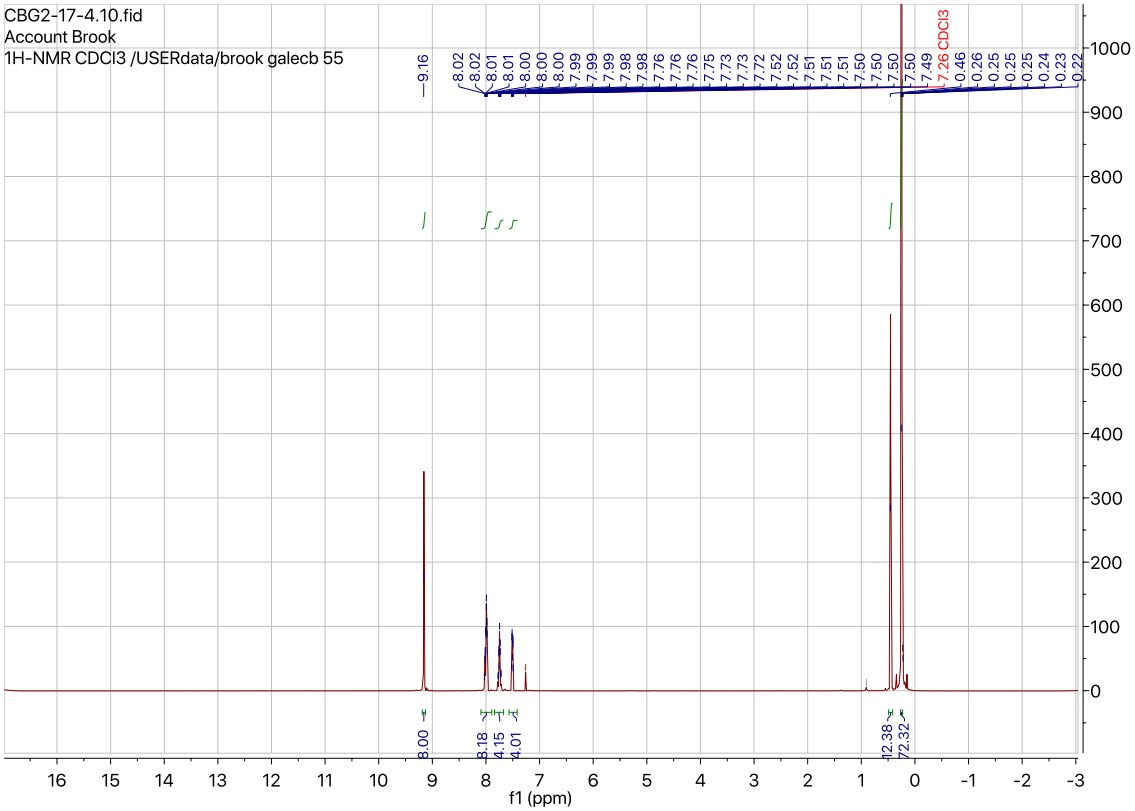

Figure 6.4: ^{1}H-NMR of Zn-TPMP-Bis-H.

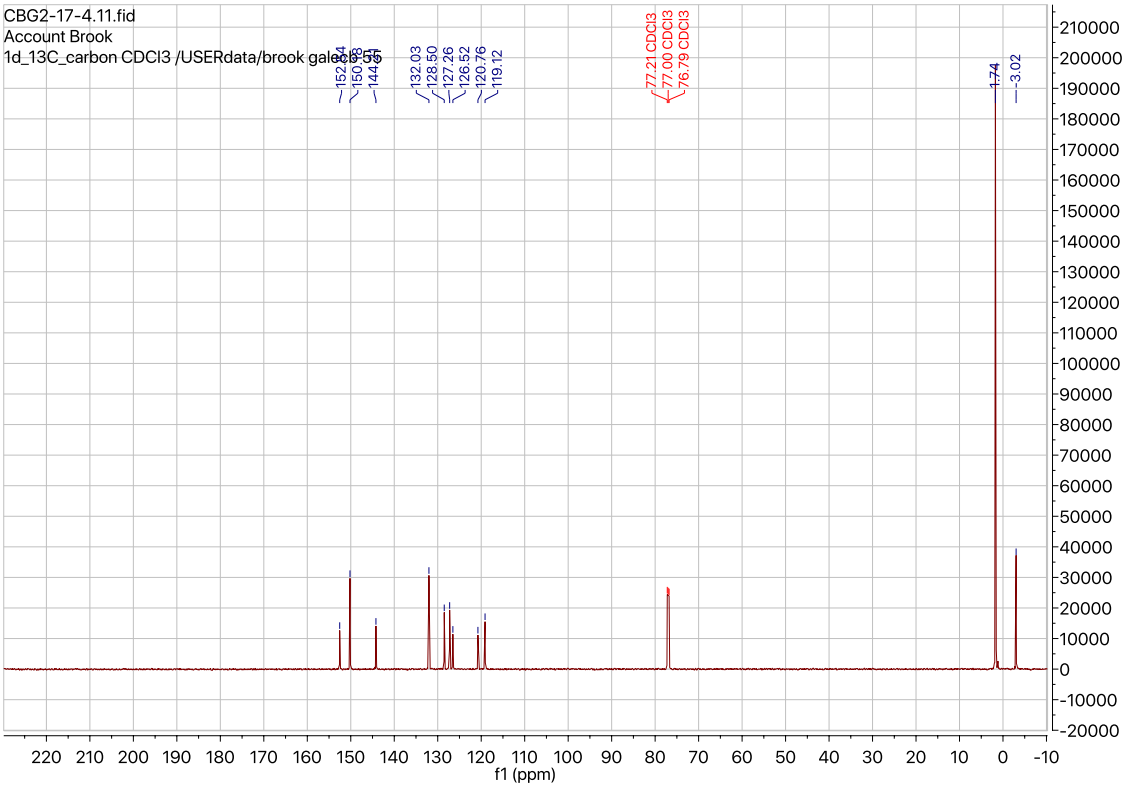

Figure 6.5: ^{13}C-NMR of Zn-TPMP-Bis-H.

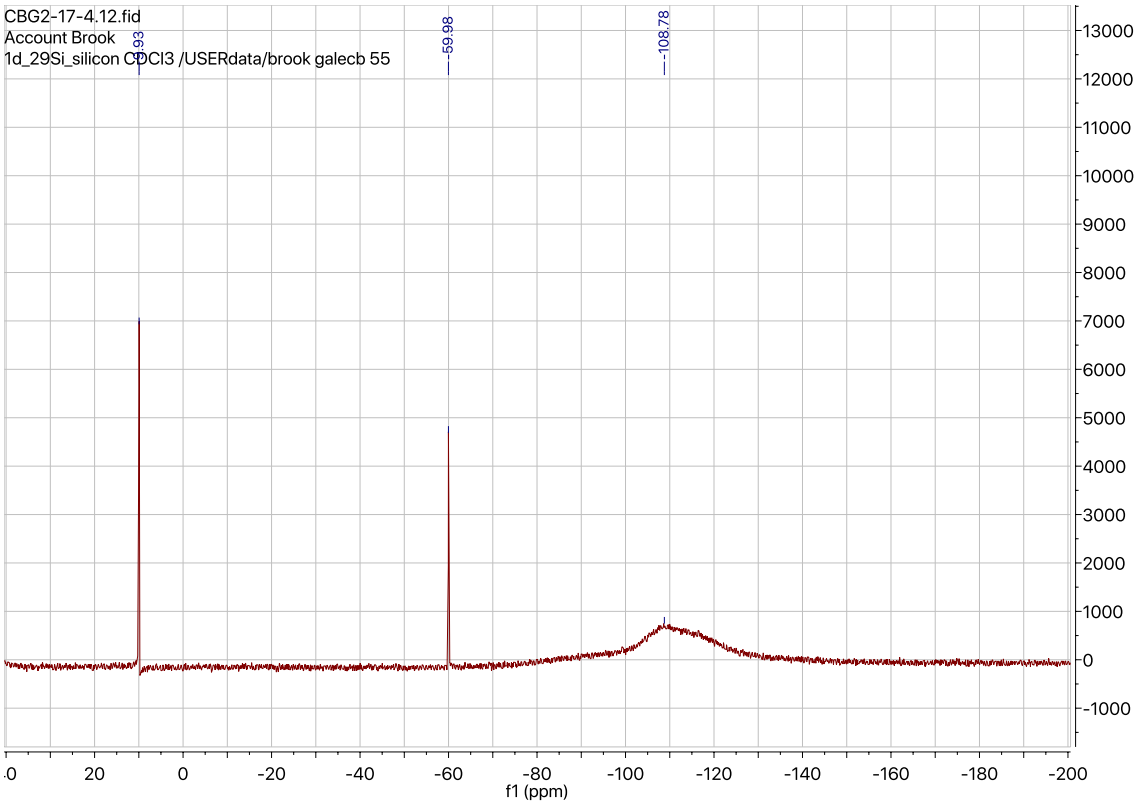

Figure 6.6: ^{29}Si NMR of Zn-TPMP-Bis-H.

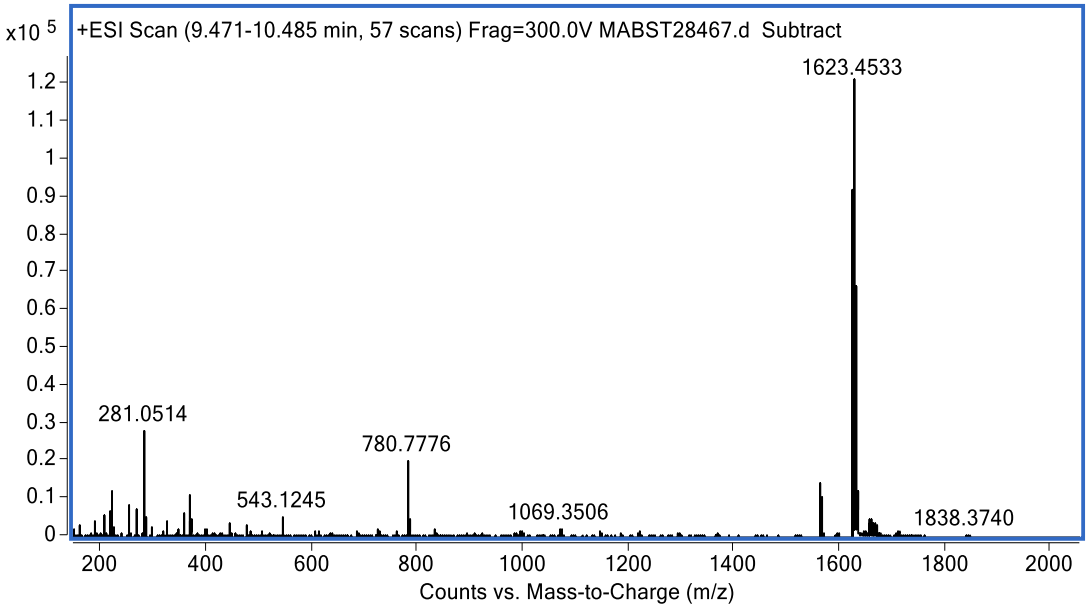

Figure 6.7: ESI-MS of Zn-TPMP-Bis-H.

6.1.3 Dielectric Properties of Zn-TPMP Elastomers

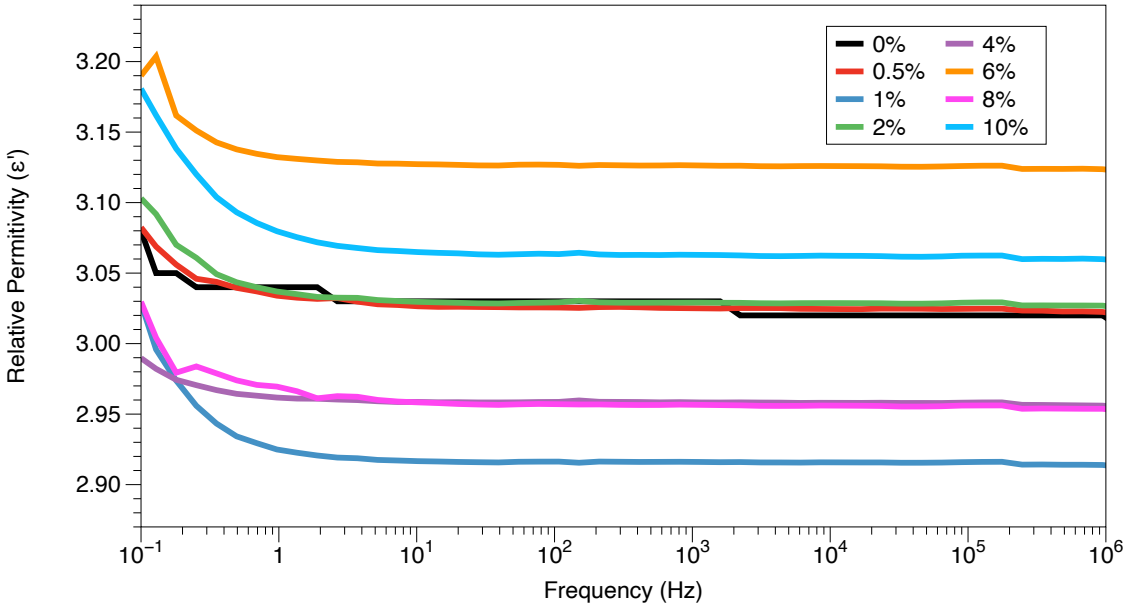

Figure 6.8: Relative permittivity of Zn-TPMP in HMS-301+DMS-V22 platinum cure system.

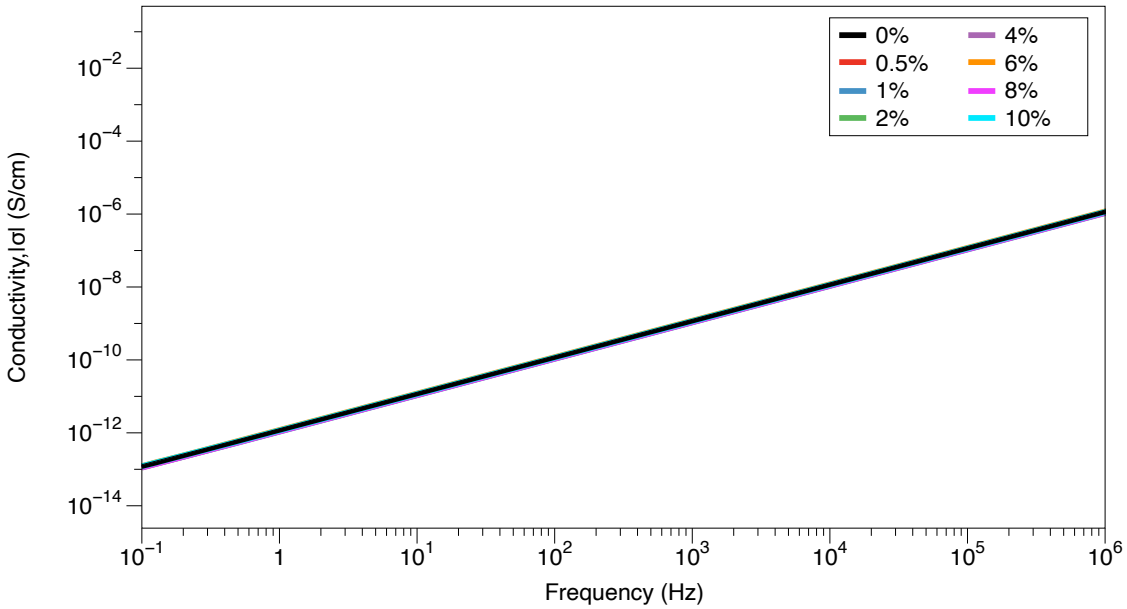

Figure 6.9: Conductivity of Zn-TPMP in HMS-301+DMS-V22 platinum cure system.

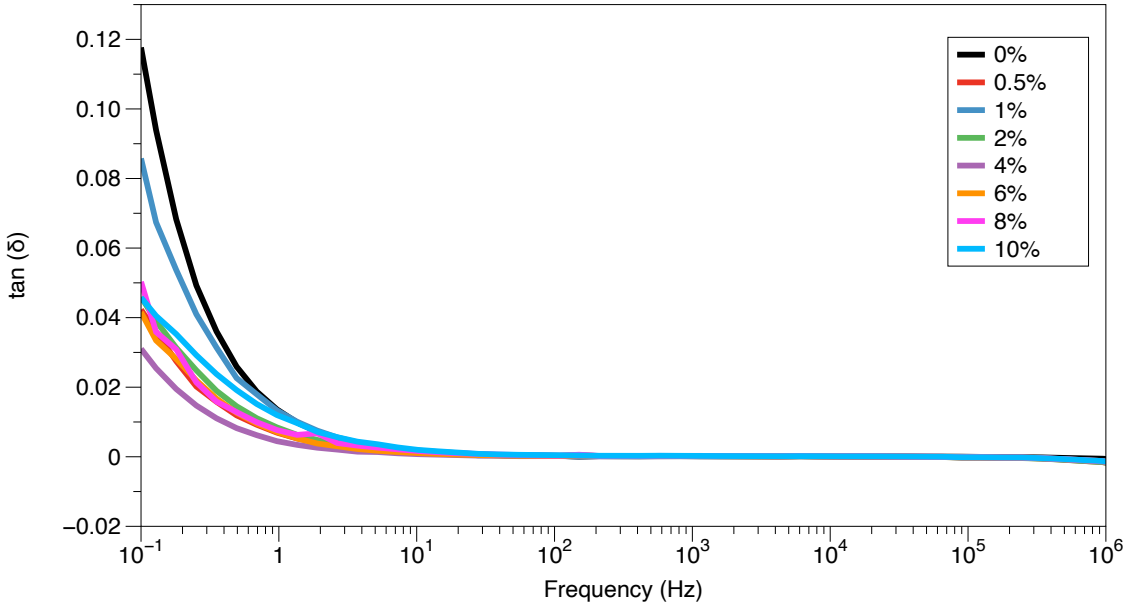

Figure 6.10: Dielectric loss of Zn-TPMP in HMS-301+DMS-V22 platinum cure system.

6.1.4 Dielectric Properties of Zn-TPMP-Bis-H Elastomers

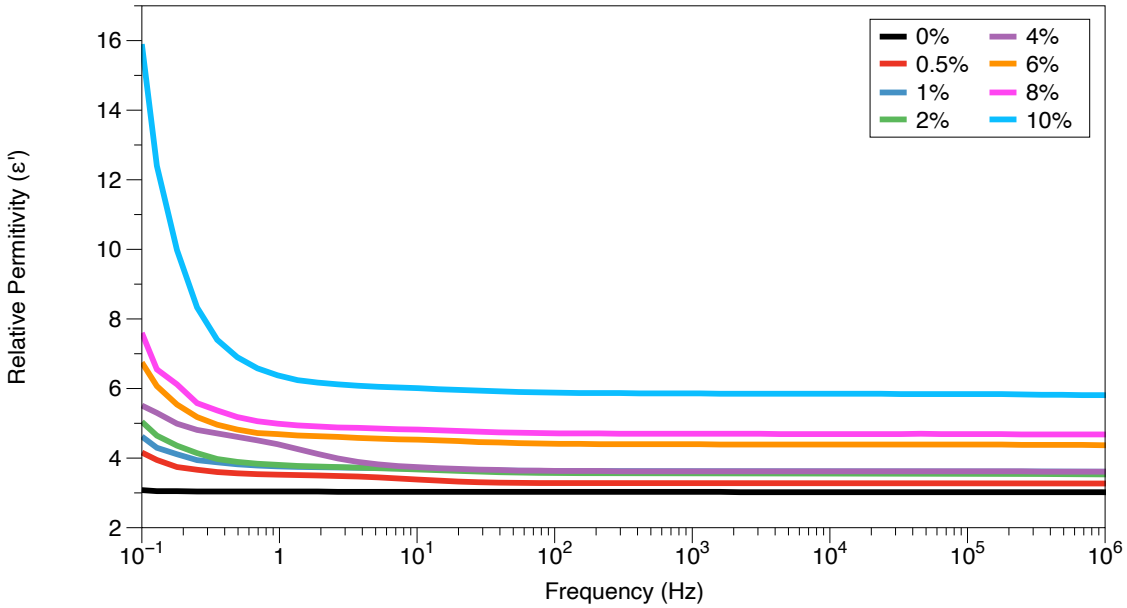

Figure 6.11: Relative permittivity of Zn-TPMP-Bis-H in HMS-301+DMS-V22 platinum cure system.

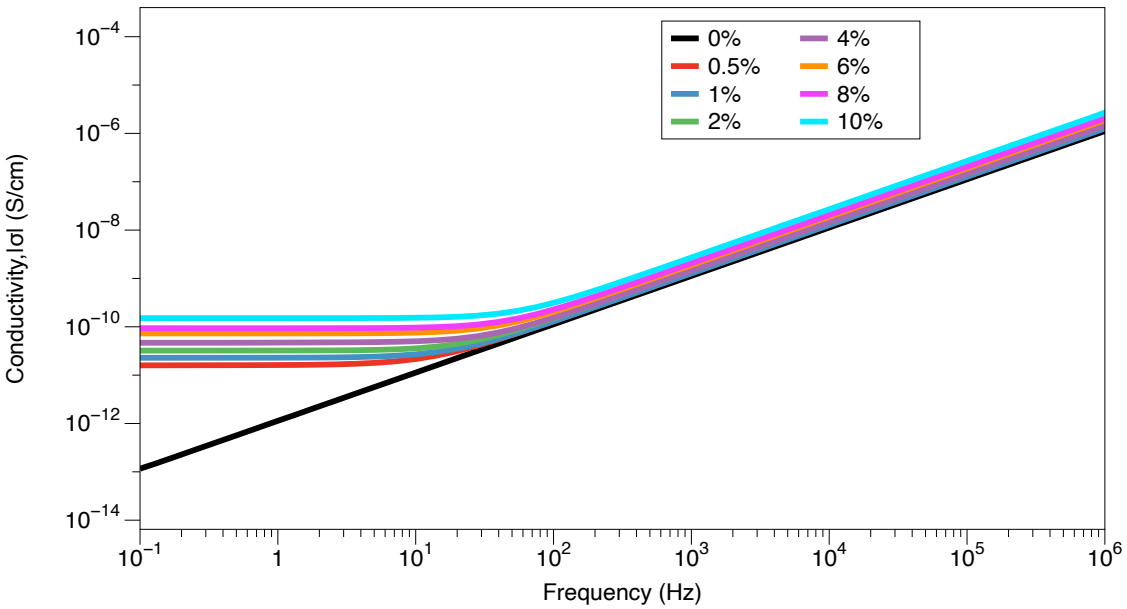

Figure 6.12: Conductivity of Zn-TPMP-Bis-H in HMS-301+DMS-V22 platinum cure system.

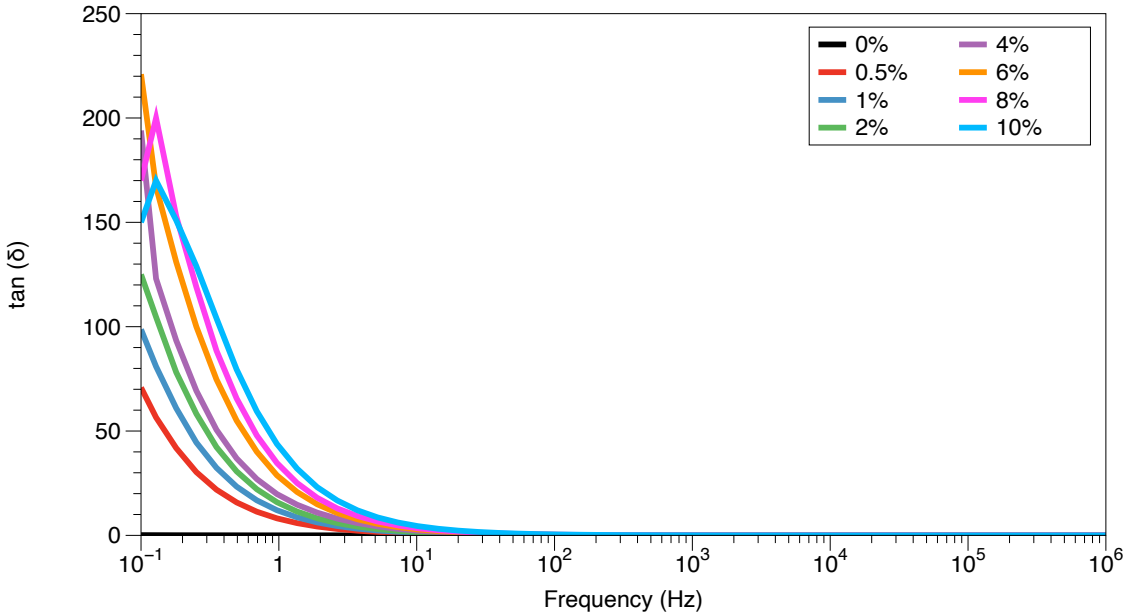

Figure 6.13: Dielectric loss of Zn-TPMP-Bis-H in HMS-301+DMS-V22 platinum cure system.

6.1.5 Dielectric Properties of Elastosil 625 Zn-TPMP-Bis-H Elastomers

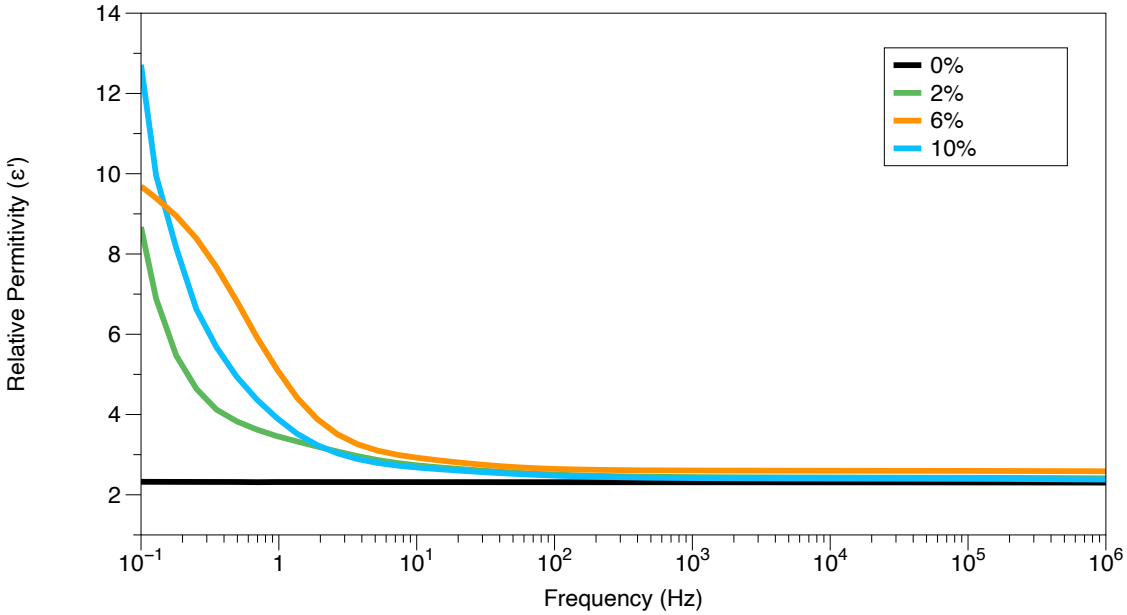

Figure 6.14: Relative permittivity of Zn-TPMP-Bis-H in Elastosil 625.

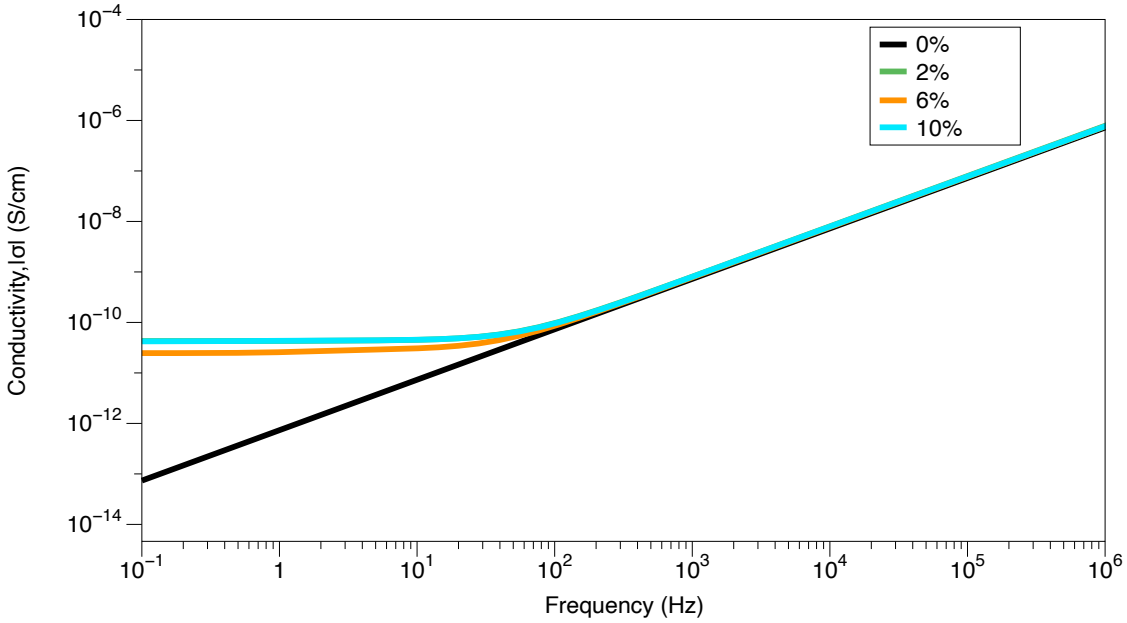

Figure 6.15: Conductivity of Zn-TPMP-Bis-H in Elastosil 625.

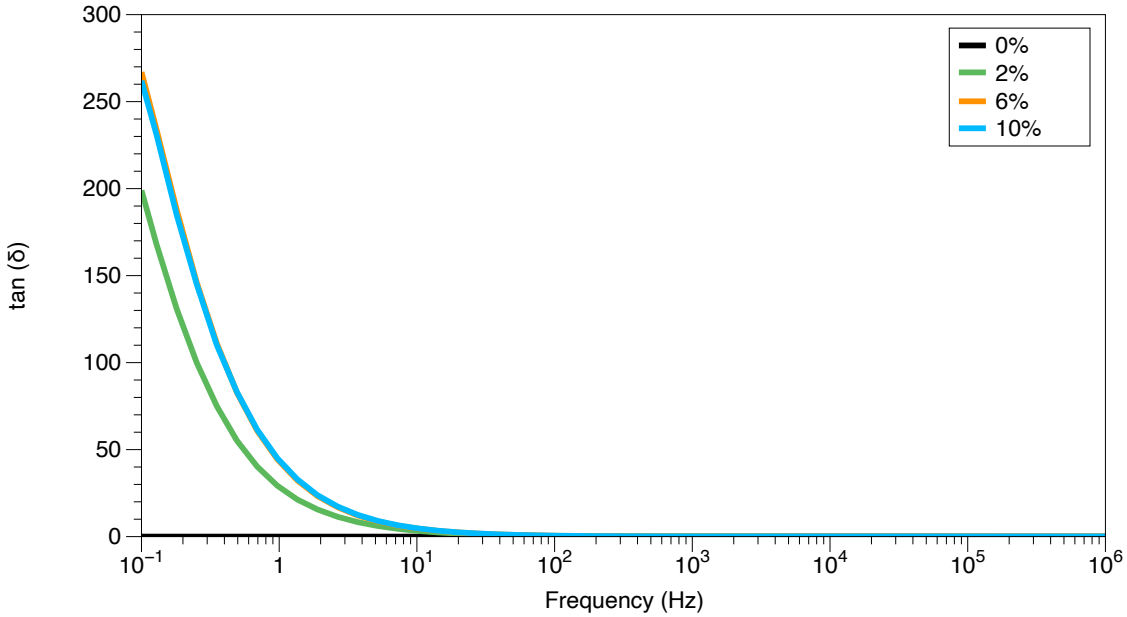

Figure 6.16: Dielectric loss of Zn-TPMP-Bis-H in Elastosil 625.

Table 6.1: Electrical breakdown results for Elastosil 625 0% Zn-TPMP-Bis-H.

Sample		Elastosil 625 0%
Sample normal thickness (μm) measured with optical microscope		107
Thickness measured with gauge (μm)	Breakdown voltage (kV)	Field Strength (V/μm)
107	10.2	95.6
107	11.1	104
107	10.6	99.3
107	10.0	93.5
105	10.0	95.6
106	11.3	107
107	10.9	102
105	10.5	100
107	10.8	101
107	10.1	94.3
108	10.0	92.8
107	10.4	97.2
Average Field Strength (V/μm)		98.4
STDEV		4.11
β		26.6
η		100
R^2		0.886

Table 6.2: Electrical breakdown results for Elastosil 625 2% Zn-TPMP-Bis-H

Sample		Elastosil 625 2%
Sample normal thickness (μm) measured with optical microscope		116
Thickness measured with gauge (μm)	Breakdown voltage (kV)	Field Strength (V/μm)
117	6.66	56.9
116	6.69	57.7
116	6.58	56.7
116	6.52	56.2
115	6.98	60.7
115	7.33	63.7
117	7.4	63.2
115	6.74	58.6
117	7.16	61.2
117	7.02	60.0
115	7	60.9
115	6.98	60.7
Average Field Strength (V/μm)		59.7
STDEV		2.39
β		27.86
η		61
R^2		0.9

Table 6.3: Electrical breakdown results for Elastosil 625 6% Zn-TPMP-Bis-H.

Sample		Elastosil 625 6%
Sample normal thickness (μm) measured with optical microscope		102
Thickness measured with gauge (μm)	Breakdown voltage (kV)	Field Strength (V/μm)
102	6.08	59.6
100	5.8	58.0
101	5.88	58.2
102	5.81	56.9
103	5.72	55.5
102	5.71	55.9
103	5.72	55.5
102	5.94	58.2
100	5.32	53.2
102	6.13	60.1
102	6.12	60
102	5.69	55.8
Average Field Strength (V/μm)		57.3
STDEV		2.1
β		31.9
η		58
R^2		0.94

Table 6.4: Electrical breakdown results for Elastosil 625 10% Zn-TPMP-Bis-H.

Sample		Elastosil 625 10%
Sample normal thickness (μm) measured with optical microscope		97
Thickness measured with gauge (μm)	Breakdown voltage (kV)	Field Strength (V/μm)
103	5.19	50.4
103	5.41	52.5
107	4.97	46.4
103	5.15	50.0
105	5.25	50.0
107	5.00	46.7
105	4.97	47.3
105	5.18	49.3
105	5.27	50.2
103	5.59	54.3
103	5.50	53.4
103	5.48	53.2
Average Field Strength (V/μm)		50.3
STDEV		2.63
β		22.0
η		52.7
R^2		0.912

6.1.6 Rheology Results/ Tensile Tests Results

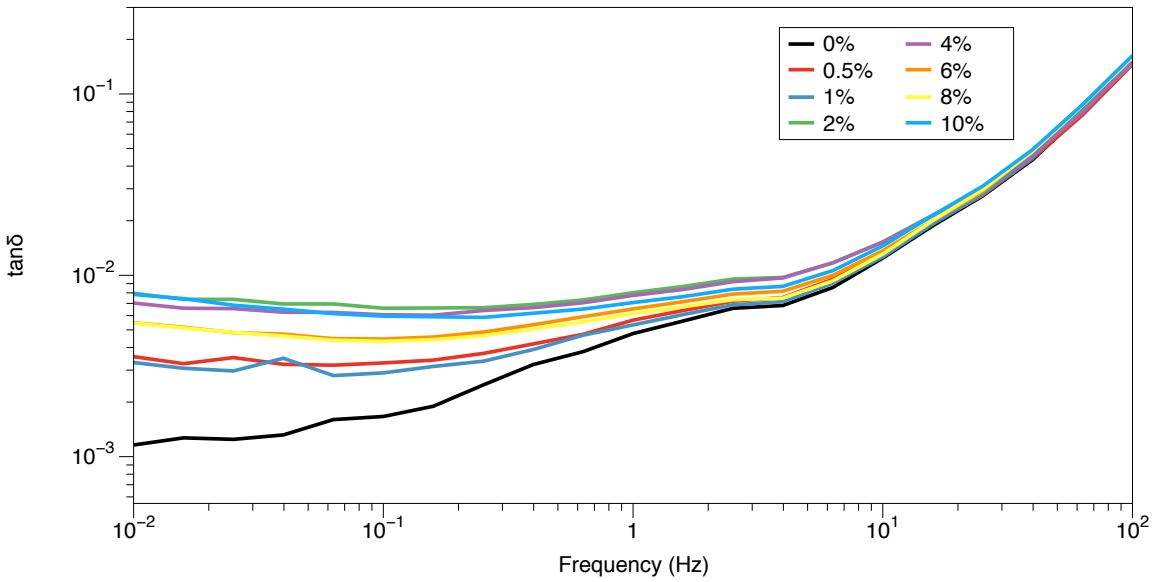

Figure 6.17: tan(δ) of Zn-TPMP elastomers, homemade formulation @25°C

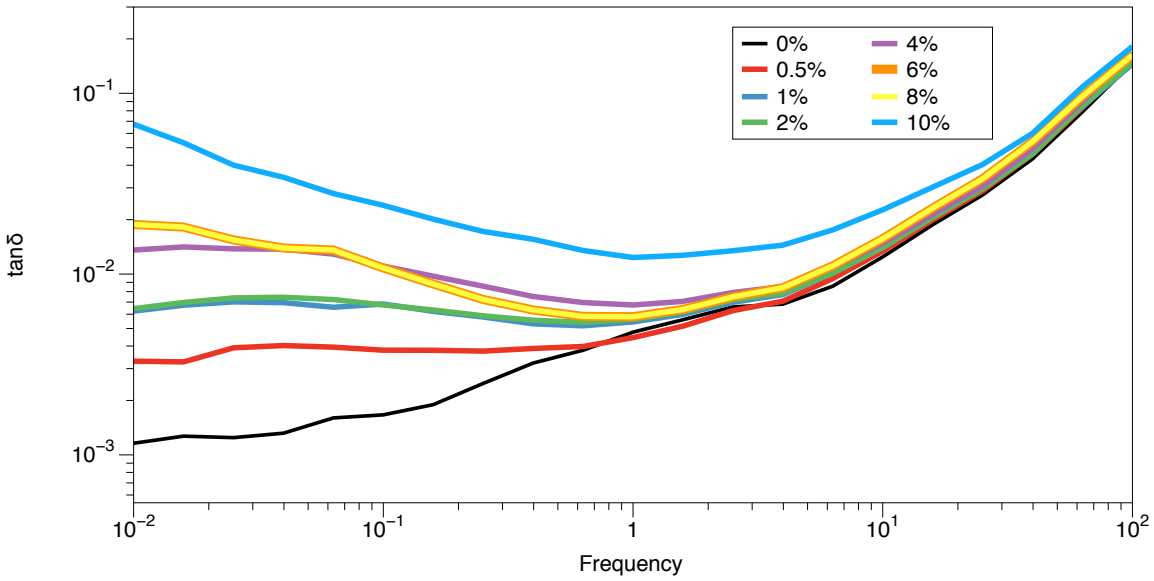

Figure 6.18: tan(δ) of Zn-TPMP-Bis-H elastomers, homemade formulation @25°C.

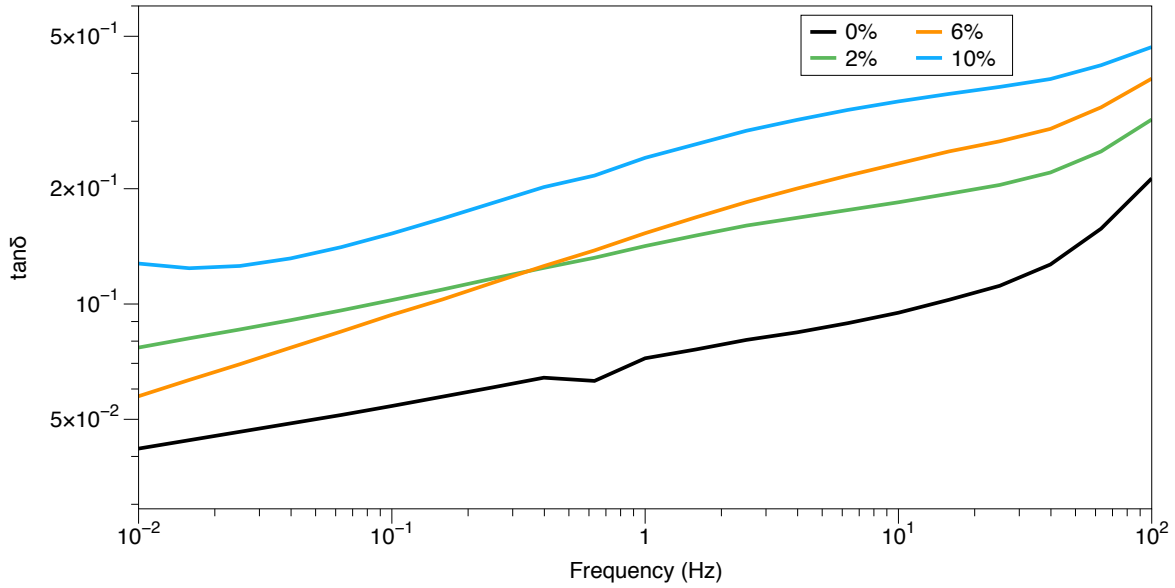

Figure 6.19: tan(δ) of Zn-TPMP-Bis-H elastomers, Elastosil 625 @25°C.

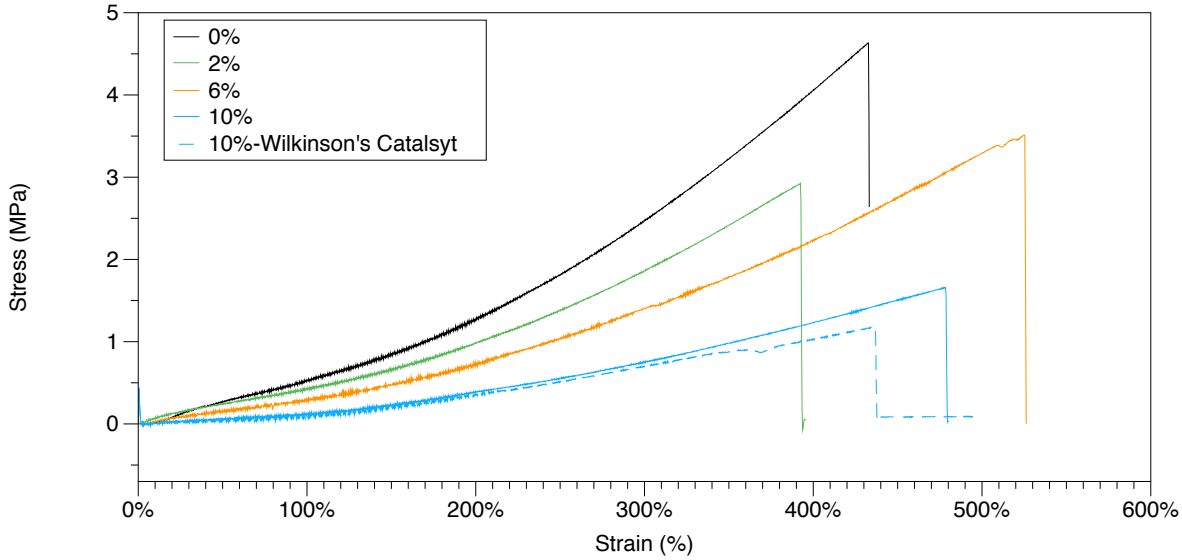

Figure 6.20:Stress-Strain curves for Elastosil 625 elastomers.

6.1.7 Elastomer Curing-Elastosil 625

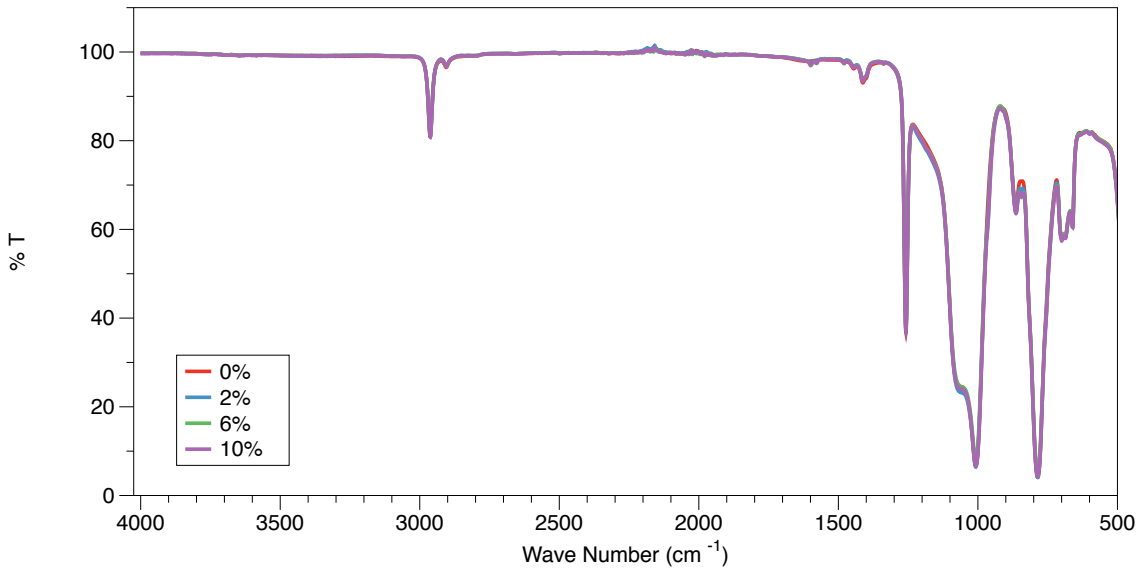

Figure 6.21: IR spectra of elastomers showing no residual Si-H.

It was important to establish whether the differences in mechanical properties of the samples containing 6 and 10% porphyrin, were a result of incomplete curing. IR spectroscopy was used to probe the samples for unreacted Si-H groups, which would indicate that that the porphyrin was quenching the catalyst. The IR spectra of the samples was obtained no peaks in the 2080-2280 cm^{-1} region, indicative of unreacted Si-H could be detected. Secondary analysis of the samples via ^{1}H-NMR was not informative as the signals corresponding to Si-CH_3 protons overwhelmed all other signals.

Table 6.5: Shore OO data for Elastosil 625 samples.

% Zn-TPMP-Bis-H	Shore OO
0	75
2	67
6	55
10	37

6.1.8 Phase Separation/ Oil Migration

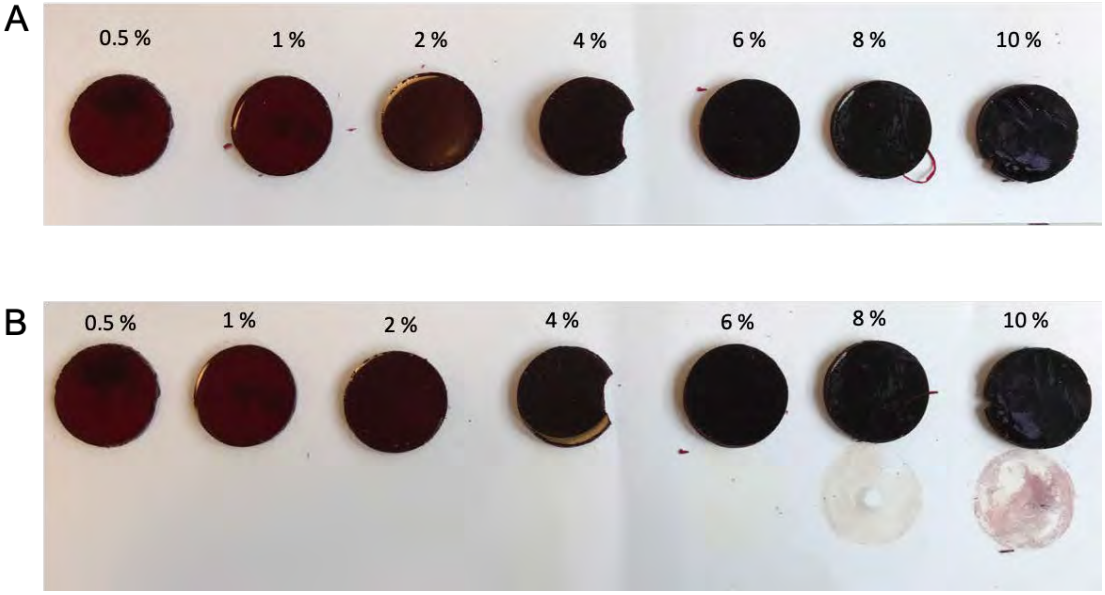

Figure 6.22: A) Zn-TPMP-Bis-H elastomers in homemade formulation placed on paper. B) Residue of elastomers left behind on paper after application of 2 kg weight to each elastomer.

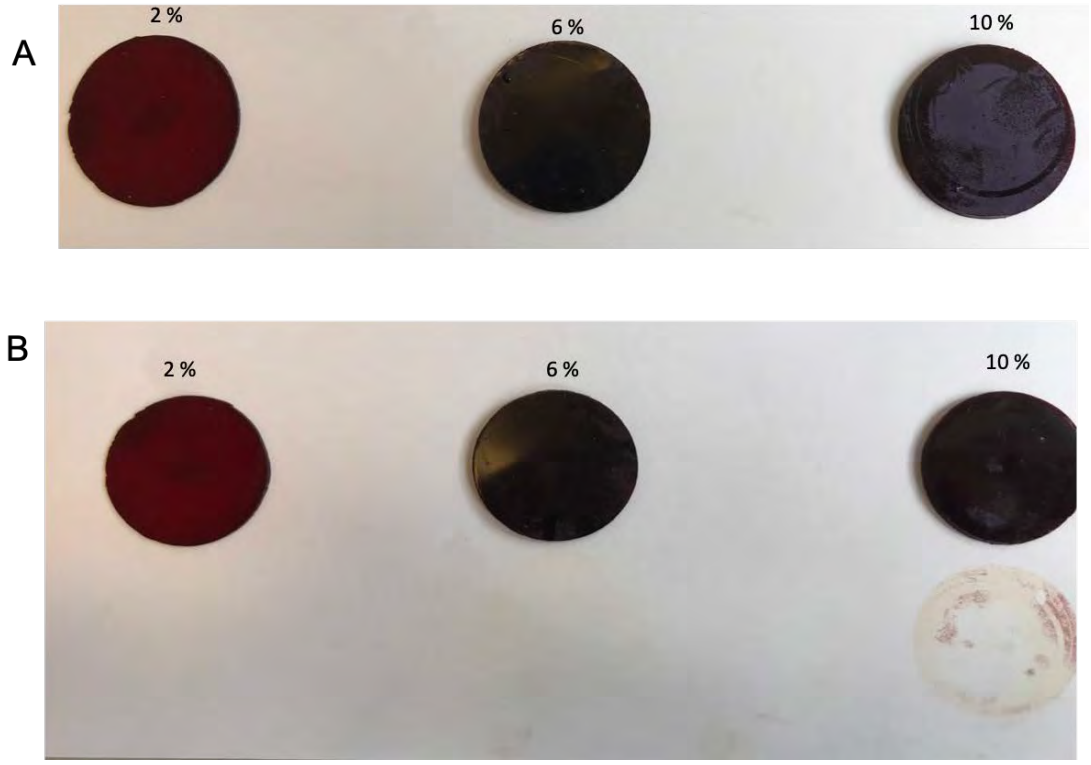

Figure 6.23: A) Zn-TPMP-Bis-H elastomers in Elastosil 625 placed on paper. B) Residue of elastomers left behind on paper after application of 2 kg weight to each elastomer.

6.2 Appendix II: Supporting Information for Chapter 3

6.2.1 Synthesis of $Si(Si_{12}O_2C_6H_{15})_4$.

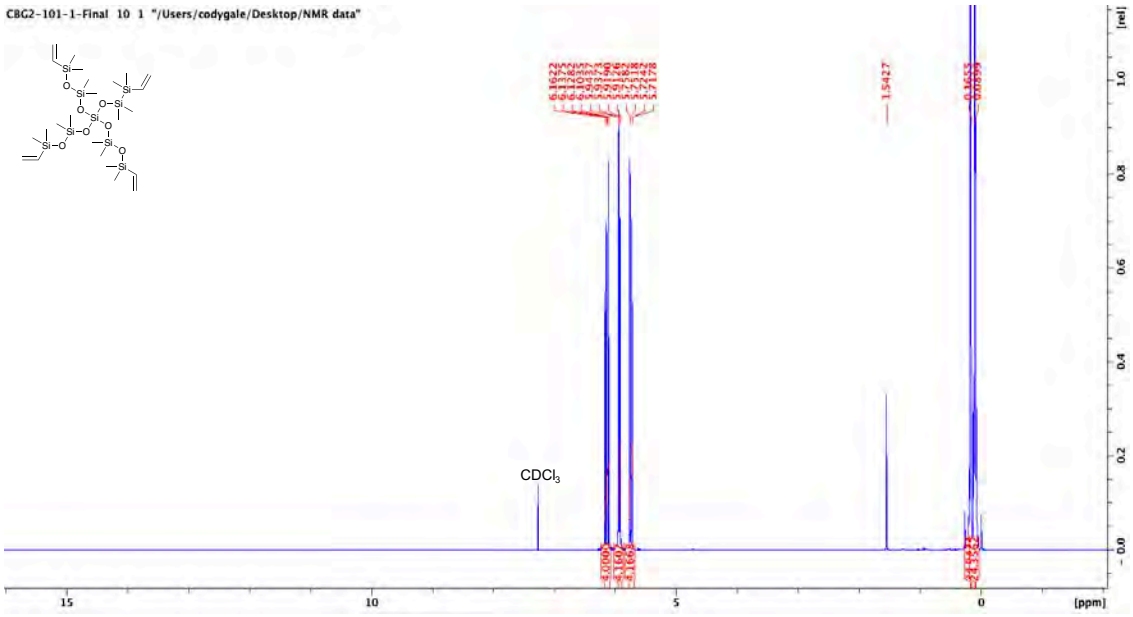

Figure 6.24: ^{1}H NMR of $Si(Si_{12}O_2C_6H_{15})_4$.

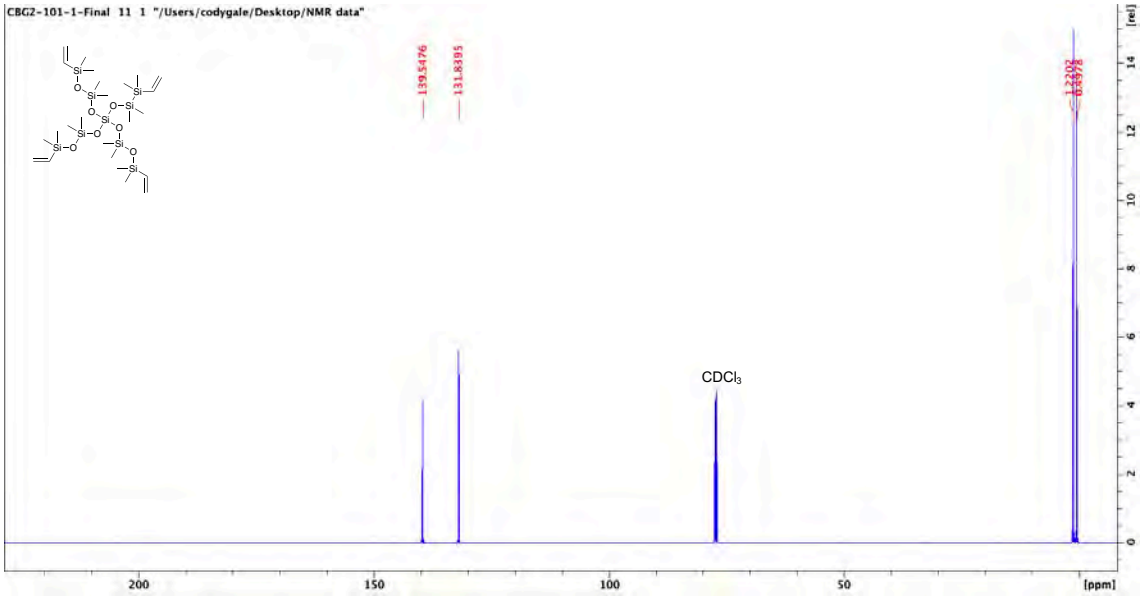

Figure 6.25: ^{13}C NMR of $Si(Si_{12}O_2C_6H_{15})_4$.

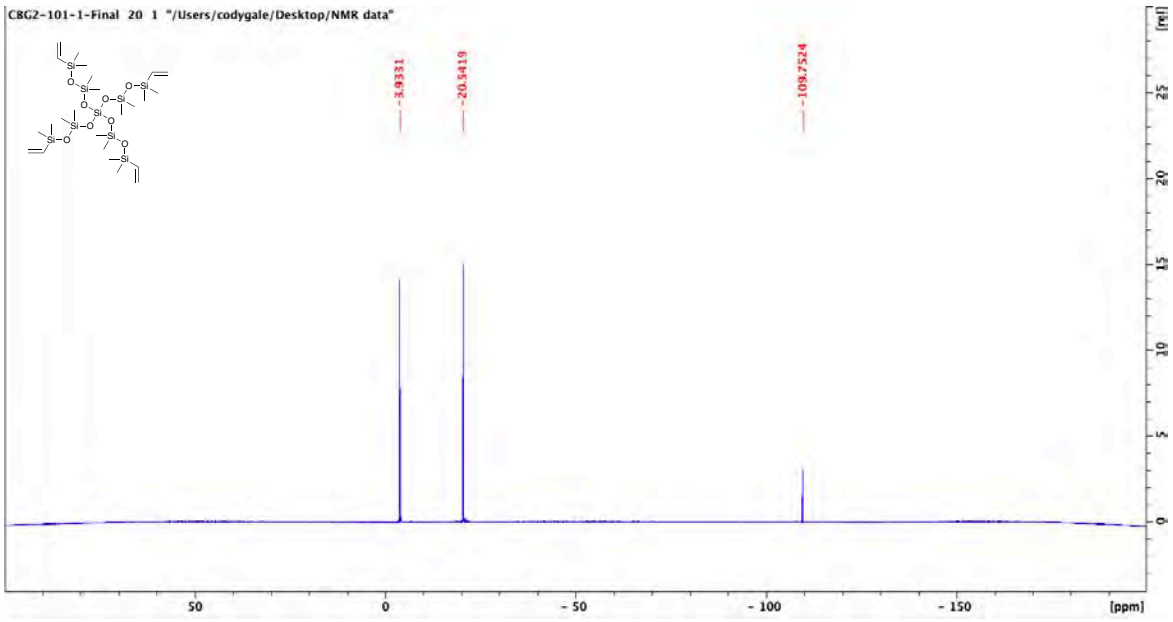

Figure 6.26: ^{29}Si NMR of $Si(Si_{12}O_2C_6H_{15})_4$.

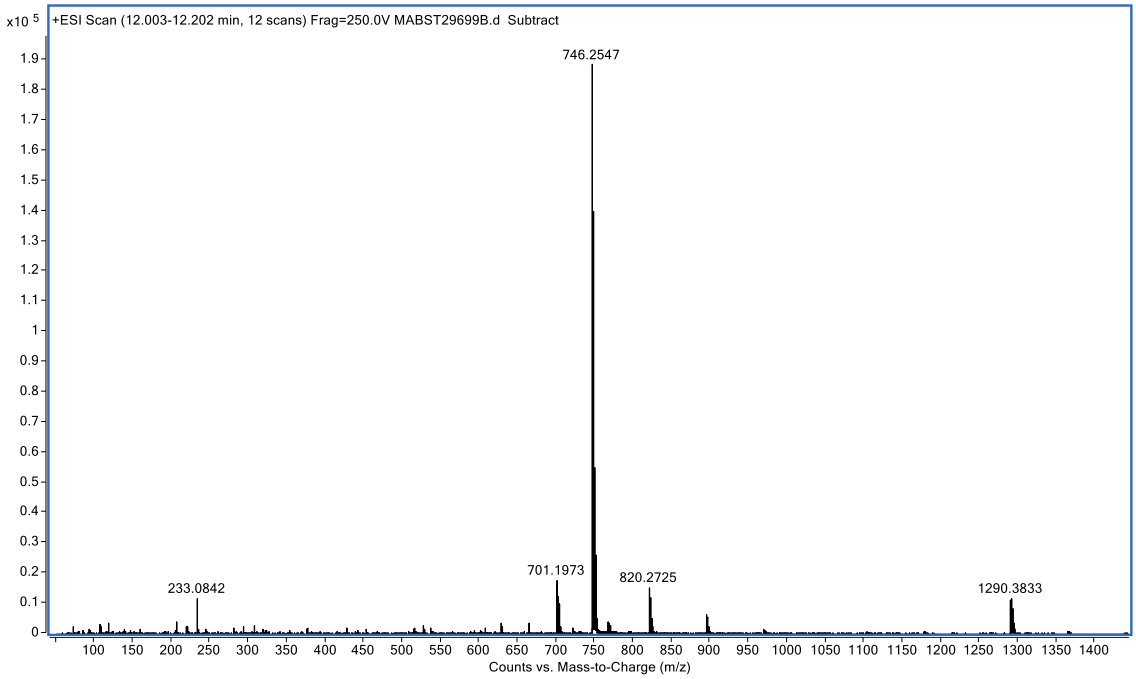

Figure 6.27: ESI-MS of $Si(Si_{12}O_2C_6H_{15})_4$.

6.2.2 Synthesis of Zn-TPMP

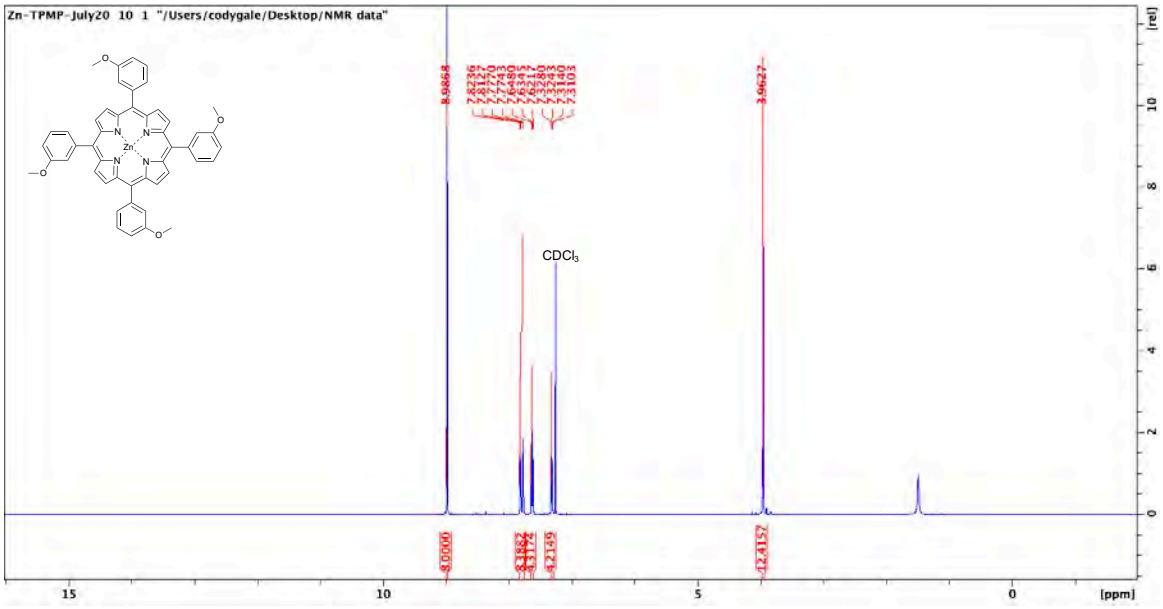

Figure 6.28: ^{1}H NMR of Zn-TPMP.

.

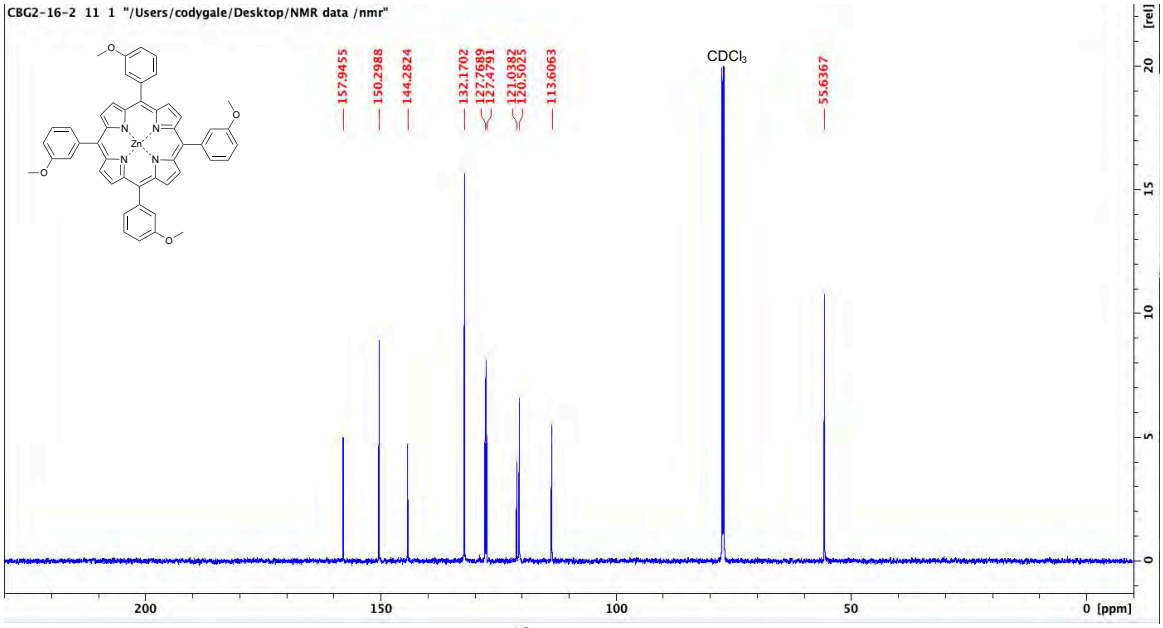

Figure 6.29: ^{13}C NMR of Zn-TPMP.

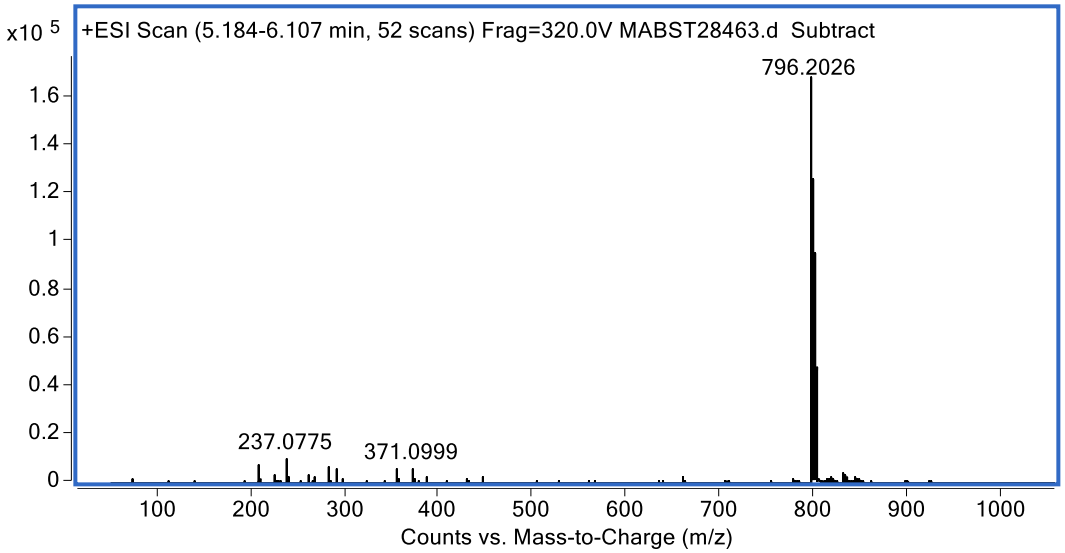

Figure 6.30: ESI-MS of Zn-TPMP.

6.2.3 Synthesis of Zn-TPMP-HV15

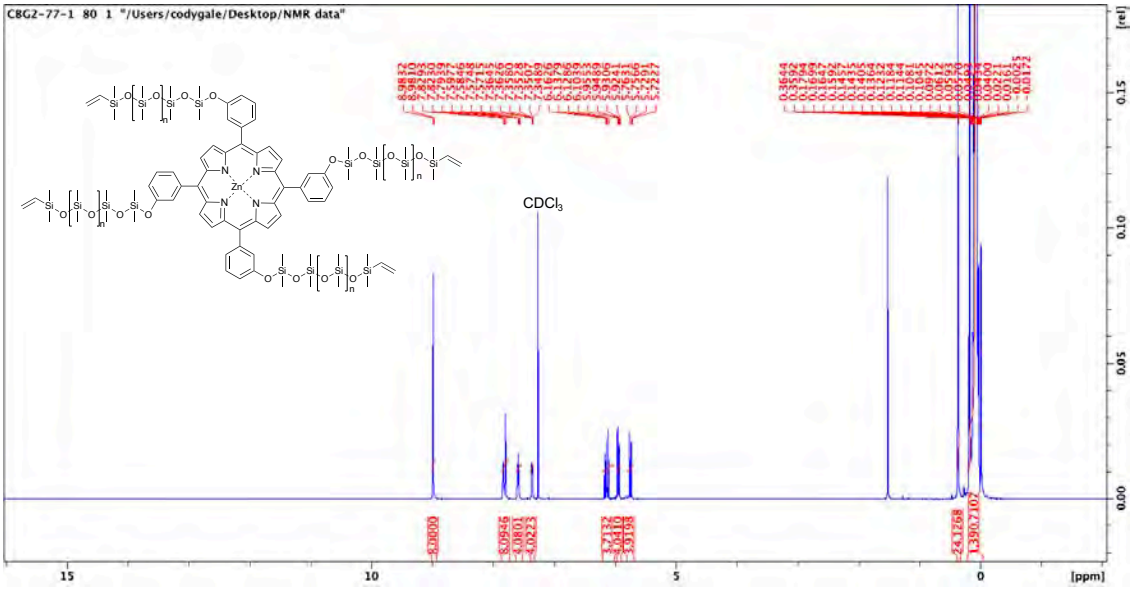

Figure 6.31: ^{1}H NMR of Zn-TPMP-HV15.

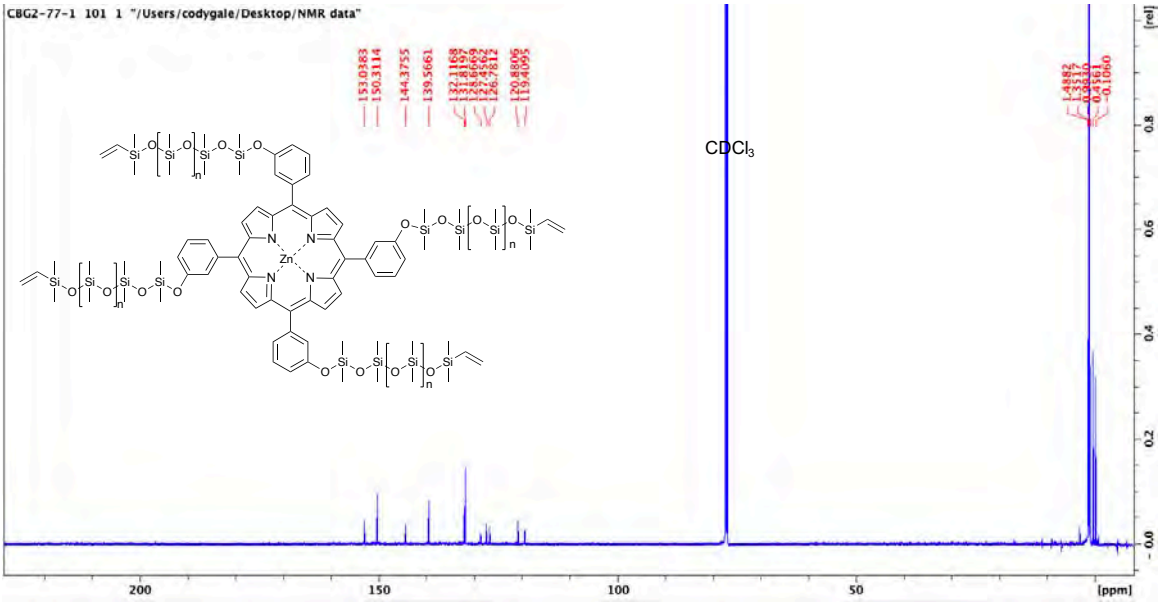

Figure 6.32: ^{13}C NMR of Zn-TPMP-Penta.

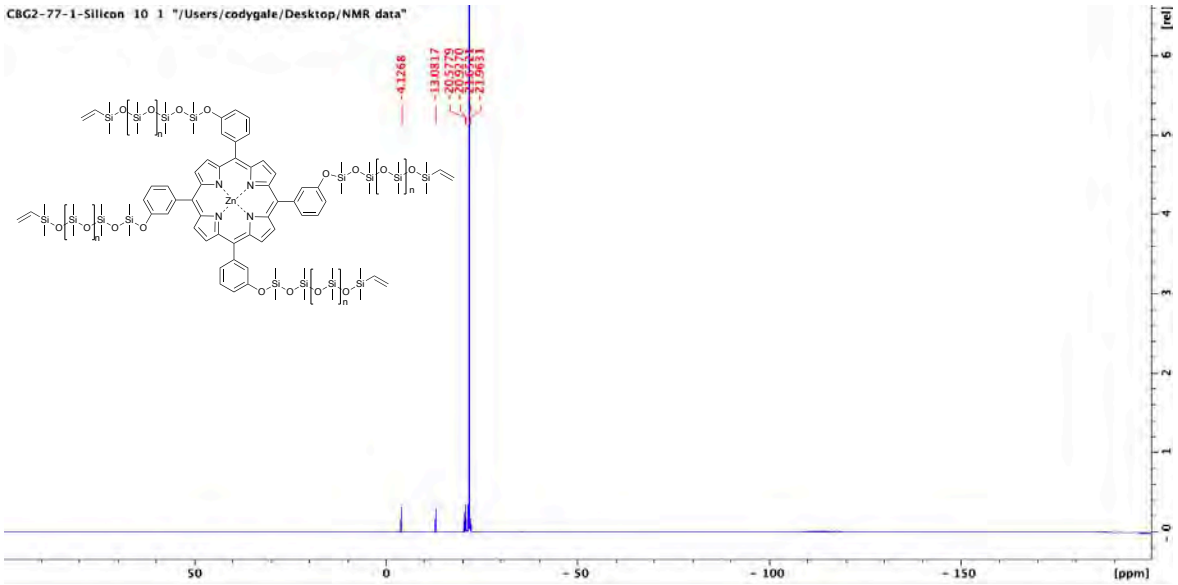

Figure 6.33: ^{29}Si NMR of Zn-TPMP-HV15.

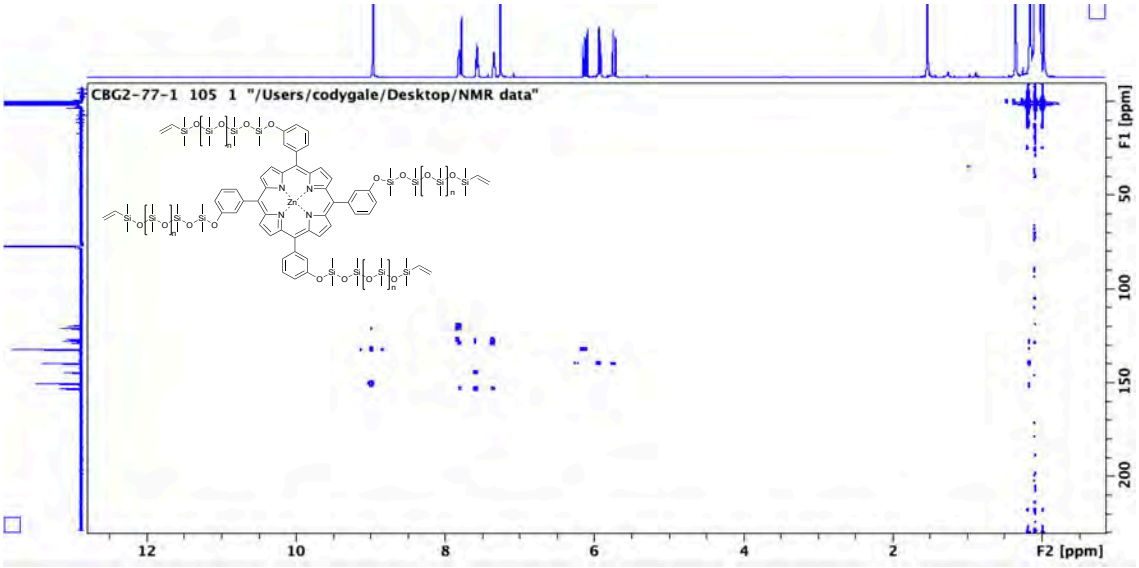

Figure 6.34: ^{1}H-^{13}C HMBC of Zn-TPMP-HV15.

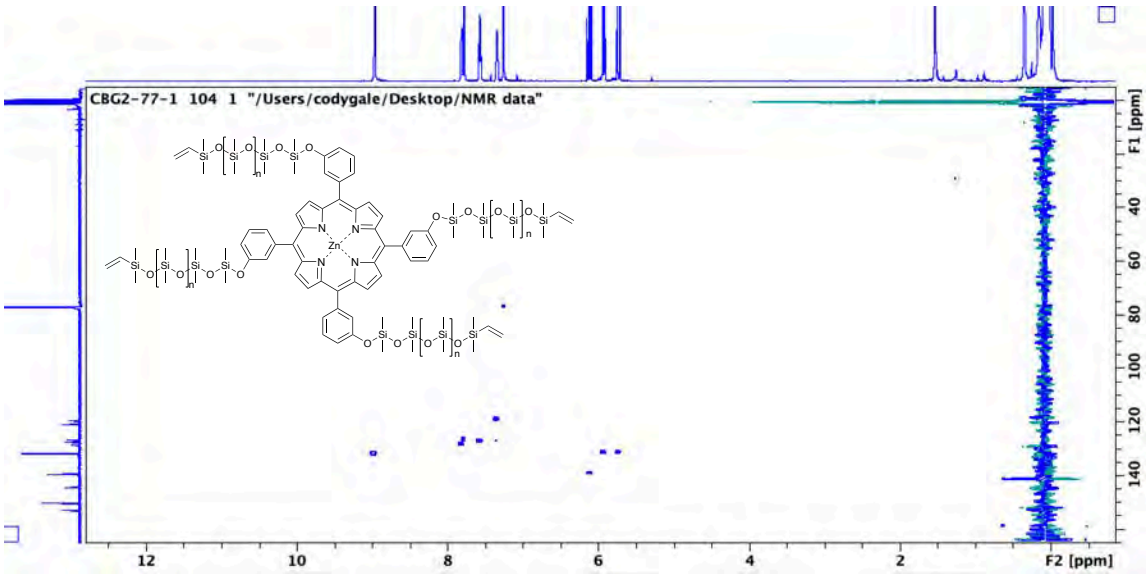

Figure 6.35: ^{1}H-^{13}C HSQC of Zn-TPMP-HV15.

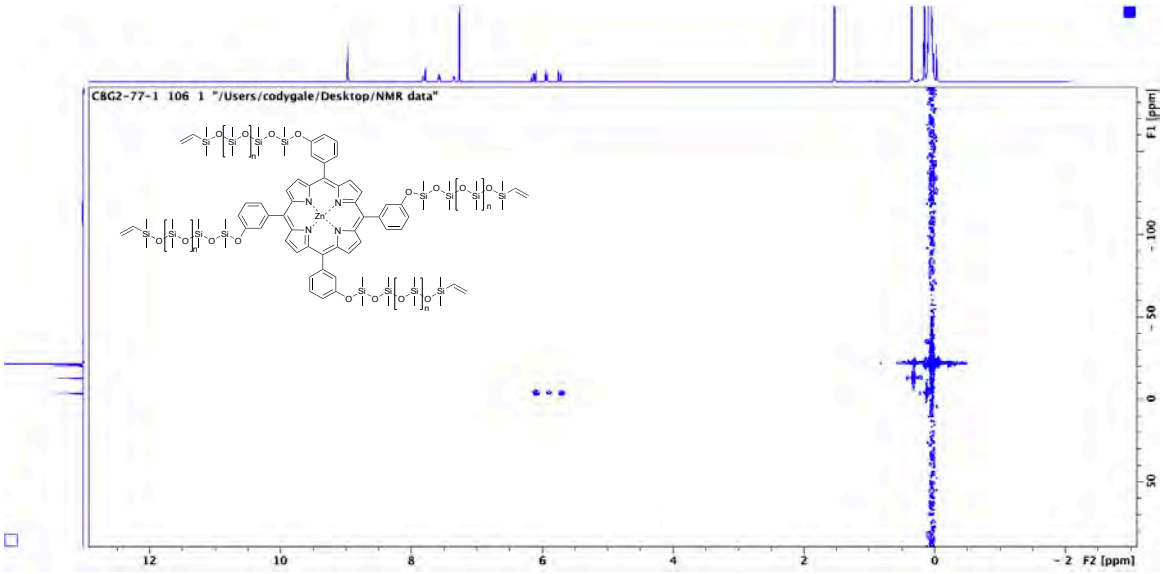

Figure 6.36: ^{1}H-^{29}Si HMBC of Zn-TPMP-HV15.

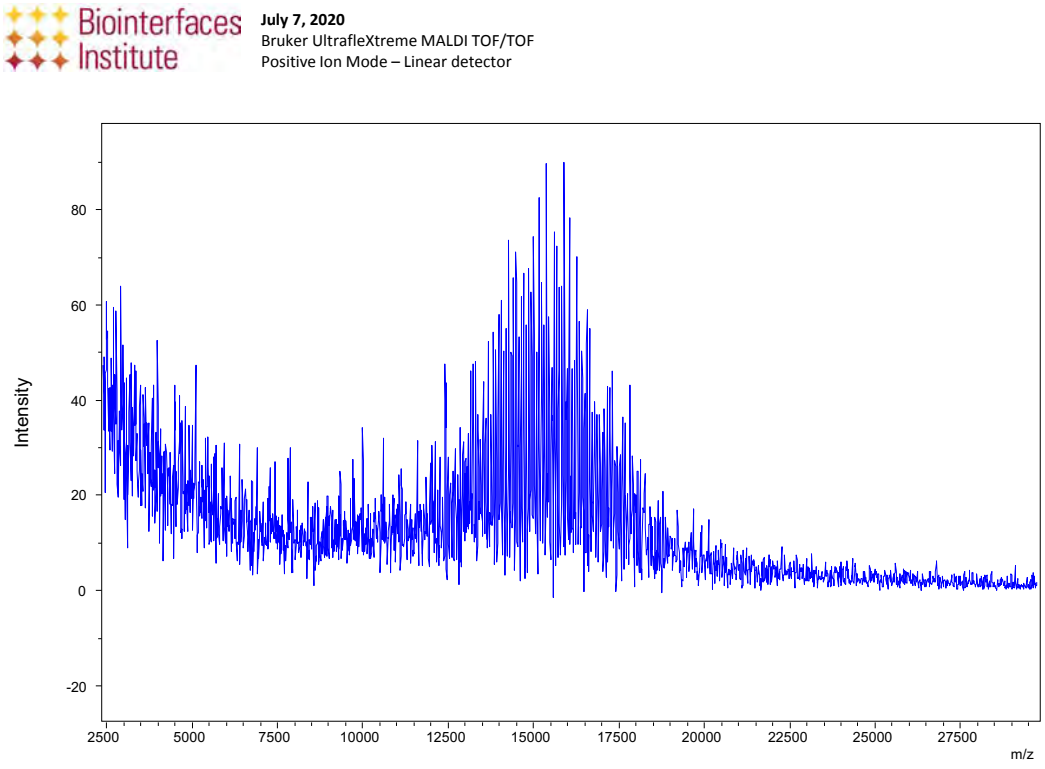

Figure 6.37: MALDI of Zn-TPMP-HV15.

6.2.4 Synthesis of Zn-TPMP-Penta

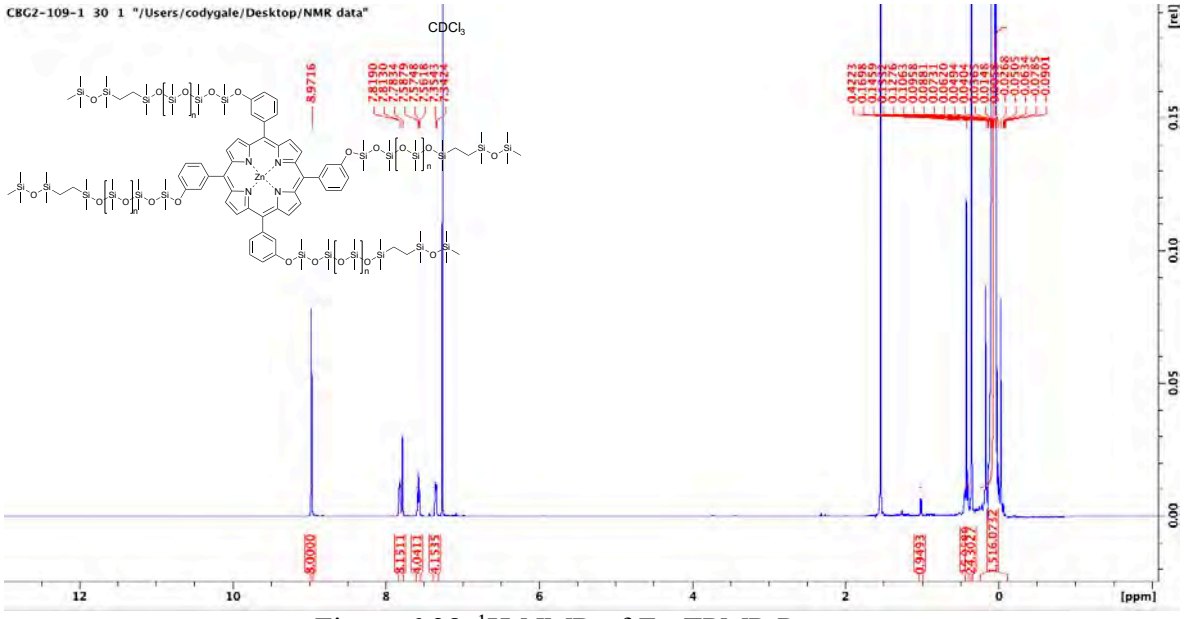

Figure 6.38: ^{1}H-NMR of Zn-TPMP-Penta

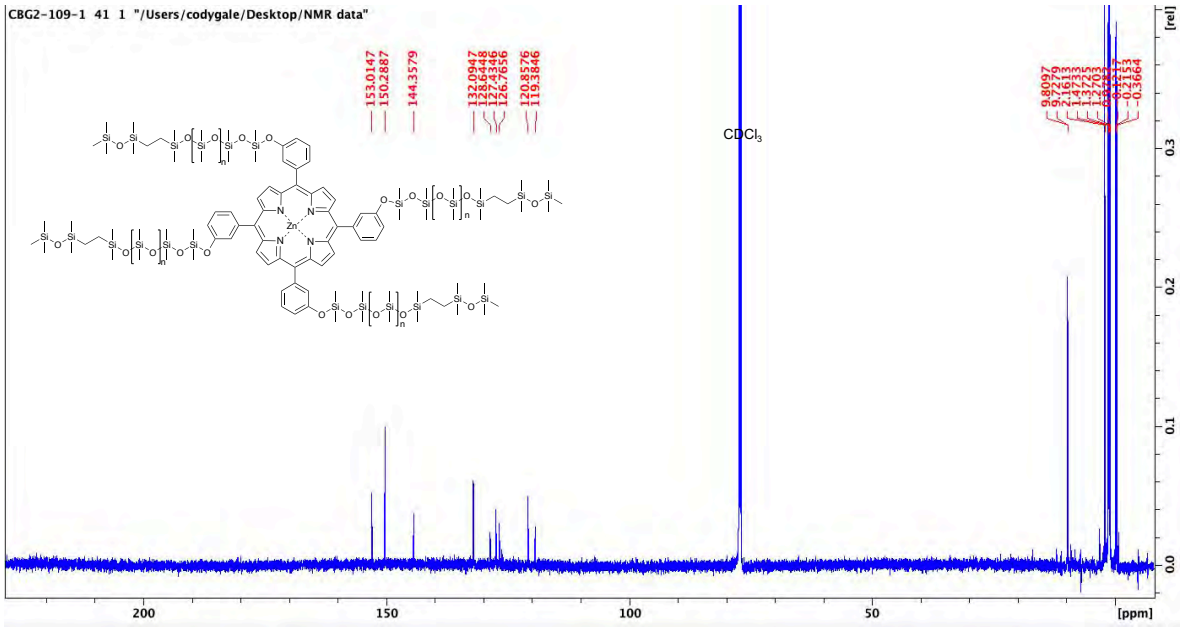

Figure 6.39: ^{13}C NMR of Zn-TPMP-Penta.

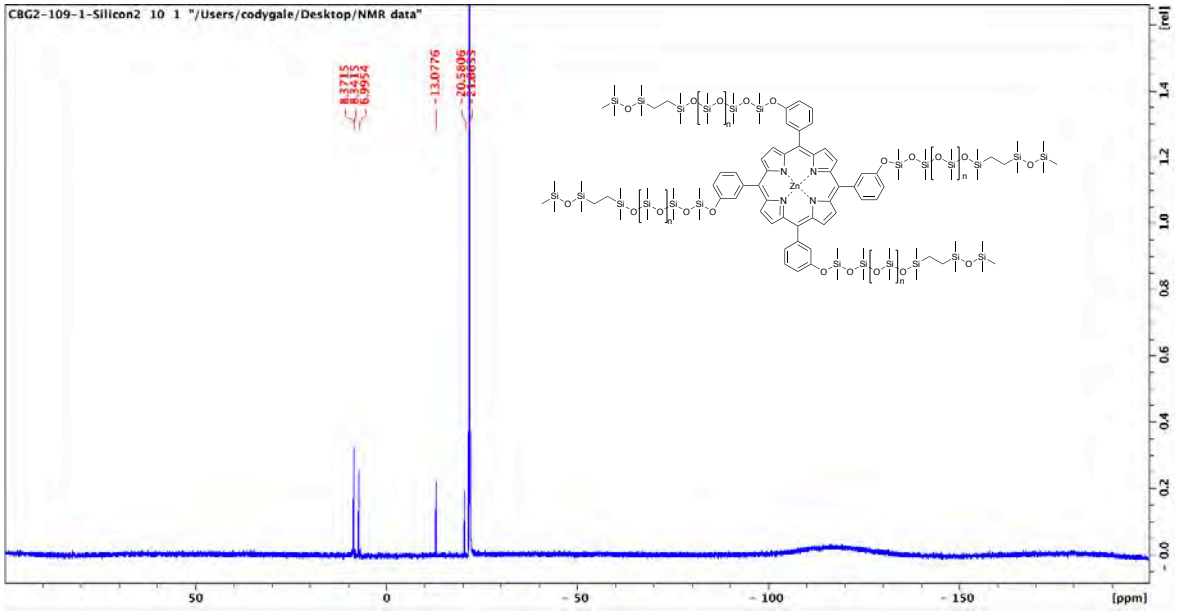

Figure 6.40: ^{29}Si-NMR of Zn-TPMP-Penta.

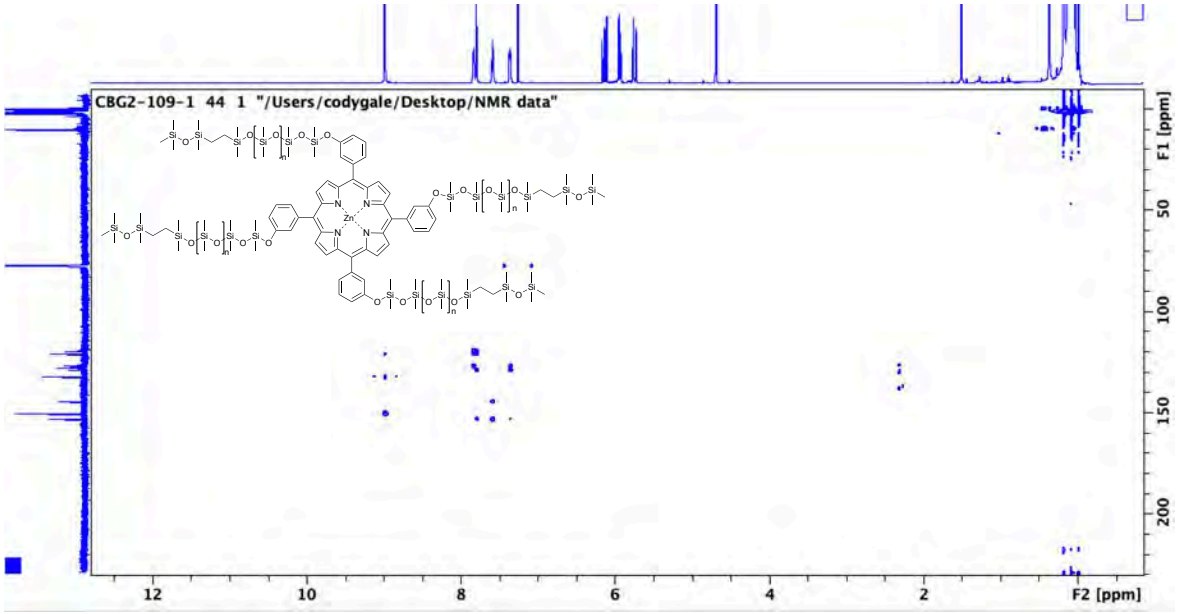

Figure 6.41: ^{1}H-^{13}C HMBC of Zn-TPMP-Penta.

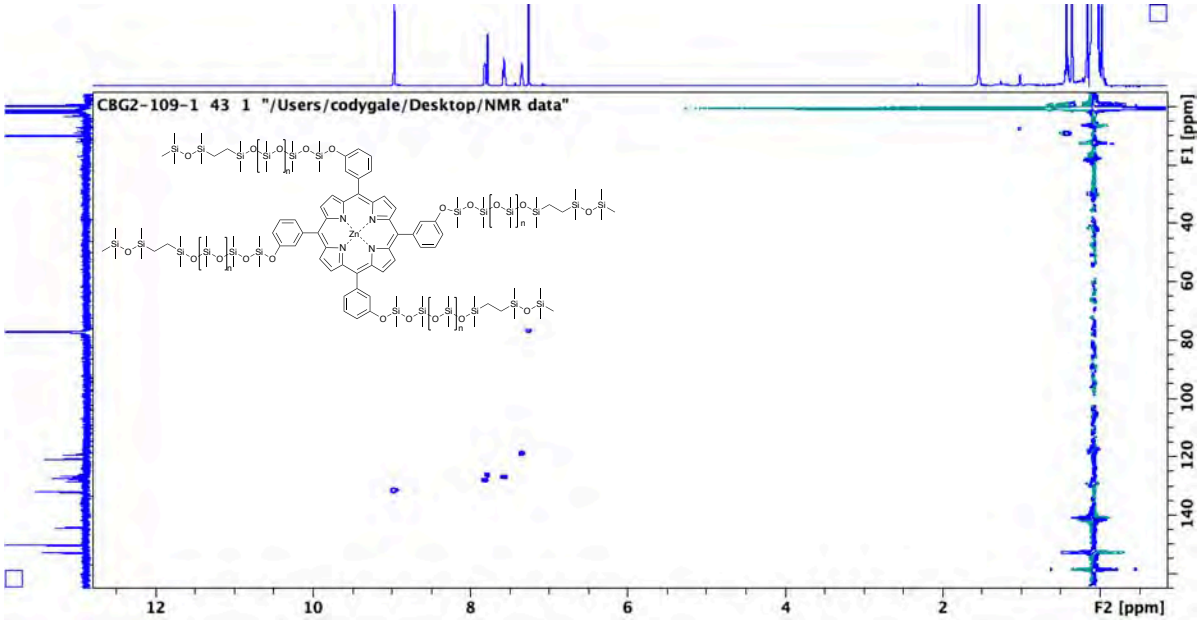

Figure 6.42: ^{1}H-^{13}C HMBC of Zn-TPMP-Penta.

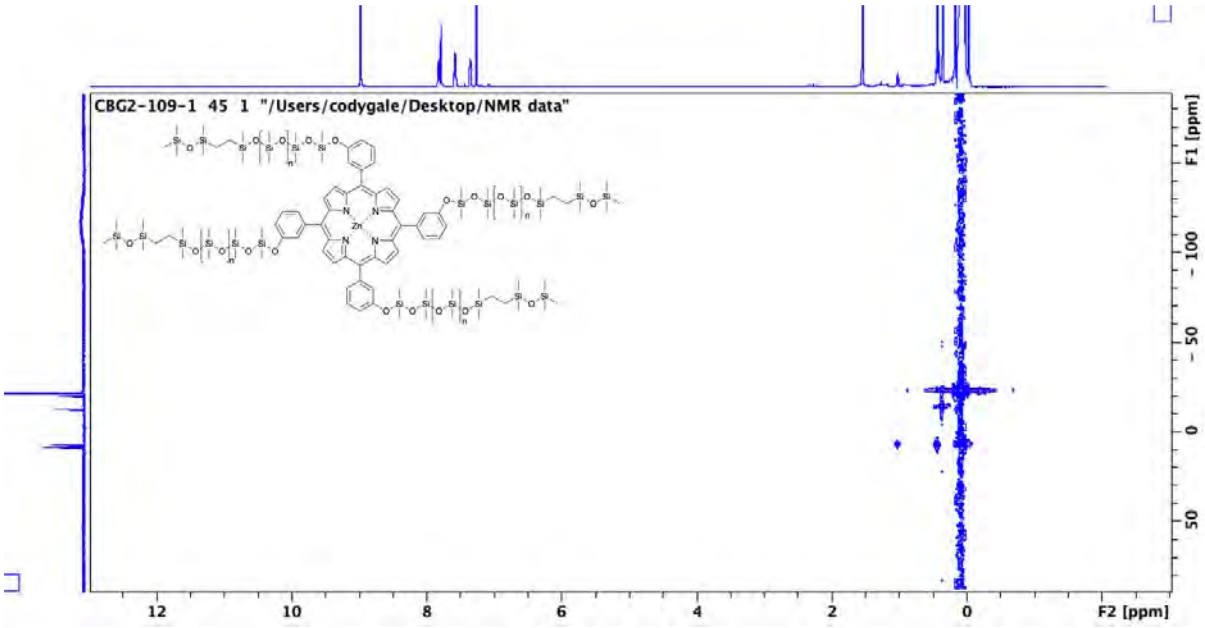

Figure 6.43: ^{1}H-^{29}Si HMBC of Zn-TPMP-Penta.

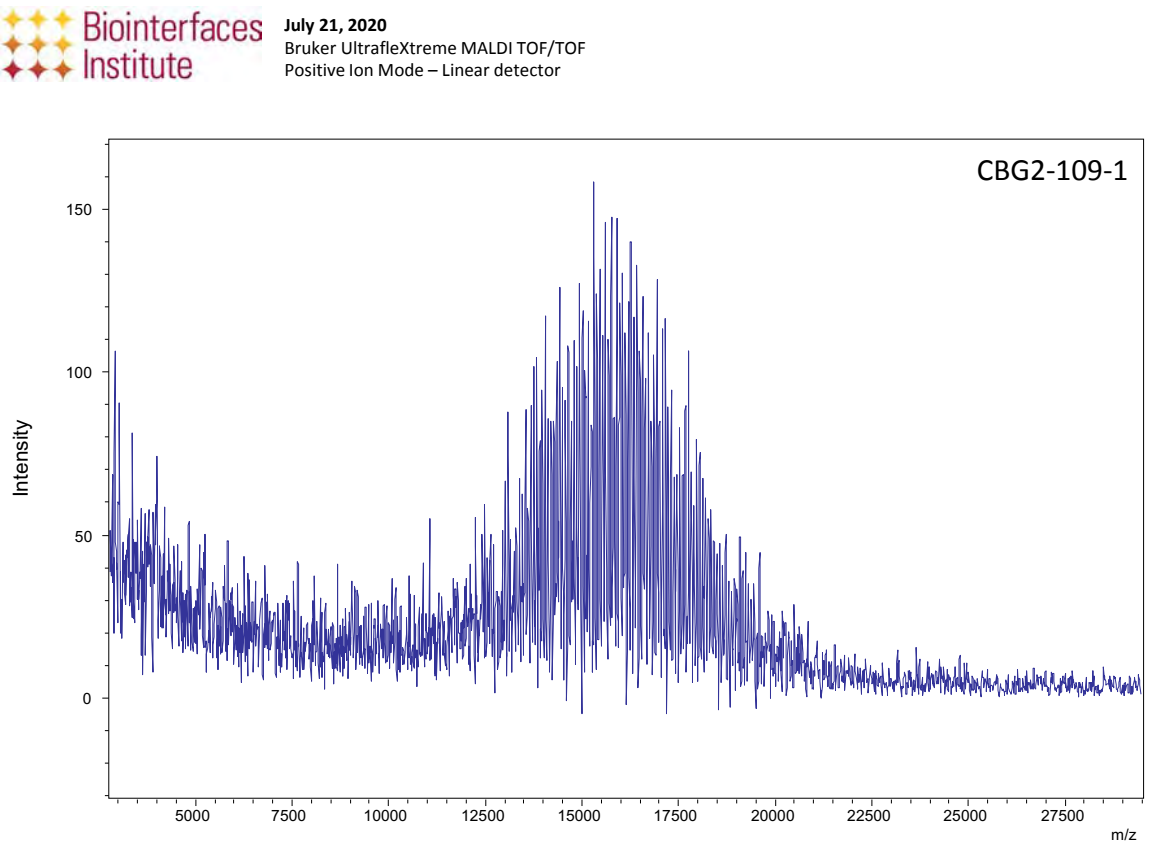

Figure 6.44: MALDI Zn-TPMP-Penta.

6.2.5 Spectral Analysis of DMS-HV15

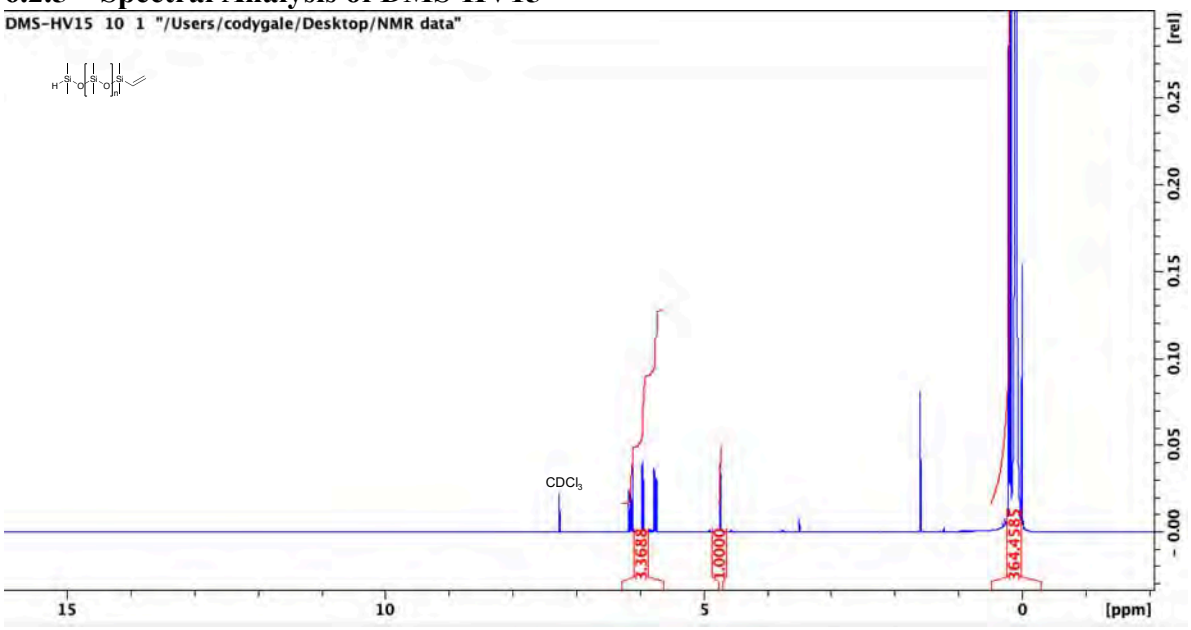

Figure 6.45: ^{1}H-NMR of DMS-HV15.

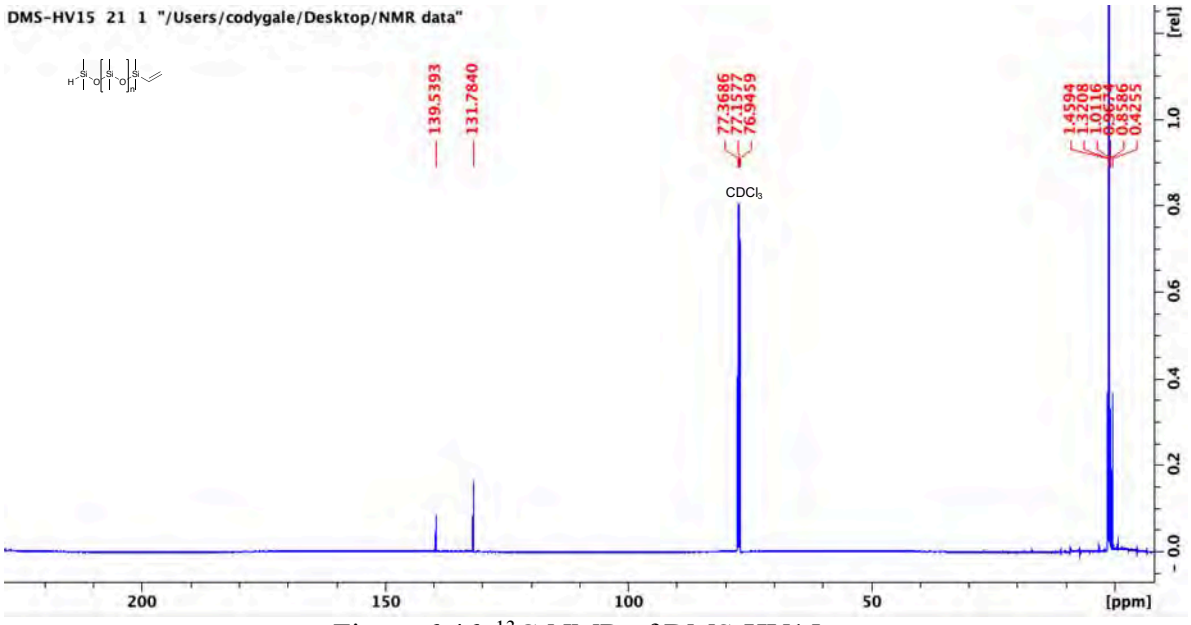

Figure 6.46: ^{13}C-NMR of DMS-HV15.

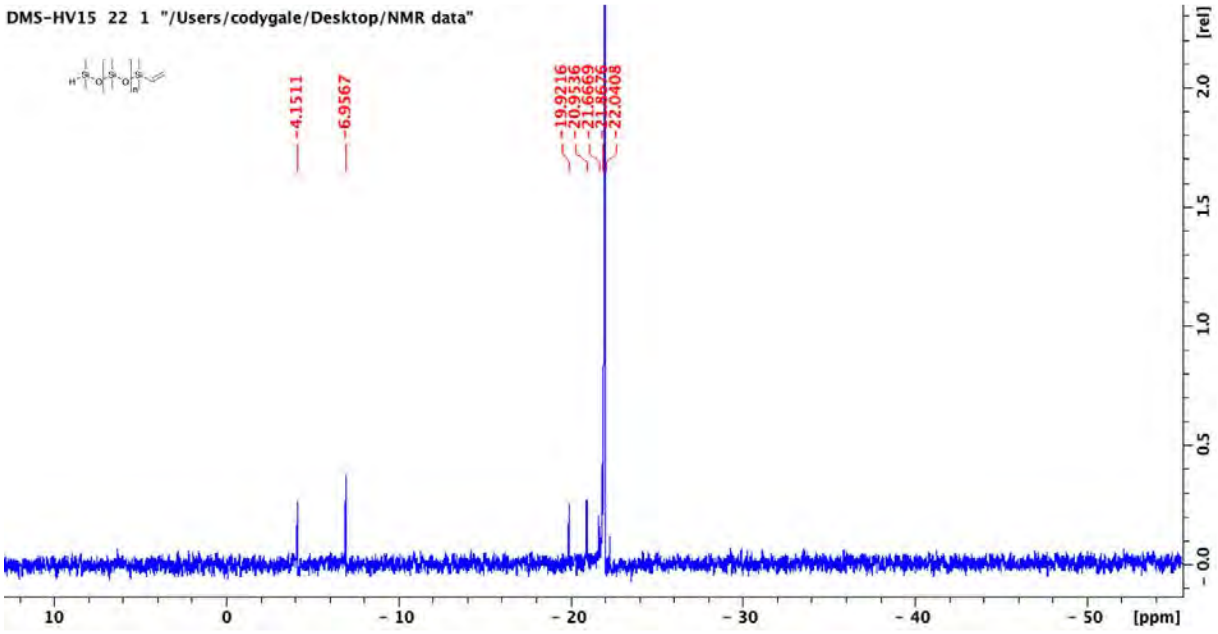

Figure 6.47: ^{29}Si-NMR of DMS-HV15.

6.2.6 Elastomer Formulations, Photobleaching and Fluorescence Data

Table 6.6: Zn-TPMP-HV15 elastomer formulations.

Concentration (M)	Mass DMS-H31 (g)	Volume DMS-H31 (mL)	Mass Zn-TPMP-HV15 (g)	Mass $Si(Si_2O_2C_6H_{15})_4$ (g)	Volume of Karstedt's Catalyst
1×10^{-3}	30.000	31.000	0.5472	0.3546	0.5
1×10^{-4}	30.000	31.000	0.0547	0.3794	0.5
1×10^{-5}	30.000	31.000	0.0054	0.3820	0.5

Table 6.7: Zn-TPMP-Penta elastomer formulations.

Concentration (M)	Mass DMS-H31 (g)	Volume DMS-H31 (mL)	Mass Zn-TPMP-Penta (g)	Mass $Si(Si_2O_2C_6H_{15})_4$ (g)	Volume of Karstedt's Catalyst
1×10^{-3}	30.000	31.000	0.5646	0.3822	0.5
1×10^{-4}	30.000	31.000	0.0565	0.3822	0.5
1×10^{-5}	30.000	31.000	0.0056	0.3822	0.5

Table 6.8: Average elastomer thicknesses measured using optical microscopy (n=9).

Concentration (M)	Photosensitizer	Average Thickness (μm)
Control	NA	170±6
1×10^{-3}	Zn-TPMP-HV15	115±7
1×10^{-4}	Zn-TPMP-HV15	111±10
1×10^{-5}	Zn-TPMP-Hv15	109±3
1×10^{-3}	Zn-TPMP-Penta	114±4
1×10^{-4}	Zn-TPMP-Penta	125±4
1×10^{-5}	Zn-TPMP-Penta	105+±10

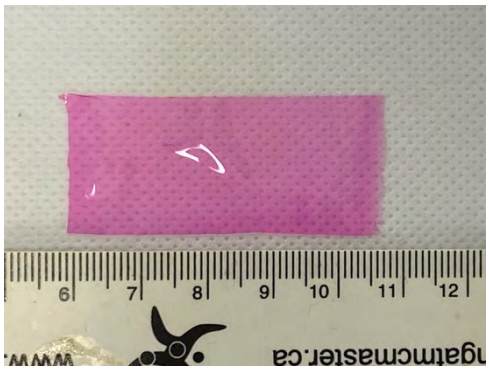

Figure 6.48: Representative image of a thin film containing Zn-TPMP-HV15 (1×10^{-3} M) before being cut for transfer into 24-well plate.

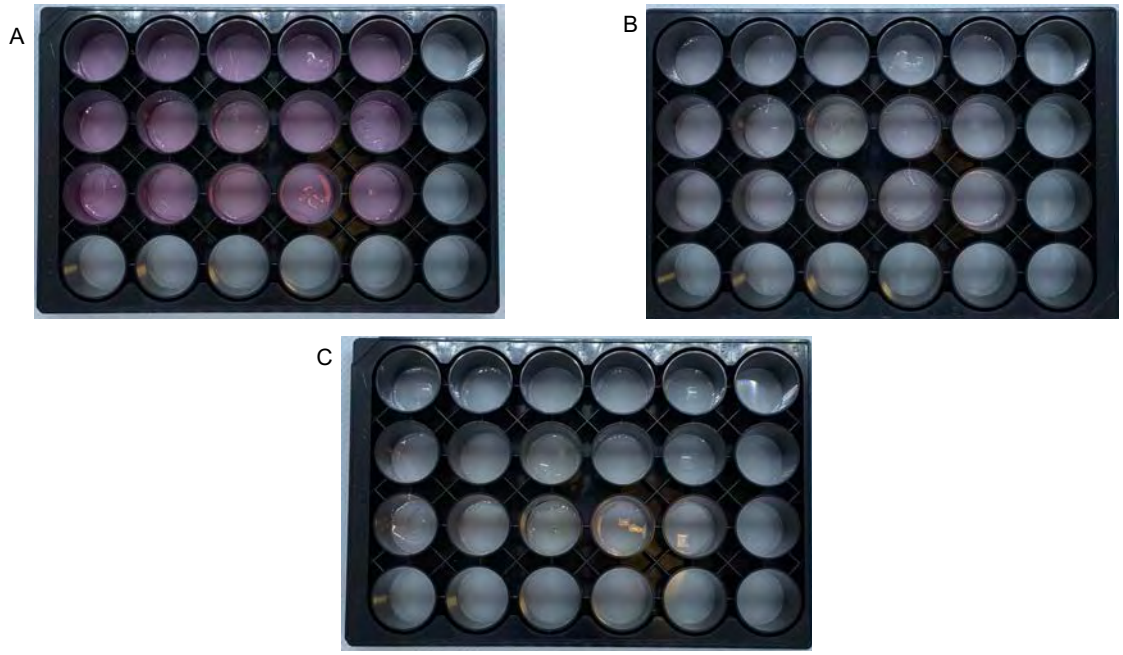

Figure 6.49: Zn-TPMP-HV15 elastomer films in 24-well plates. A) 1×10^{-3} M B) 1×10^{-4} M C) 1×10^{-5} M.

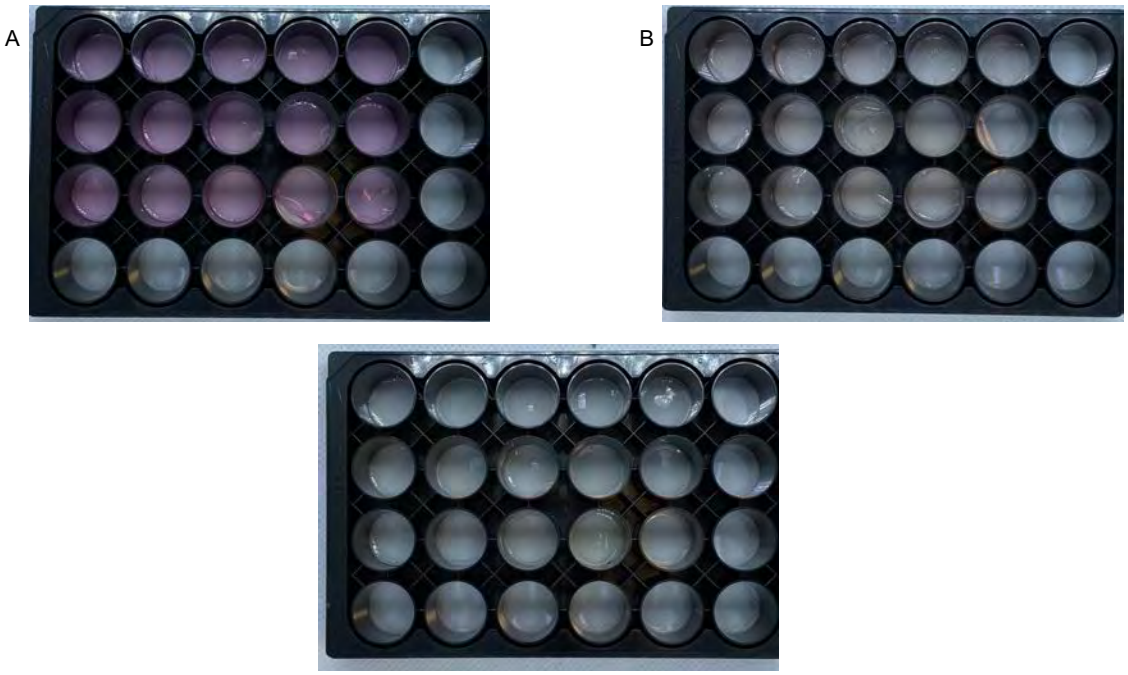

Figure 6.50: Zn-TPMP-Penta elastomer films in 24-well plates. A) 1×10^{-3} M B) 1×10^{-4} M C) 1×10^{-5} M

Table 6.9: Average Fluorescence Intensity of samples (n=12).

Photosensitizer	Concentration	Fluorescence Intensity
Zn-TPMP-HV15	1×10^{-3}	71494±1358
	1×10^{-4}	34278±1430
	1×10^{-5}	9383±4031
Zn-TPMP-Penta	1×10^{-3}	66172±1867
	1×10^{-4}	24945±3845
	1×10^{-5}	1749±252

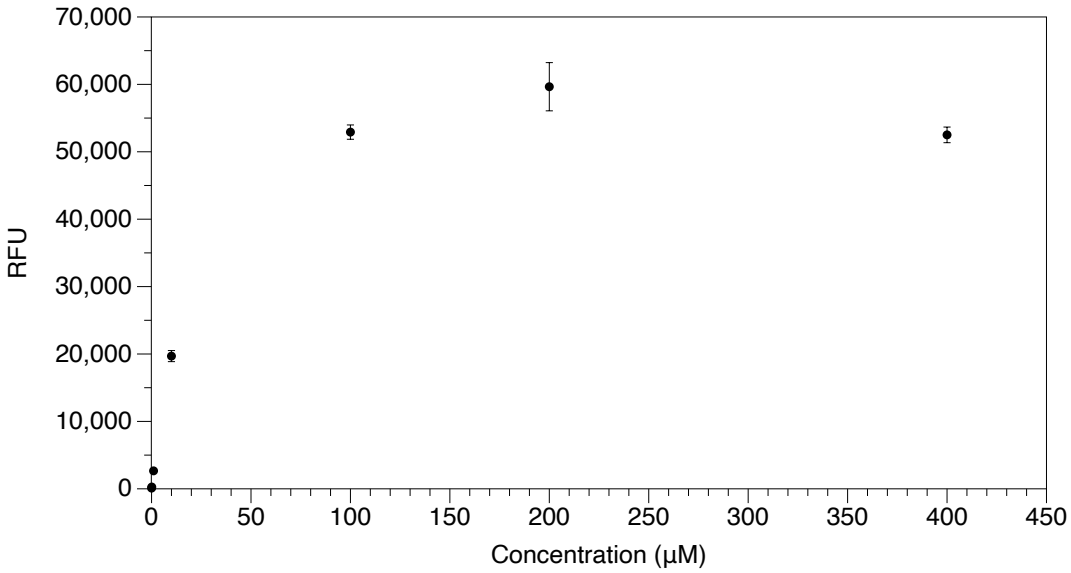

Figure 6.51: Fluorescence Intensity vs concentration calibration curve

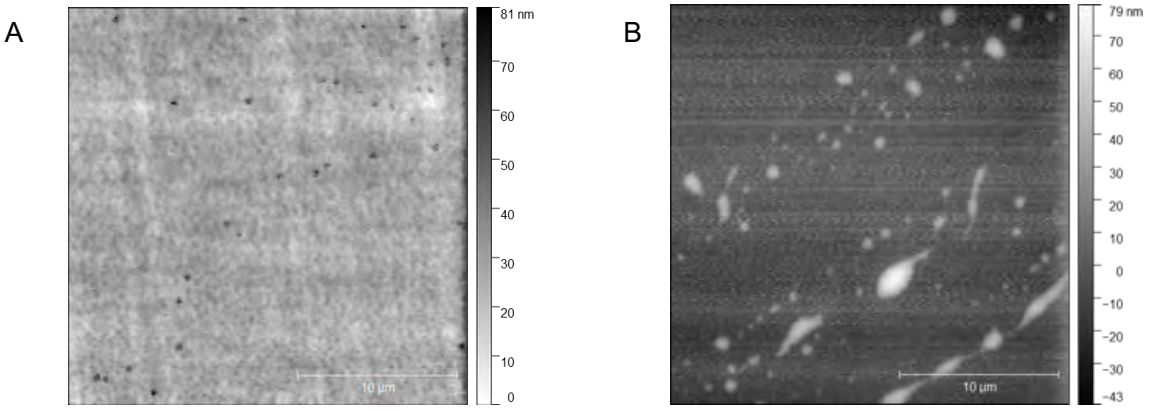

Figure 6.52: A) AFM image of Zn-TPMP-HV15 elastomer film (1×10^{-3}M). B) AFM image of Zn-TPMP-Penta elastomer film (1×10^{-3}).

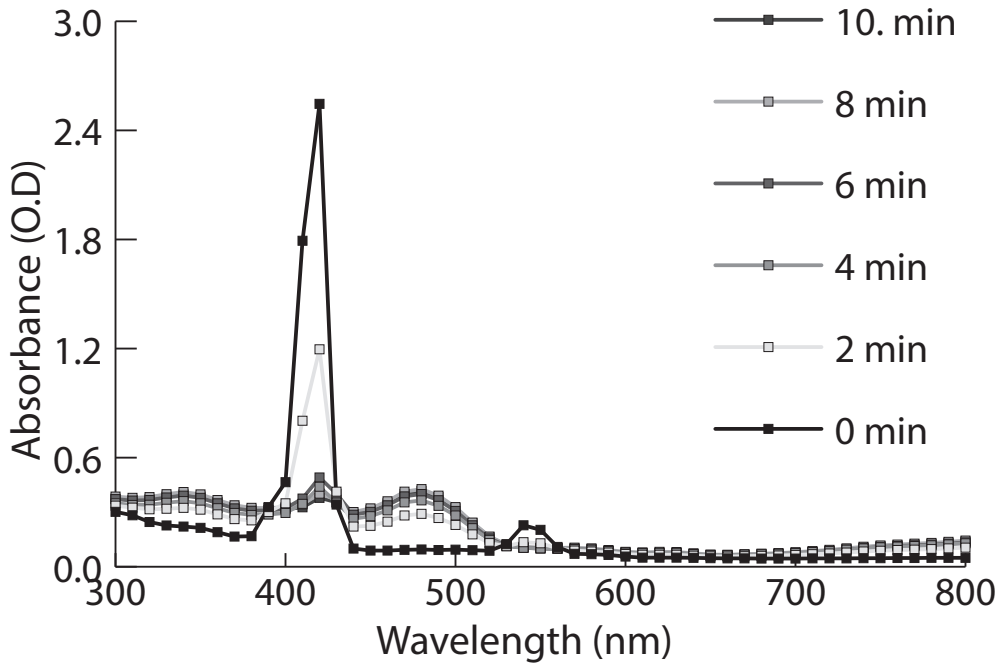

Figure 6.53: Photobleaching of Zn-TPMP-HV15 (1×10^{-3} M).

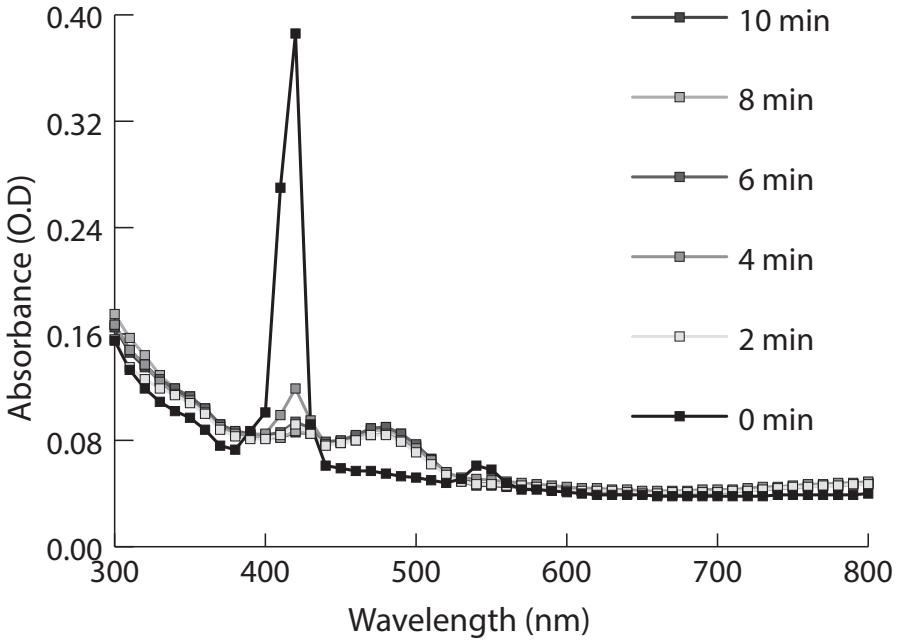

Figure 6.54: Photobleaching of Zn-TPMP-HV15 (1×10^{-4} M).

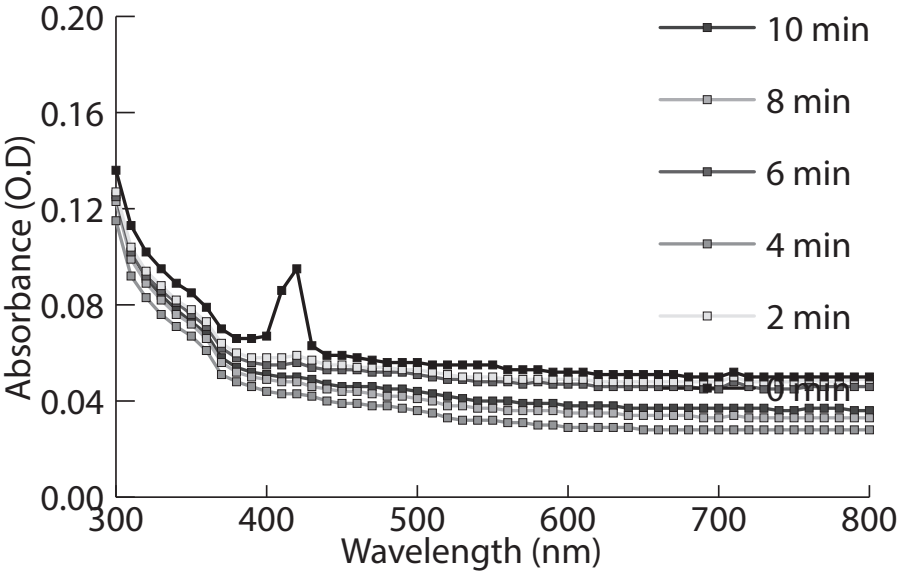

Figure 6.55: Photobleaching of Zn-TPMP-HV15 (1×10^{-5} M).

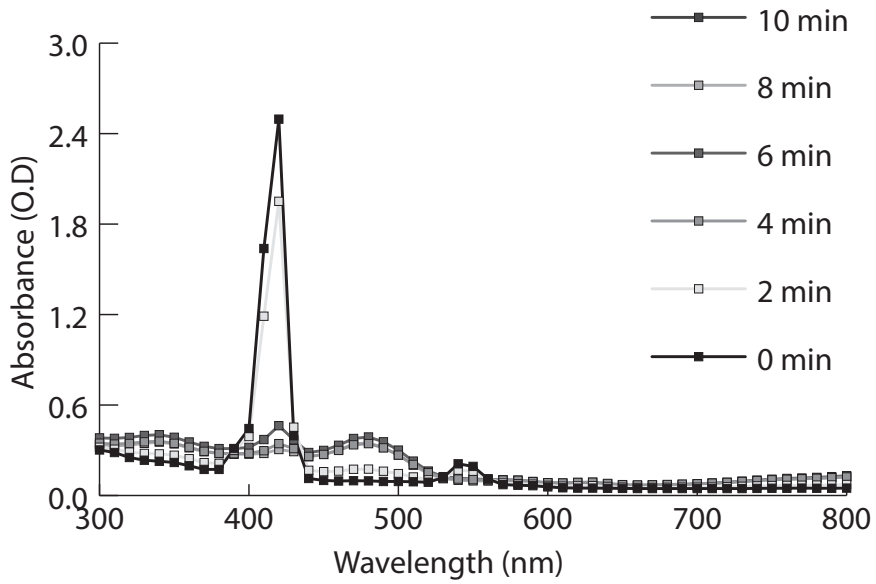

Figure 6.56: Photobleaching of Zn-TPMP-Penta (1×10^{-3} M).

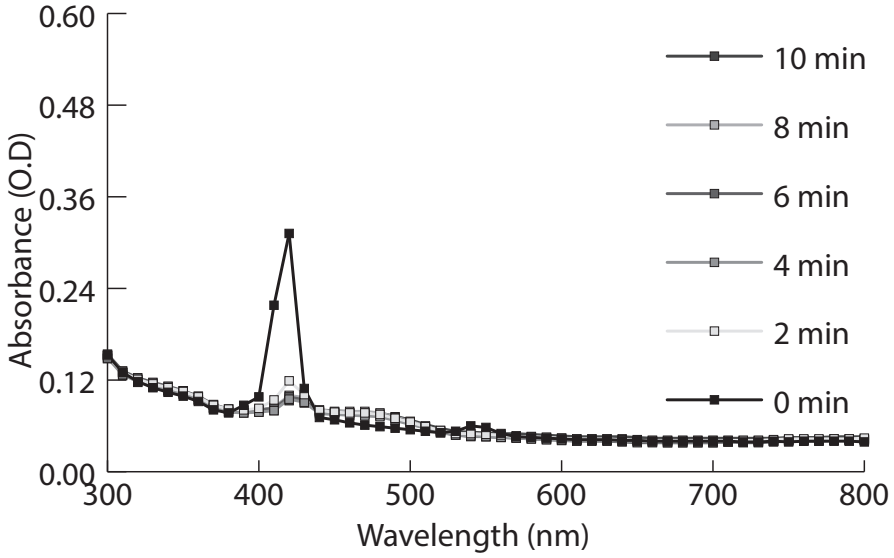

Figure 6.57: Photobleaching of Zn-TPMP-Penta (1×10^{-4} M).

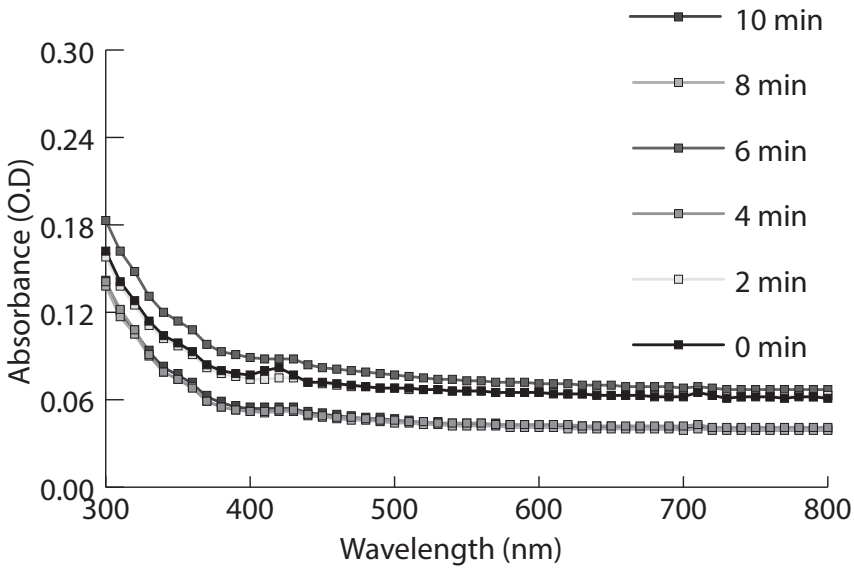

Figure 6.58: Photobleaching of Zn-TPMP-Penta (1×10^{-5} M).

6.3 Appendix III: Supporting Information for Chapter 3

6.3.1 Lineweaver-Burke Plots

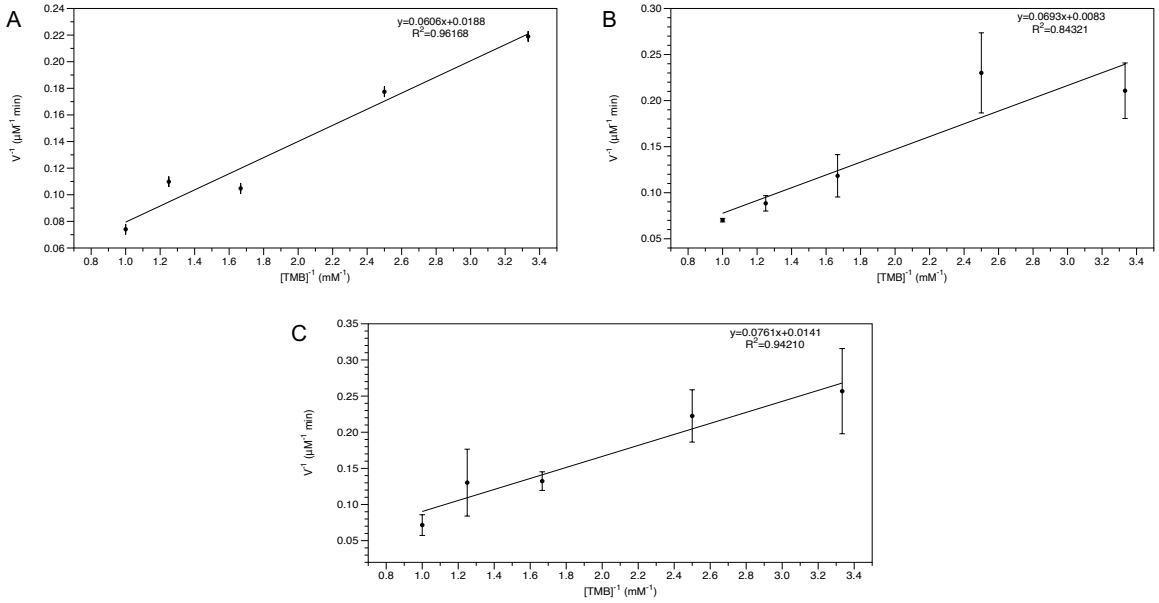

Figure 6.59: Lineweaver-Burke plots for first reaction cycle with TMB. A) **H-E-NN** 1:1. B) **H-E-NN** 1:2. C) **H-E-NN** 1:4.

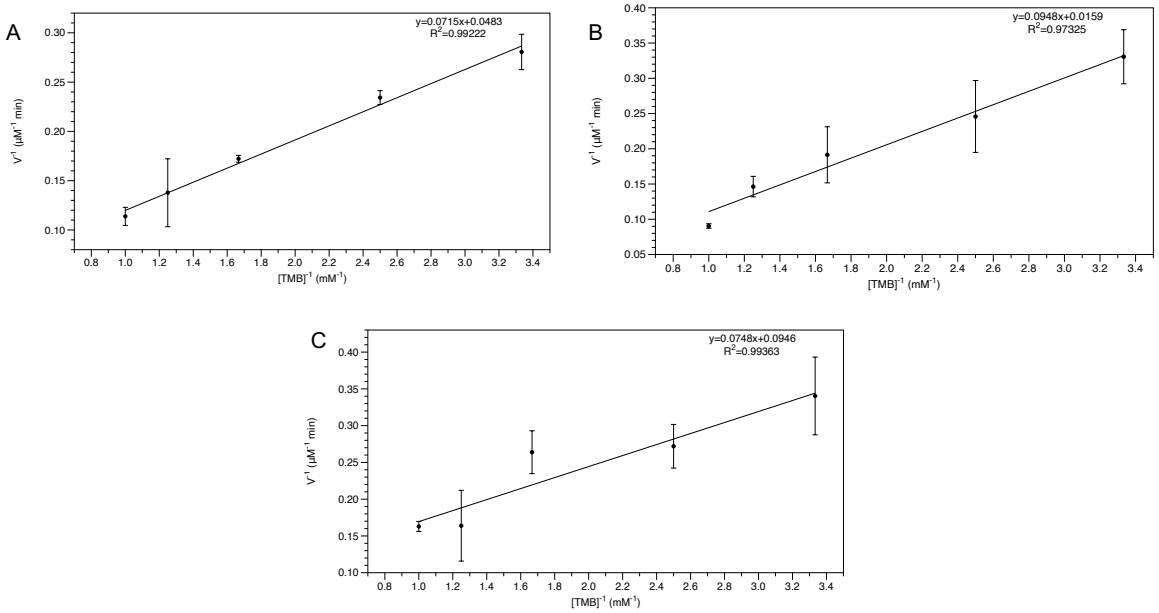

Figure 6.60: Lineweaver-Burke plots for second reaction cycle with TMB. A) **H-E-NN** 1:1. B) **H-E-NN** 1:2. C) **H-E-NN** 1:4.

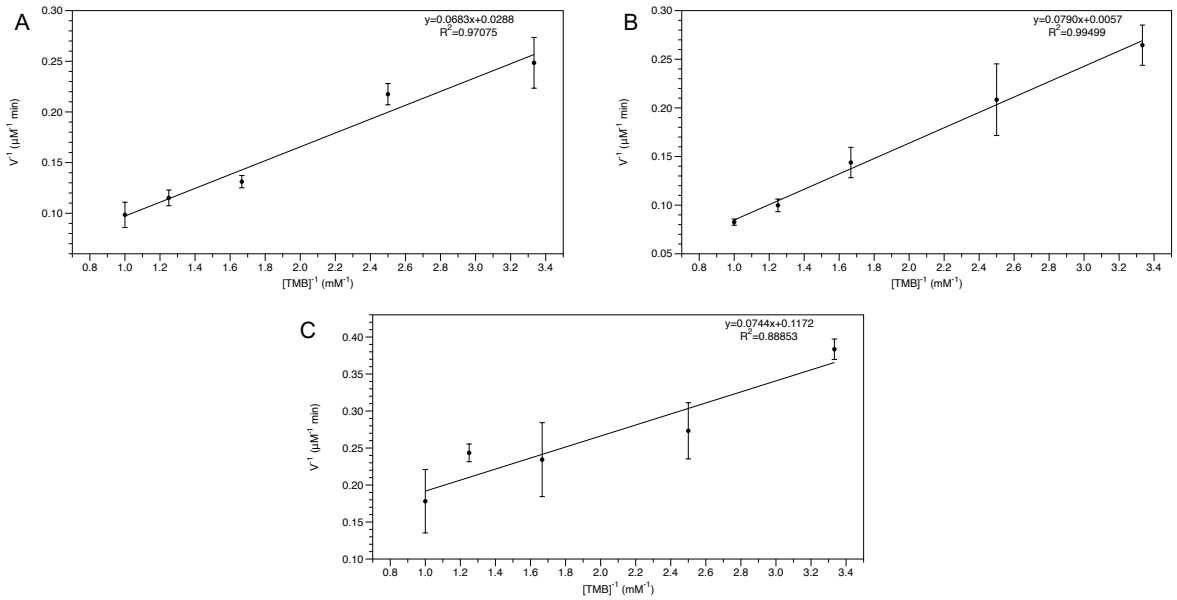

Figure 6.61:Lineweaver-Burke plots for first reaction cycle with TMB. A) H-E-NN 1:1. B) H-E-NN 1:2. C) H-E-NN 1:4.

6.3.2 Images of Elastomers

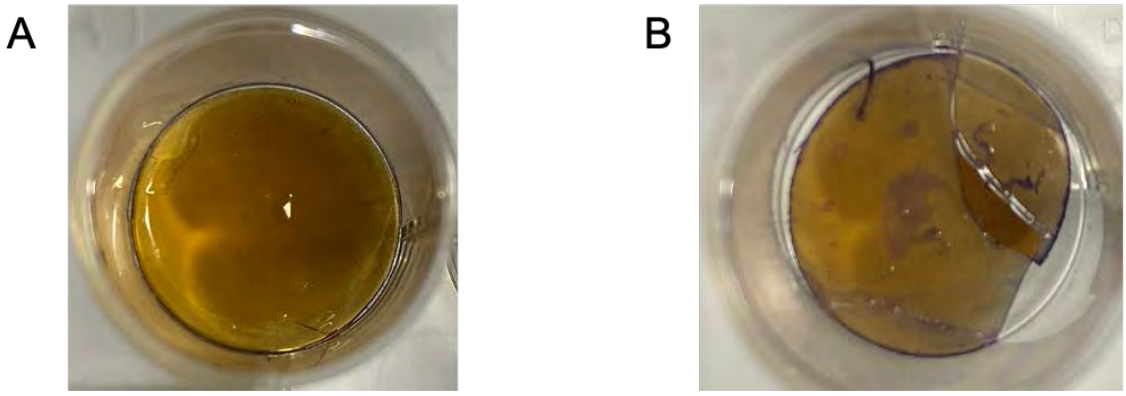

Figure 6.62:A) H-E-NN 1:4 elastomer pre-exposure to TMB. B) H-E-NN 1:4 elastomer post-exposure to TMB (3rd cycle).

Figure 6.63: Poor quality H-A-N 1:1 elastomer film cast with higher viscosity oils.

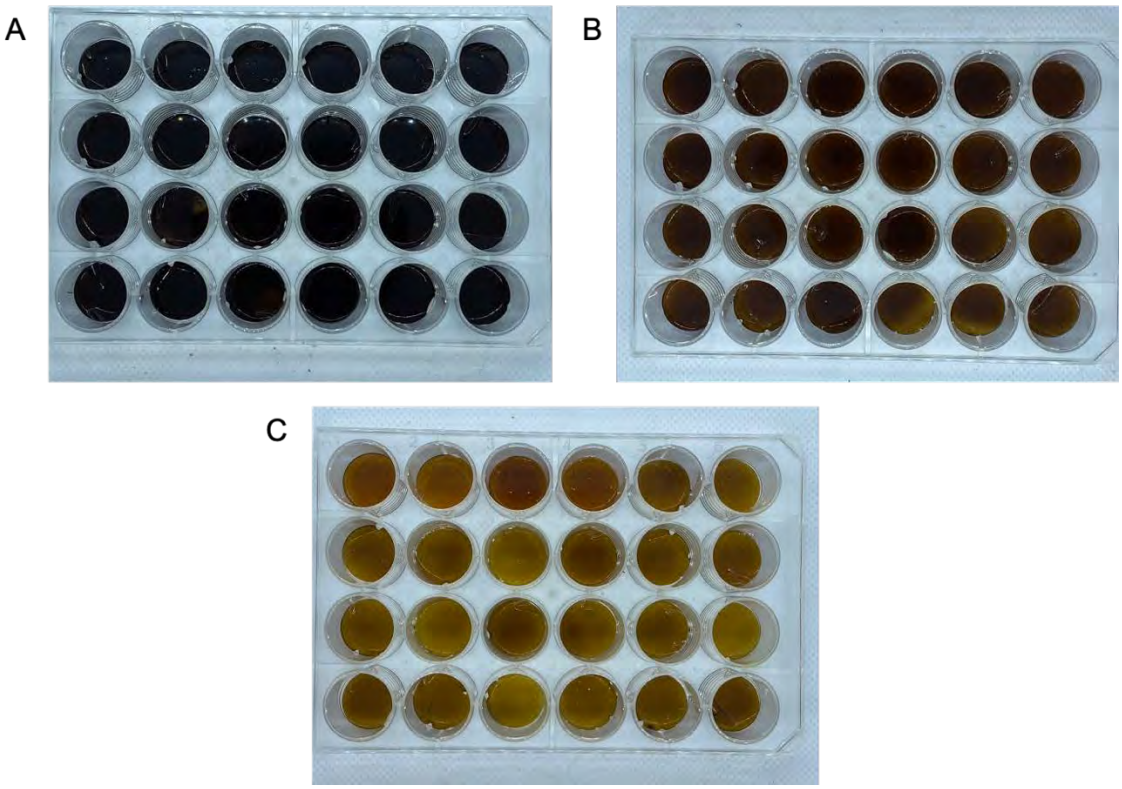

Figure 6.64:A) H-E-NN 1:1. B) H-E-NN 1:2. C) H-E-NN 1:4.